

Phase transitions of lipid bilayers

a mesoscopic approach

Phase transitions of lipid bilayers

a mesoscopic approach

ACADEMISCH PROEFSCHRIFT

ter verkrijging van de graad van doctor
aan de Universiteit van Amsterdam,
op gezag van de Rector Magnificus
prof. mr. P.F. van der Heijden
ten overstaan van een door het college voor promoties ingestelde commissie,
in het openbaar te verdedigen in de Aula der Universiteit

op dinsdag 23 maart 2004 te 10.00 uur

door

Marieke Kranenburg
geboren te Leiderdorp

Promotiecommissie:

Promotor:

- prof. dr. ir. B. Smit

Overige leden:

- dr. P.G. Bolhuis
- prof. dr. S. Brul
- prof. dr. D. Frenkel
- prof. dr. J.A. Killian
- prof. dr. E MacKintosh
- prof. dr. A.E. Mark

Faculteit der Natuurwetenschappen, Wiskunde en Informatica

The research reported in this thesis was carried out at the Department of Chemical Engineering, Faculty of Science, University of Amsterdam (Nieuwe Achtergracht 166, 1018 WV Amsterdam, The Netherlands). Financial support was provided by NWO (Dutch Science Foundation) through PIONIER.

Gedrukt door: Drukkerij MacDonald/SSN bv, Nijmegen. Met dank aan Carlie Segboer.

Voorwoord

Vaak wordt gezegd dat je een proefschrift eigenlijk voor jezelf schrijft, om aan de buitenwereld te laten zien wat je gedaan hebt. Maar waaruit bestaat die buitenwereld? Uit wetenschappers, maar meestal hebben zij de inhoud al vernomen uit artikelen, en uit je eigen familie, vrienden en kennissen. Normaal leest 'de gewone mens' alleen het dankwoord en bekijkt de mooie plaatjes, de rest is toch te ingewikkeld. Toegegeven, ik doe het zelf ook. Maar dan komt het punt dat je je eigen proefschrift schrijft en denkt: ik wil eigenlijk aan iedereen uitleggen waarmee ik vier jaar bezig ben geweest. Ten eerste omdat de popularisering van de scheikunde mijn interesse heeft en ik het een uitdaging vind moeilijke dingen op een eenvoudige manier uit te leggen. En ten tweede omdat dit boekje inderdaad niet alleen naar de specialisten gaat, maar ook naar de familie, de vrienden, de buurman enzovoorts. En dan is het wel zo leuk als zij er ook iets van begrijpen.

Daarom heb ik in dit proefschrift een poging gedaan om alle doelgroepen te bereiken en zodoende heb ik voor een bepaalde opzet gekozen. De inleiding heb ik geprobeerd zo te schrijven dat iedereen de essentie van het onderzoek kan begrijpen. Na deze inleiding volgen een aantal wetenschappelijke hoofdstukken met een meer gedetailleerde beschrijving van het model en de verkregen resultaten. Tenslotte is er een uitgebreide 'Samenvatting voor iedereen', waarin ik in een paar pagina's de resultaten van het onderzoek in eenvoudiger taal uitleg.

Op deze manier hoop ik met dit proefschrift een net wat breder publiek te bereiken dan gemiddeld. Idealistisch? Misschien. Ik realiseer me dat dit proefschrift niet tot een revolutie gaat leiden in de bèta-wetenschappen. Maar alle kleine beetjes helpen.

Contents

Voorwoord	i
1 Introduction	1
1.1 The cell membrane	2
1.2 Lipids and lipid bilayers	3
1.3 Computer simulations	6
1.4 This thesis	8
2 Computer simulations	11
2.1 Introduction	12
2.2 Dissipative Particle Dynamics	13
2.3 Constant surface tension simulations	15
2.4 Inter- and intramolecular interactions	16
2.4.1 Repulsion parameters α_{ij}	16
2.4.2 Constructing lipids	17
2.4.3 Reduced units	18
2.5 Testing the MC-DPD scheme	18
2.6 Structural quantities of a lipid bilayer	20
3 Phase behavior of monotail lipids	23
3.1 Introduction	24
3.2 Computational details	25
3.3 Results and Discussion	26
3.3.1 The lipid ht_9	27
3.3.2 Phase behavior as a function of tail length	34
3.4 Conclusions	37
4 Coarse graining a phospholipid	39
4.1 Introduction	40
4.2 Computational details	41
4.3 Parameter sets	42
4.3.1 Coarse-grained models	45

4.4	Results and Discussion	48
4.4.1	Model I: bead volume 30 \AA^3	49
4.4.2	Model II: bead volume 90 \AA^3	51
4.4.3	Changing temperature and lipid topology	52
4.4.4	Driving forces in the formation of a bilayer	54
4.5	Conclusions	56
5	Phase behavior of double tail lipids	57
5.1	Introduction	58
5.2	Computational details	60
5.3	The lipid $h_3(t_4)_2$	61
5.3.1	Phase behavior as a function of temperature and head group interaction	62
5.3.2	The rippled phase	66
5.4	Influence of tail length	68
5.5	Discussion	70
5.5.1	Phase behavior as a function of temperature and tail length	71
5.5.2	Anomalous swelling	72
5.5.3	Structure of the rippled phase	75
5.6	Conclusions	78
6	Induced interdigitation	79
6.1	Introduction	80
6.2	Computational details	82
6.3	Effect of an additional bead in the head group	83
6.4	Induced interdigitation by alcohols	86
6.4.1	Phase behavior	87
6.4.2	Structure of the interdigitated phase	90
6.4.3	Longer chain alcohols	93
6.5	Conclusions	95
	References	97
	Summary	103
	Samenvatting	107
	Curriculum Vitae	113
	Publications and presentations	115
	Dankwoord	117

I

Introduction

1.1 The cell membrane

The cell is the most important unit in life. In 1665 Hooke observed that the tissue of a cork plant was divided into tiny compartments, which he called cells (*cellulae* means rooms). In 1840 improved observations on many tissues led to the hypothesis that all organisms exist either as single cells or aggregates of cells. More than a century of study later this hypothesis was confirmed. Moreover, there is no relation between the size of the cells and the size of an organism. All cells are of about the same size; a larger organism has just more cells than a small one.

An (eukaryotic) cell can be regarded as a factory, in which different processes take place. The cell is surrounded by the so-called cell membrane, in which the cytosol, a semi fluid, is contained (see figure 1.1) [1, 2]. In this cytosol the organelles are located: membrane-surrounded structures in which specialized functions are carried out. The major organelles are the nucleus, the mitochondria, the endoplasmic reticulum and the Golgi complex. Most cells of higher organisms are specialized in function, for example in the production and the export of one or a few molecular products. However, despite their different function, they are all composed of the same kinds of lipids, proteins, nucleic acids, and polysaccharides.

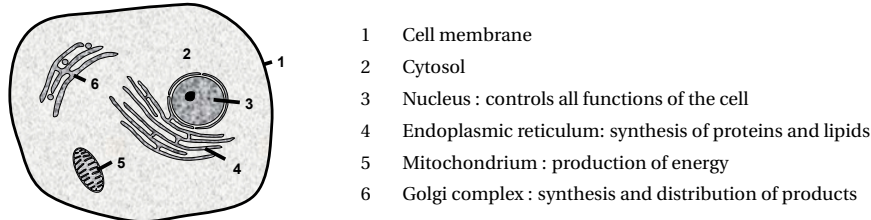


Figure 1.1: Schematic overview of an eukaryotic cell with the most common organelles of both plants and animals

The membranes play an important role in the protection of the cell or organelle from its surroundings. The membrane, however, is more than just a protective wall. It contains highly selective gates (proteins), that regulate the transport of nutrients in certain directions. In this way, a cell or organelle can create its own environment and thus it can perform its specific function.

The common representation of a membrane of an eukaryotic cell is known as the Fluid Mosaic Model, that was proposed by Singer and Nicolson (see figure 1.2) [3]. The essence of the model is that membranes are two-dimensional solutions of oriented (phospho)lipids and globular proteins. The basis of the membrane are the lipids that are arranged in a bilayer. This bilayer has a dual role: it is a solvent for the integral membrane proteins and it is a permeability barrier. Both the lipids and the

proteins can undergo lateral movement (in the plane of the bilayer) and rotational movement (around its molecular axis perpendicular to the membrane). A small proportion of the lipids interact specifically with some membrane proteins and may thus be essential for the function of these proteins.

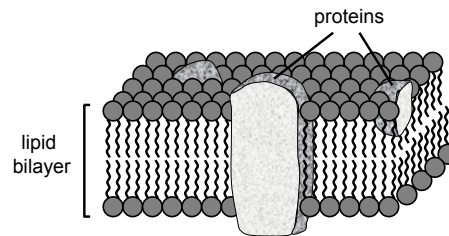


Figure 1.2: The Fluid Mosaic model of a cell membrane: a mosaic of numerous protein molecules dissolved in a fluid bilayer of lipids

1.2 Lipids and lipid bilayers

From the previous section it is clear that the lipid bilayer plays an important role in the cell membrane. Before discussing the properties of a bilayer, we will first look at a lipid, the building block of a bilayer, in more detail.

Lipids are so-called amphipathic molecules, meaning that one molecule contains both a polar, hydrophilic ("water-loving") head group, which tends to associate with water, and one or more hydrophobic ("water-fearing"), water repelling, tails. Due to this amphipathic character, lipids associate together in water, a process called self-assembly. The hydrophobic parts stick together, while the hydrophilic head groups are in contact with water. Dependent on the shape of the lipid and the concentration of lipids in water, different structures can form (see figure 1.3) [4–7], of which the lipid bilayer is a particular one. If the head group is large with respect to the hydrophobic part, the lipids will form a micelle: a globular structure in which the head groups are surrounded by water and the hydrophobic tails are sequestered inside. The opposite is the formation of the inverse micelle, formed if the tails are bulky and the head group is relatively small. The third and most important structure in biology is the lipid bilayer. The lipids are comprised of a large head group and mostly two hydrophobic tails. This yields a roughly cylindrical molecule, which can easily pack in parallel to form extended sheets. The various structures can transform from one to another by changing the solution conditions such as the electrolyte concentration, the pH, or temperature.

The formation of lipid bilayers is a rapid and spontaneous process, with the hydrophobic interactions as the main driving force (*i.e.* the hydrophobic effect). Water

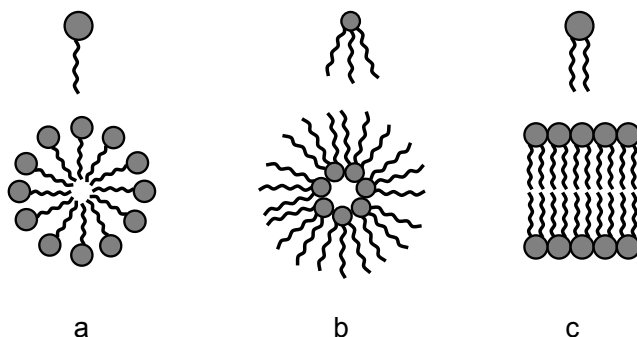


Figure 1.3: Self-assembly of lipids in water gives different structures, dependent on the molecular structure of the lipid: (a) micelle, (b) inverse micelle, and (c) bilayer. The filled circles represent the hydrophilic head groups of the molecules and the wavy lines the hydrophobic tails.

molecules are released from the hydrophobic tails as these tails become sequestered in the interior of the bilayer. Additionally, the vanderWaals attractive forces between the tails favor a close packing. And finally, the lipid bilayers are stabilized by the electrostatic interactions and the formation of hydrogen bonds in the head group region [2, 8].

The most abundant lipids in biological membranes are the phospholipids. In figure 1.4 a schematic drawing of a phospholipid is given, together with an example. The backbone of a phospholipid is glycerol. To this glycerol unit two hydrocarbon tails, derived from the fatty acids, are connected. These fatty acid chains contain an even number of carbon atoms, typically between 12 and 24, of which the 16, and 18 carbon fatty acids are the most common ones. The tails can be both saturated or unsaturated, meaning that one or more double bonds between carbon atoms are present. At the remaining carbon atom of the glycerol the hydrophilic head group is attached. This head group consists of a phosphate group and an alcohol group. Different alcohols lead to a variation in head groups and thus a variation in properties of the lipid bilayer.

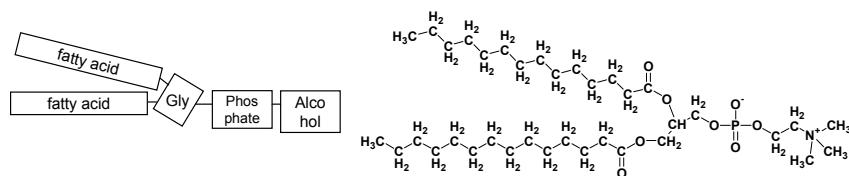


Figure 1.4: Schematic drawing of the components of a phospholipid (left) and the phospholipid DiMyristoylPhosphatidylCholine (right). 'Gly' denotes the glycerol group.

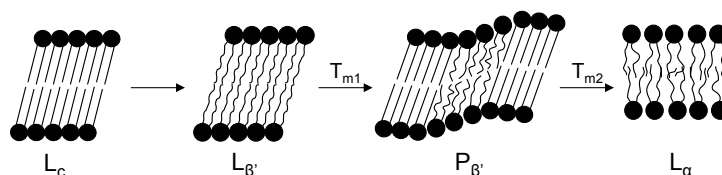


Figure 1.5: Schematical representations of the lipid bilayer phases during a heating process. T_{m1} and T_{m2} denote the pretransition and the main transition, respectively.

The most common phospholipids are the PhosphatidylCholines (PC's), in which the alcohol group is a choline (see the example in figure 1.4). The bilayers of these lipids undergo three phase transitions within the temperature range of 10°C to 80°C [9]. In figure 1.5 these phases are drawn in order of increasing temperature. The lowest temperature phase is the L_c phase, also called the subgel phase, which transforms to the gel phase or $L_{\beta'}$ phase upon heating. In both phases the hydrocarbon tails are tilted with respect to the bilayer normal, but in the $L_{\beta'}$ phase the head group is more hydrated (*i.e.* surrounded by water). The transition from the L_c phase to the $L_{\beta'}$ phase is called the subtransition. Increasing temperature further leads to the formation of the the rippled ($P_{\beta'}$) phase. The transition is called the pretransition and in this $P_{\beta'}$ phase, the bilayer is not flat, but corrugated. Finally, the bilayer undergoes the transition to the liquid crystalline or fluid L_{α} phase, which is called the main transition or the chain order/disorder transition. In this phase, the bilayer is a two-dimensional fluid, meaning that the lipids are free to move in the plane of the bilayer. The hydrocarbon chains become disordered and therefore the transition to the L_{α} phase is regarded as the melting of the bilayer.

Lipid	n_C	T_{m1}	T_{m2}
DMPC	14	15.3	24.0
DPPC	16	35.5	41.5
DSPC	18	51.0	54.3
DAPC	20	62.1	64.1

Table 1.1: Pretransition (T_{m1}) and main transition (T_{m2}) temperatures (in $^{\circ}\text{C}$) of various PhosphatidylCholines (PC's) dependent on the number of carbon atoms in the hydrocarbon chains n_C [10].

The various transition temperatures are characteristic for the lipid of which the bilayer consists. The pre- and main- transition temperatures increase with increasing tail length of the lipid (see table 1.1), but decrease with increasing head group hydration and unsaturation of the alkyl chains. In the latter case the transition temperatures are not only influenced by the number of double bonds in the chains, but also by position. In case of a pure phospholipid bilayer the transition to another phase is very sharp and takes place over a temperature range of $0.8 - 1.5^{\circ}\text{C}$. How-

ever, this temperature range varies in the presence of cholesterol, proteins, cations, or small molecules that interact with the bilayer.

The nature of the head group and the presence of small molecules interacting with the bilayer do not only influence the transition temperatures, but also the structure of the low temperature phases of the bilayer. If the head group is small, the stable phase is a gel phase (L_{β}), in which the tails do not show a tilt with respect to the bilayer normal (see figure 1.6(a)). If small amphiphilic molecules are added to the bilayer, the low temperature phase is the interdigitated $L_{\beta I}$ phase. In the interdigitated phase, the terminal methyl groups of the lipid chains of two opposing layers do not face each other, but are located near the head group region of the opposing layer (figure 1.6(b)).

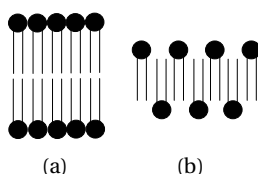


Figure 1.6: Schematical representation of (a) the L_{β} phase and (b) the $L_{\beta I}$ phase.

Let us now return to the cell membrane. As explained, the basis of the cell membrane is the lipid bilayer, in which the hydrophilic head groups stick into the water and the hydrocarbon tails are sequestered in the middle. Not only the lipids are amphiphilic, but also the proteins in the cell membrane have a hydrophilic and a hydrophobic region. The organization of the lipids around the proteins plays a crucial role in the functioning of the proteins. If this organization changes due to changes in composition, temperatures or additives to water, the lateral pressure on the different parts on the protein will change [11] or the hydrophobic part of the protein will be exposed to water (the so-called "hydrophobic mismatch"), causing the disfunctioning of the protein. Therefore, knowledge of the behavior of lipid bilayers is very important for our understanding of the functioning of the cell.

1.3 Computer simulations

In recent years many experimental techniques, such as X-ray crystallography, electron microscopy, infra-red and Raman spectroscopy, have been developed to characterize the structure of a membrane. Despite these developments, the precise functioning of membranes is still not well understood [12]. Therefore, a better characterization of the (phase) behavior of lipid membranes and the interaction between lipids and proteins is needed. This insight can be gained by performing computer simulations on detailed atomistic models based on realistic microscopic interactions.

The most used method to simulate biological systems, like lipid membranes, at an atomistic scale, is Molecular Dynamics (MD). In this method all interactions between the individual atoms are taken into account. Let us take one of the simplest systems, a bilayer of DMPC (see figure 1.4), as an example. To calculate the properties of a fully hydrated bilayer, 64 lipids and 1645 water molecules are needed [13], which gives a total of 12.487 atoms. For all these atoms both the intramolecular interactions (bonds, angles, dihedral angles) and the intermolecular interactions (van der Waals forces, hydrogen bonds, electrostatic interactions) must be described and calculated in every time step. This costs a lot of CPU time and thus these MD simulations are restricted to a small part of the bilayer (the length scale) and 1 or 2 nanoseconds (the time scale). Recently the progresses in computational techniques and the increased power of computers have allowed to reach time scales of 100 nanoseconds [14, 15], but there are still various phenomena that occurs at longer time and length scales. These time and length scales are still not reachable by all-atom simulations and therefore other methods have been developed.

Although an all-atom model is seen as the realistic description of a biological membrane, such a model assumes that the quantumchemical nature of the interactions is not essential for our understanding of some of the properties of a membrane. Similarly, one can assume that some of the atomic details can be ignored, while preserving the essential aspects of the molecular structure. In such a mesoscopic approach, clusters of atoms are replaced by spheres, which are connected by harmonic springs. A commonly used approach is to apply MD simulations, in which the interactions between the clusters of atoms are described by a Lennard-Jones potential [16–20]. An alternative approach is to use Dissipative Particle Dynamics, which is more efficient compared to MD for these models.

Dissipative Particle Dynamics (DPD) was originally developed to simulate complex fluids. A fluid particle is to be understood as *"being very small compared with the volume of the body under consideration, but large compared with the distances between the molecules"* [21]. In many DPD studies, a particle represents three water molecules or three methylene (CH₂) groups. Between the particles, there is a soft repulsive potential, in which the characteristics of water and the lipids are described. All particles repel each other, but the repulsive force between, for example, two water particles will be less than the repulsion between a water particle and an oil particle. In this way, a phase separation between oil and water is obtained. In case of a lipid, we end up with a set of repulsion parameters, describing the interactions between the hydrophilic particles, hydrophobic particles and water. The advantage of this technique is that due to the coarse graining much larger length and time scales can be reached. Compared to molecular dynamics simulations on an all-atom system, DPD on such a coarse-grained model can be 4 to 5 orders of magnitude more efficient [16, 22]. This gain in CPU time allows us to study longer time and length scales

than is possible with MD on an all atom model.

1.4 This thesis

Since the structure of the lipid bilayer plays a crucial role in the functioning of the cell, it is interesting to study the properties and the behavior of lipid membranes using computer simulations at longer time and length scales than has been achieved with Molecular Dynamics. Dissipative Particle Dynamics seems to be a very promising method to simulate such bilayers. However, DPD is a relatively new simulation technique and till now, only a few investigations on lipid membranes have been published [22–26].

The aim of this thesis is twofold. First of all, we investigated how much detail should be added to a mesoscopic model of a lipid to reproduce the experimental observations. Questions that arise are, for instance:

- Is it sufficient to have a representation of a lipid, in which the model only contains the basic features of a lipid or should the model be more detailed?
- Related to the previous question: what level of coarse-graining is needed? Should a DPD particle represent one, two, three, or even more water molecules?
- Which set of repulsion parameters should be used and what happens if we change some of the parameters?

Once we have optimized the model, the logical next step is to investigate the properties of a lipid bilayer, which are difficult to answer experimentally. Examples of some experimental questions, that we try to answer in this thesis are:

- The formation of the rippled phase during the heating and cooling process of a lipid bilayer. As can be seen in figure 1.5, the plane of the bilayer in the gel phase and the fluid phase is flat, while in the rippled phase it is corrugated. Since more than 30 years the appearance of this ripple has been puzzling. Why does the ripple appear? What does it look like at a molecular scale? Is the swelling of the bilayer at the main transition coupled to the appearance of the rippled phase?
- It is proposed that the formation of an interdigitated phase is caused by an increased distance between the lipid head groups. This can be achieved in various ways: by changes of the chemical structure of the lipid and by the addition of salts or small amphiphilic molecules, like alcohols or anesthetics, to the bilayer. One may wonder whether the increase in separation of the head groups in itself is sufficient to cause interdigitation. Experimentally this question is difficult to answer, because it is hard to isolate a single cause and effect relation. *In silico* this is however quite easy as we can turn interactions on and off at will. In case of the addition of small amphiphilic molecules to the bilayer, we

are able to directly count the molecules involved in the interdigitation, which is not possible experimentally.

In chapter 2, we give a description of the simulation technique applied, the model, and the structural quantities of a bilayer, needed to characterize the different phases. With these definitions, we investigate the phase behavior of the most simple model of a lipid, that consists of one hydrophilic head bead connected to a single hydrophobic tail in chapter 3. From the results obtained with this model, we can predict the conditions under which interdigitation in a bilayer consisting of monotail lipids can be induced. In chapter 4 we address the question of the choice of repulsion parameters and of which level of coarse graining is needed to reproduce the experimental characteristics of a bilayer consisting of double tail lipids. We find that a model consisting of a head group of three hydrophilic beads connected to two hydrophobic beads gives the best result. With this model, we study the phase behavior of a lipid bilayer in chapter 5. By changing the interaction between the head groups of the lipid, we observe the formation of various phases and special attention is given to the formation of the rippled phase. In the last chapter we return to the induction of the interdigitated phase, but now in a bilayer containing double tail lipids. Interdigitation is induced in two ways: 1. by changes in the chemical structure of the lipid head group, and 2. by the addition of small amphiphilic molecules to the bilayer.

II

Computer simulations

Abstract

In this chapter a combined scheme of Dissipative Particle Dynamics (DPD) and Monte Carlo (MC) is used to simulate a lipid bilayer. DPD is a mesoscopic simulation method in which several atoms are represented by a single particle. A soft repulsive conservative force between the particles causes the self assembly of lipids in water. To obtain a tensionless state of the bilayer, we perform MC moves, in which we can impose the condition of a zero interfacial tension. In this chapter, the details of the simulation method are described and we show that, dependent on the lipid topology, different structures are observed during the self assembly of the lipids. We also describe the various structural quantities of the bilayer, calculated during the simulations.

2.1 Introduction

Phase behavior of lipid bilayers has been studied theoretically using phenomenological models [27–29]. Whereas these models give important information on the general aspects of the phase diagram, they are less convenient to study effects of changes in the chemical structure of the lipids. For this type of questions molecular simulations are more convenient. At present it is possible to study the formation of lipid mesophases using all-atom molecular simulations [30], but these simulations are too time consuming to study the phase behavior. An alternative approach is to use a mesoscopic model, in which general aspects of changes in the chemical structure and interactions between the lipids can be studied [16, 17, 22, 23]. Here, we present a mesoscopic model that allows us to study transitions between the various mesoscopic bilayer phases.

We use Dissipative Particle Dynamics (DPD) [31] to simulate our system. In a DPD simulation one uses, in addition to the conservative forces between the particles, a dissipative and a random force. The dissipative and random forces are chosen such that a proper Boltzmann distribution of configurations is sampled corresponding to the intermolecular interactions from which the conservative interactions are derived [32]. In analogy with previous simulations using the DPD technique, we use soft-repulsive interactions to mimic the coarse-grained interactions between the lipids and water molecules. Groot and Rabone [22] have shown that compared to a molecular dynamics (MD) simulation on an all atom system, DPD on a coarse-grained model can be 4 to 5 orders of magnitude more efficient. Since these MD-simulations are very demanding, they are often limited to a single temperature and type of lipid [33]. The efficiency gained by DPD allows us to compute complete phase diagrams.

A biological membrane is not subject to external constraints and therefore adopts a configuration which is tensionless. In a molecular simulation in which the total area and number of lipid molecules are fixed, the resulting membrane has a non-zero surface tension. Lipowski and coworkers [34] emphasize the importance of simulating at exactly the area for which the surface tension is zero. Whereas in ref. 34 this area is determined iteratively, we use a different approach. To ensure that our simulations are performed in a tensionless state, we use an ensemble in which we can impose the surface tension. After a randomly selected number of DPD steps we perform a Monte Carlo move in which we change the area of our bilayer in such a way that the total volume of the system remains constant. The importance of this method is that it also allows us to observe directly phase transitions in which the area per lipid changes.

2.2 Dissipative Particle Dynamics

Dissipative Particle Dynamics (DPD) is a relatively new simulation method, introduced in 1992 by Hoogerbrugge and Koelman [31]. By combining several aspects of Molecular Dynamics and lattice-gas automata, it captures hydrodynamic time and length scales much larger than can be reached with the first method and it avoids the lattice artifacts of the latter method. Hoogerbrugge and Koelman showed both by simulations and theoretical derivation that the DPD algorithm obeys the Navier-Stokes equations. The original scheme was modified in 1995 by Español and Warren [35] to ensure that a proper Boltzmann distribution is generated.

One of the most attractive features of DPD is the versatility in simulating complex fluids. A DPD particle represents a ‘fluid package’ or a cluster of atoms, that moves according to the Newton’s equations of motion, interacting with other particles through a dissipative, a random, and a conservative force. By changing the conservative force between different types of particles a fluid can be made ‘complex’. The simplest example is the phase separation of two immiscible fluids by assuming two types of particles [36, 37]. A second application is in the simulation of colloidal particles [38–40], in which a colloid is represented by freezing some of the particles. Another application of DPD is in computing phase diagrams of polymers [41–45] and surfactants [46–50]. By joining consecutively particles with springs, one can construct coarse-grained models of the polymers or surfactants. Dilute polymer solutions are modeled by a set of polymer molecules interacting with other dissipative particles. Also, rheological properties [51, 52], solutions confined between walls [53], and polymer melts [54] have been studied. Recently, DPD has also been used to study the behavior of a lipid bilayer [22–24, 55]. In this thesis we further investigate lipid bilayers with DPD ¹.

A DPD particle represents the center of mass of a cluster of atoms. The particles interact via a force consisting of three contributions, all of them pairwise additive. The total force on a particle i consists of a dissipation force \mathbf{F}^D , a random force \mathbf{F}^R , and a conservative force \mathbf{F}^C , and can then be written as the sum of these forces [31, 57]:

$$\mathbf{f}_i = \sum_{i \neq j} (\mathbf{F}_{ij}^D + \mathbf{F}_{ij}^R + \mathbf{F}_{ij}^C) \quad (2.1)$$

The first two forces in equation 2.1 are of the form:

$$\begin{aligned} \mathbf{F}_{ij}^D &= -\eta w^D(r_{ij})(\hat{\mathbf{r}}_{ij} \cdot \mathbf{v}_{ij})\hat{\mathbf{r}}_{ij} \\ \mathbf{F}_{ij}^R &= \sigma w^R(r_{ij})\zeta_{ij}\hat{\mathbf{r}}_{ij} \end{aligned} \quad (2.2)$$

where $\mathbf{r}_{ij} = \mathbf{r}_i - \mathbf{r}_j$ and $\mathbf{v}_{ij} = \mathbf{v}_i - \mathbf{v}_j$, with \mathbf{r}_i and \mathbf{v}_i representing the position and the

¹See ref. [56] for a nice review on DPD and its applications

velocity of particle i , respectively. $\hat{\mathbf{r}}_{ij}$ is the unit vector, η is the friction coefficient, σ the noise amplitude, and ζ_{ij} a random number taken from a uniform distribution, which is independent for each pair of particles. The combined effect of these two forces is a thermostat, which conserves (angular) momentum, and hence gives the correct hydrodynamics at sufficiently long time and length scales.

Español and Warren [35] have shown that the equilibrium distribution of the system is the Gibbs-Boltzmann distribution if the weight functions and coefficients of the drag and the random force satisfy:

$$w^D(\mathbf{r}) = [w^R(\mathbf{r})]^2 \quad (2.3)$$

$$\sigma^2 = 2\eta k_B T \quad (2.4)$$

The weight function $w^R(\mathbf{r})$ is chosen as

$$w^R(\mathbf{r}) = \begin{cases} (1 - r/r_c) & (r < r_c) \\ 0 & (r \geq r_c) \end{cases} \quad (2.5)$$

where r_c is the cut-off radius, which gives the extent of the interaction range. In this case, all forces assume the same functional dependence on the interparticle distance \mathbf{r}_{ij} as the conservative force \mathbf{F}_{ij}^C , which is usually of the form

$$\mathbf{F}_{ij}^C = \begin{cases} a_{ij}(1 - r_{ij}/r_c)\hat{\mathbf{r}}_{ij} & (r_{ij} < r_c) \\ 0 & (r_{ij} \geq r_c) \end{cases} \quad (2.6)$$

where the coefficient $a_{ij} > 0$ is a parameter expressing the maximum repulsion strength.

The equations of motion are integrated with a modified velocity Verlet algorithm [57].

$$\begin{aligned} \mathbf{r}_i(t + \Delta t) &= \mathbf{r}_i(t) + \Delta t \mathbf{v}_i(t) + \frac{1}{2}(\Delta t)^2 \mathbf{f}_i(t) \\ \tilde{\mathbf{v}}_i(t + \Delta t) &= \mathbf{v}_i(t) + \lambda \Delta t \mathbf{f}_i(t) \\ \mathbf{f}_i(t + \Delta t) &= \mathbf{f}_i(\mathbf{r}_i(t + \Delta t), \tilde{\mathbf{v}}_i(t + \Delta t)) \\ \mathbf{v}_i(t + \Delta t) &= \mathbf{v}_i(t) + \frac{1}{2} \Delta t (\mathbf{f}_i(t) + \mathbf{f}_i(t + \Delta t)) \end{aligned} \quad (2.7)$$

in which $\tilde{\mathbf{v}}$ is a prediction for the new velocity \mathbf{v} . The original velocity-Verlet algorithm would be recovered for $\lambda = 0.5$.

Groot and Warren explain in their paper [57] that the temperature can be controlled by three factors, the time step Δt , the noise level σ , and the λ in the Verlet algorithm. We use a density $\rho = 3$, $\sigma = 3$, $\lambda = 0.65$, and $\Delta t = 0.03$.

2.3 Constant surface tension simulations

In most molecular simulations of membranes one uses a fixed number of lipid molecules and a fixed area, combined with periodic boundary conditions. This corresponds to an infinitely large flat membrane. In general such a system has a non-zero surface tension. It is an important question whether this corresponds to the surface tension of a real membrane. If not constrained a membrane will adopt the conformation corresponding to the lowest free energy, *i.e.*, a tensionless state [58]. However, in an atomistic molecular dynamics study of a membrane, Feller and Pastor [59, 60] observed that a tensionless state did not reproduce the experimental value of the area per lipid. Their explanation of this result is that, since the typical fluctuations and out-of-plane variation of a macroscopic membrane do not develop in a small patch of a membrane, a positive surface tension (stretching) must be imposed in order to recover the experimental value of the area per lipid. Recently, Marrink and Mark [14] simulated much larger patches of membranes up to 1800 lipids. Their calculations show that in a stressed membrane the area per lipid depends on the system size, or, for a fixed area, the surface tension decreases if the system size is increased. This is in agreement with the conclusions of Feller and Pastor. On the other hand, it was found that, that for a tensionless membrane the equilibrium area does not depend on the system size and hence that there is no need to impose a surface tension to reproduce the experimental surface area in case of a stress free membrane.

Simulations at constant surface tension have been introduced by Chiu *et al.* [61], and the constant surface tension ensemble (NVT γ) has been considered in literature. The corresponding equation of motion for Molecular Dynamics simulations have been derived by Zhang *et al.* [62]. Here we use a different approach, based on a Monte Carlo (MC) scheme, to simulate a membrane at a given state of tension (of which the tensionless state is a particular case). We use an hybrid simulation scheme that combines DPD to evolve the positions of the particles and MC moves to change the shape of the simulation box [23]. The importance of this method is that it allows us to observe directly transitions in which the area per lipid changes.

Consider a system with a constant number of particles N , a constant temperature T , and a constant volume V , in which an interface of area A is present. If we take a rectangular simulation box, with dimensions L_{\parallel} parallel to the interface (yz -plane), and L_{\perp} perpendicular to the interface (x -axis), so that the system volume is $V = L_{\perp} L_{\parallel}^2$ and the area of the interface $A = L_{\parallel}^2$, we define a transformation of the box size which changes the area and the height but keeps the volume constant. Such a transformation can be written in the form

$$\begin{aligned} L'_{\parallel} &= \chi L_{\parallel} \\ L'_{\perp} &= \frac{1}{\chi^2} L_{\perp} \end{aligned} \quad (2.8)$$

where χ is the parameter of the transformation. We use a set of scaled coordinates $\mathbf{s} \in [0, 1]$, defined as

$$\mathbf{r} = (L_{\parallel} s_x, L_{\parallel} s_y, L_{\perp} s_z) \quad (2.9)$$

By a transformation of the box dimensions with χ , the coordinates of the particles rescale as

$$\mathbf{r}' = \left(\chi L_{\parallel} s_x, \chi L_{\parallel} s_y, \frac{1}{\chi^2} L_{\perp} s_z \right) \quad (2.10)$$

By changing χ , the above expression generates a transformation of coordinates which preserves the total volume of the system, hence no work against the external pressure is performed.

The MC move is accepted with a probability [23].

$$\text{acc}(o \rightarrow n) = \min \left(1, \frac{\exp[-\beta(U_n - \gamma A_n)]}{\exp[-\beta(U_o - \gamma A_o)]} \right) \quad (2.11)$$

where o and n indicate the old and the new configuration, respectively. U denotes the energy, γ the surface tension, A the area of the bilayer and $\beta = 1/k_B T$.

The described scheme can be applied to impose any value of the surface tension; in our simulations we impose $\gamma = 0$ to obtain a tensionless state.

2.4 Inter- and intramolecular interactions

2.4.1 Repulsion parameters a_{ij}

In our model, we distinguish three types of particles: w , h , and t to mimic water, head and tail atoms of a lipid, respectively.

The value of the repulsion parameter for water-like particles is chosen such that the simulated compressibility of DPD water at room temperature corresponds to the experimental value [50,57]. If the bead density of the system is chosen equal to $\rho r_c^3 = 3$, the correct compressibility of water is obtained for $a_{ww} = 25k_B T$. To model the amphiphilic nature of the lipids, the repulsion parameters a_{ij} (eq.2.6) between two beads, which are both hydrophilic (hydrophobic), are smaller than the ones between hydrophilic and hydrophobic beads. The interaction parameters we generally use (shown in table 2.1) are the same used by Groot in ref. 50, with the exception of a_{tt} (tail-tail), which we increased from 15 to 25 to avoid unrealistically high densities in the bilayer hydrophobic core. A more detailed discussion on these parameters is given in chapter 4.

a_{ij}	w	t	h
w	25	80	15
t	80	25	80
h	15	80	35

Table 2.1: Values of the repulsion parameter a_{ij} (see equation 2.6) used in the simulations

2.4.2 Constructing lipids

Lipids are constructed by connecting head and tail beads with springs. Two typical examples of our coarse-grained models are depicted in figure 2.1. In both models the tail(s) can have different lengths. We denote a single-tail lipid by $h_m t_n$, and a double-tail lipid by $h_m (t_n)_2$, where in both cases m is the number of beads in the head and n is the number of beads in the tail(s).

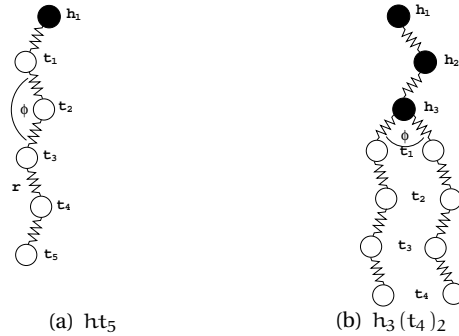


Figure 2.1: Two examples of model lipids with their nomenclature: (a) single tail lipid and (b) double tail lipid. Black particles represent head beads and white particles tail beads.

The spring potential is of the form

$$U_r = \frac{1}{2}k_r(r - r_0)^2 \quad (2.12)$$

The equilibrium distance is set to $r_0 = 0.7$. We determined the spring constant k_r by imposing that in a typical lipid 98% of the bond distance distribution lies within one r_c . The value $k_r = 100$ was found to satisfy this requirement. To control the chain flexibility, an additional bond-bending potential between three consecutive bonds is added:

$$U_\phi = \frac{1}{2}k_\phi(\phi - \phi_0)^2 \quad (2.13)$$

where k_ϕ is the bending constant, ϕ is the angle between two consecutive bonds, and ϕ_0 is the equilibrium angle.

2.4.3 Reduced units

We use reduced units with r_c as the unit of length, the mass m of a particle as the unit of mass, and $a_{ww} = 1$ as the unit of energy. The length scale depends on two factors in our mesoscopic simulation: the particle density ρ and the number of (water) molecules represented by one particle N_m (e.g. the mapping factor). The particle density ρ is the total number of DPD particles N_w divided by the volume V (in units of r_c^3): $\rho = N_w/V$. The particle density and the mapping are used to define the value of r_c . For instance: we have N_w water beads in a volume V , then

$$\rho = N_w/V = 1/v \quad (2.14)$$

where v is the volume in DPD units (r_c^3) of one DPD water particle. Let v' be the volume of one water molecule in \AA^3 ($=30 \text{\AA}^3$), then we have:

$$vr_c^3 = v'N_m \quad (2.15)$$

substituting v by the expression of equation 2.14

$$r_c = \sqrt[3]{v'N_m\rho} \quad (2.16)$$

If we take, for example, $N_m = 3$ and $\rho = 3$ as the level of coarse graining, then $r_c = 6.46 \text{\AA}$ and if we take $N_m = 1$ and $\rho = 3$, then $r_c = 4.48 \text{\AA}$.

From this coarse-graining procedure, the interaction parameters are defined in units of $k_B T$. To use reduced units, we define $k_B T_o = 1$ where T_o is room temperature. The interaction parameters can then be expressed in these reduced units, *i.e.* the a_{ww} parameter has been fitted to give the correct compressibility of water at room temperature and at the assumed density. In principle, we could use the same procedure to match the compressibility of water at different temperatures. This gives, however, a temperature dependent a parameter which would make the interpretation of our results more complex. Therefore we have chosen to keep the parameters fixed and only change the temperature. In the following we will use the notation T^* to indicate the reduced temperature.

2.5 Testing the MC-DPD scheme

In this work, all simulations are performed at the condition of zero surface tension using the described hybrid MC-DPD scheme. A typical simulation required 100,000 cycles of which 20,000 cycles were needed for equilibration. Per cycle it is chosen whether 50 DPD time steps are performed or an attempt to change the area of the box was made. We have optimized the relative number of MD and MC moves to

sample as efficiently as possible. On average in 70% of the cycles DPD time steps are performed. The equilibration is finished when the area of the bilayer fluctuates around the equilibrium value. Explicit calculation of the surface tension confirmed that indeed a state of zero surface tension was simulated. The volume of the system remained constant during all simulations. This implies that as the temperature is changed the total pressure also (slightly) changes; the pressure ranges from 20.9 to 21.8 in the temperature range applied.

As described in the introduction, the structure of an aggregate of lipids depends, among others, on the chemical structure of the lipid (see section 1.2). We start our simulation by performing an NVT simulation on randomly distributed lipids in water, meaning that the area of the yz -plane of the simulation box is fixed. Dependent on the number of lipids in the system and the lipid structure different structures are formed (see figure 2.2. In this figure we plotted different final configurations of simulations performed on a system of 200 lipids and 4000 water particles at $T^* = 1.0$. If a lipid bilayer is formed, the surface tension of the bilayer is not equal to zero. To obtain the tensionless state, we continue the simulation by using the combined MC-DPD scheme. In almost all simulations, the bilayer stays the stable phase. However, sometimes we find that by applying the zero surface tension scheme, the bilayer falls apart and a different structure is obtained.



Figure 2.2: The final configuration of the lipid self assembly on a system with 200 lipids and 4000 water particles at $T^* = 1.0$. Depending on the lipid structure different phases are obtained: phase separation with inverted micelles (left), cylindrical micelle (middle), and bilayer (right). The black spheres represent the hydrophilic head group and the grey lines the hydrophobic tails. The water particles are not shown.

In the simulations described in this thesis, we often change the head-head repulsion parameter to study the influence of the head group interactions. In principle, it is then possible that other phases than a bilayer are obtained. However, we see that only changing the head-head repulsion parameter is not sufficient to obtain structures like (inverted) micelles and that, in the time scales studied, the bilayer is the stable phase. To ensure that our simulations were sufficiently long to observe the stable phase, we repeated some simulations starting from a random distribution of

lipids. These simulations all reproduced bilayer phases.

To test finite-size effects, we performed a series of simulations of bilayers of different sizes (200, 800 and 1800 lipids). In figure 2.3 the area per lipid as function of the number of MC cycles is plotted for these different systems. After a period of equilibration, all the bilayers converge to the same value of the area per molecule. Our results are in agreement with those of Marrink and Mark [14], *i.e.*, the area per lipid in a tensionless bilayer is almost independently of the system size.

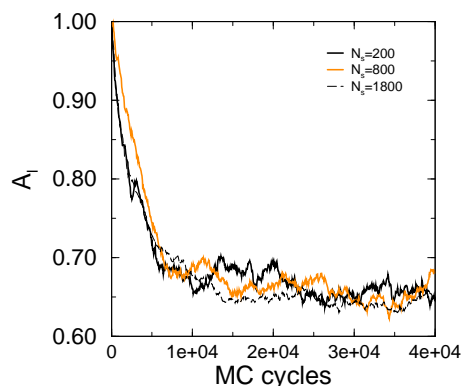


Figure 2.3: Instantaneous area per lipid A_l , as function of the number of MC cycles, for bilayers of different sizes. The lines correspond to bilayers of 200, 800, and 1800 lipids.

2.6 Structural quantities of a lipid bilayer

Lipid bilayers are experimentally described using structural properties, which are defined in figure 2.4. In this section we describe how these quantities are obtained from our simulation results.

Area per molecule and bilayer thickness

A central quantity is the area per lipid molecule, which is experimentally determined by diffraction and NMR studies. The area per lipid is directly related to the bilayer thickness by $D_B = 2V_L/A$, where V_L is the volume of a lipid in the bilayer obtained by volumetric measurements [63]. The values of the area per lipid of DPPC in the fluid phase L_α vary from 56 \AA^2 to 72 \AA^2 [64], with $62\text{-}63 \text{ \AA}^2$ as the most commonly used value, indicating that this quantity has a large uncertainty.

In simulations it is easy to obtain the area per molecule, bilayer thickness, and hydrophobic thickness independently. The bilayer is formed in the yz -plane of the simulation box and thus x is normal to the bilayer. To compute the area per lipid A_l

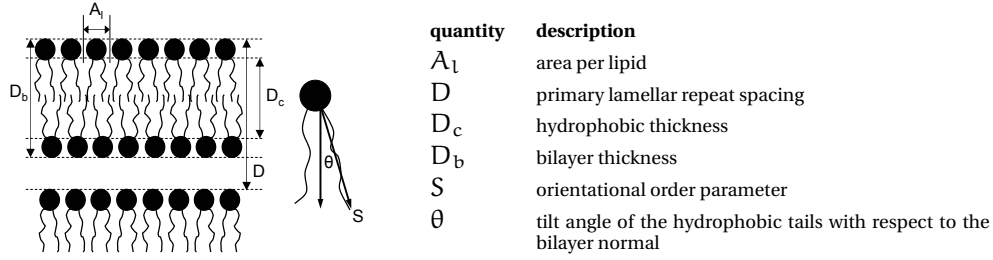


Figure 2.4: Graphical representation of some structural bilayer quantities. In our simulations the primary lamellar repeat spacing is not calculated, because we only study a single bilayer in water. The reason to mention this quantity is that in many experimental studies, results are explained in terms of this spacing.

we simply divide the total area in the yz -plane (after equilibration, at a state of zero surface tension) by half the number of lipids in the bilayer, since, on average, the number of molecules in each side of the bilayer is equal.

The bilayer thickness is computed as the average distance between the head groups of two opposing lipids. D_c is the thickness of the hydrophobic core, computed as the average distance along the bilayer normal between the first bead (or beads in case of double tail lipids) in the tail(s) of the lipids in one layer and the ones in the opposite layer:

$$D_c = \left| \langle x_{t_1}^{(1)} \rangle - \langle x_{t_1}^{(2)} \rangle \right| \quad (2.17)$$

where $\langle x_{t_1}^{(i)} \rangle$ is the average z position of the first tail bead(s) of the lipids in monolayer i . In case of the bilayer thickness D_b the thickness of the head-group region is also included.

Orientational order parameters and tilt angle

Another quantity used in determining the structure of lipid bilayers is the orientational order parameter. The order parameter can be directly measured by deuterium substitution NMR spectroscopy, and is given by

$$S = \frac{1}{2} \langle 3 \cos^2 \theta - 1 \rangle \quad (2.18)$$

where θ is the angle between the orientation of the vector along a given C-H bond and the bilayer normal.

In our mesoscopic model, however, the hydrogen atoms are not present, hence we must use a different definition. The mathematical expression is the same as in equation 2.18, but the tilt angle θ is now defined as the angle between the orientation

of the vector along two beads in the chain and the bilayer normal:

$$\cos \theta = \frac{\mathbf{r}_{ij} \cdot \hat{\mathbf{n}}}{r_{ij}} = \frac{x_{ij}}{r_{ij}} \quad (2.19)$$

where $\hat{\mathbf{n}}$ is a unit vector normal to the bilayer and $\mathbf{r}_{ij} = \mathbf{r}_i - \mathbf{r}_j$ is the vector between beads i and j ($r_{ij} = |\mathbf{r}_{ij}|$). The order parameter has value 1 if this vector is on average parallel to the bilayer normal, 0 if the orientation is random, and -0.5 if the bond is on average parallel to the bilayer plane.

With this definition of the angle θ , we can compute the order parameter for a vector between any two beads in the lipid. We are interested in characterizing the overall order of the chains and the local order. For the first quantity we define the indexes of the vector \mathbf{r}_{ij} in equation 2.19 as: $i = t_N$ and $j = t_1$, where t_N is the last bead in the lipid tail and t_1 is the first one. We call S_{tail} the corresponding order parameter. For the local order we define $i = t_{n+1}$ and $j = t_n$ with the index n increasing going toward the tail end, and call the corresponding order parameter S_n . If n is taken progressively from the head group to the tail end of the molecule, a plot of the corresponding order parameters, S_n , gives an indication of the persistence of order through the bilayer core.

Chain overlap and interdigitation

To further characterize the bilayer structure and to investigate the presence of an interdigitated phase, we characterize the extent of interpenetration of the hydrophobic tails of the lipids on opposite sides of the bilayer, by defining the chain overlap D_{overlap} , as

$$D_{\text{overlap}} = \frac{2L_x - D_c}{L_x}. \quad (2.20)$$

L_x is the average chain length in the direction normal to the bilayer, *i.e.* the average distance projected on the bilayer normal (x -axis) between the first bead in the tail t_1 and the last one t_N :

$$L_x = \left| \langle x_{t_1} \rangle - \langle x_{t_N} \rangle \right|. \quad (2.21)$$

D_c is the hydrophobic thickness as defined in equation 2.17.

In the next chapters we will see that at high temperatures the chain overlap is mainly due to the disorder of the molecules, while at low temperatures the chain overlap can be seen as an effective interdigitation of the chains.

III

Phase behavior of monotail lipids

Abstract

In this chapter we study the phase behavior of the simplest mesoscopic model of a phospholipid, that consists of a hydrophilic head group and one hydrophobic tail. With this mesoscopic lipid-water model we observe the formation of the liquid crystalline phase (L_α) and gel phases in which the tails are interdigitated ($L_{\beta I}$) or non-interdigitated (L_β). For double-tail lipids experiments show all three phases, while for single-tail lipids only L_β and L_α are observed. We show that at sufficiently high head-head repulsion the $L_{\beta I}$ phase is stable for single-tail lipids. This suggests that it might be possible to induce an $L_\beta \rightarrow L_{\beta I}$ transition by adding chaotropic salts.

3.1 Introduction

In the previous chapter, we discussed the technique to study the self-assembly and the phase behavior of lipid bilayers. An important question in the development of a mesoscopic model is how much chemical detail should be included in the model. Often, a model consisting of a hydrophilic head group and a single hydrophobic tail is used as a model of a phospholipid. In this chapter, we investigate if such a model correctly describes the (phase) behavior of double tail phospholipids. A second goal of this chapter is to compare the results of our simulations with experiments that are performed on monotail lipids.

The phase behavior of different PC's has been determined experimentally (see [9] for a review). All PC's have a low temperature $L_{\beta'}$ phase (see figure 3.1). In this phase the bilayer is a gel: the chains of the phospholipids are ordered and show a tilt relative to the bilayer normal. At higher temperature the L_{α} phase is the stable phase. This phase is the liquid crystalline state of the bilayer in which the chains are disordered and tail overlap due to this thermal disorder is possible. This phase is physiologically the most relevant [63].

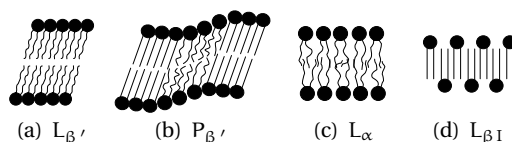


Figure 3.1: Schematical drawings of the various bilayer phases. The characteristics of these phases are explained in the text. The filled circles represent the hydrophilic head group of a phospholipid and the lines represent the hydrophobic tails.

Under normal conditions the two monolayers of a bilayer contact each other at the terminal methyl group of their hydrophobic chains, while their hydrophilic head groups are in contact with water. However, it is known experimentally that at low temperatures an interdigitated state, in which the terminal methyl groups of one monolayer interpenetrate the opposing layer, is also possible. This $L_{\beta I}$ phase does not spontaneously form in bilayers of symmetrical chain phospholipids, but has to be induced by changes in the environment or in the molecular structure (see chapter 6 for more details). Interdigitation reduces the bilayer thickness, and this can, for example, affect the diffusion of ions across the bilayer or influence the activity of membrane proteins. It has been proposed [65, 66] that specific interactions are not important in the formation of an interdigitated phase, and that the main driving force that induces interdigitation is an increase in the head group surface area, which results in the creation of voids between the molecules. Since voids in the bilayer core are energetically unfavorable, they are filled up by molecules of the opposite mono-

layer.

This mechanism suggests that the formation of an interdigitated phase should be a general phenomenon. This would imply that an interdigitated phase could also be induced in bilayers of, for example, single-tail lipids. The fact that for single-tail lipids the interdigitated phase has not been observed experimentally, is one of the motivations to investigate the molecular aspects underlying the formation of an interdigitated phase in more detail.

Our simulations correctly describe the hydrophobic tail length dependence of this transition and the effect of adding salt. In addition, the simulations predict that both the interdigitated and non-interdigitated phases can be formed in systems with single-tail lipids.

3.2 Computational details

In this investigation we consider lipids with one head segment connected to a single tail with variable length (see figure 3.2). Two consecutive beads are connected by harmonic springs with spring constant $k_r = 100.0$ and $r_0 = 0.7$. A harmonic bond bending potential between three consecutive beads is added with a bending constant $k_\phi = 10$ and an equilibrium angle $\phi_0 = 180^\circ$.

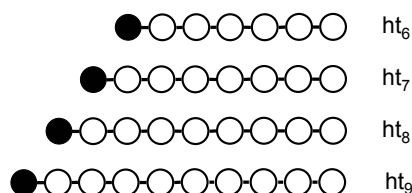


Figure 3.2: Models used in this study with their nomenclature. The black particles represent the head beads and the white particles the tail beads.

The repulsion parameters used are $a_{ww} = a_{tt} = 25$, $a_{wh} = 15$, and $a_{wt} = 80$ (see equation 2.6, chapter 2). In addition, we vary the head-head interaction parameter (a_{hh}) to study the effect of changing the interactions between the hydrophilic segments of a lipid. In a real system the head-head interactions can be changed by, for example, adding salt to the system.

All our simulations are performed on a tensionless bilayer of 200 lipids. The total number of particles was 3500. The overall density of the system is $\rho = 3$. We initialize our system by distributing lipids randomly in water and we observe the self-assembly of a bilayer using DPD simulation only. After the bilayer is formed, we perform, in ad-

dition to the DPD moves, Monte Carlo moves in which we change the area as well. A typical simulation required 100,000 cycles of which 20,000 cycles were needed for equilibration. All the results are expressed in the usual reduced units, *i.e.* using r_c as the unit of length and repulsion parameter $\alpha = 1$ as unit of the energy.

3.3 Results and Discussion

In this section we first describe in detail the different phases of a bilayer formed by single tail lipids consisting of one head bead and nine tail beads (ht_9), which we study at different reduced temperatures, from $T^* = 0.8$ to $T^* = 1.5$. At a fixed head-head repulsion of $\alpha_{hh} = 35$ an interdigitated gel phase is formed at low temperatures, while at $\alpha_{hh} = 15$ the non-interdigitated L_β phase is formed. We then investigate the influence of changing the interactions between the head groups and we show that we obtain the non-interdigitated L_β phase or the interdigitated $L_{\beta I}$ phase dependent on the head-head repulsion parameter (see figure 3.3). Finally, we investigate the influence of tail length and we compare our results with experimental data on single-tail lipids.

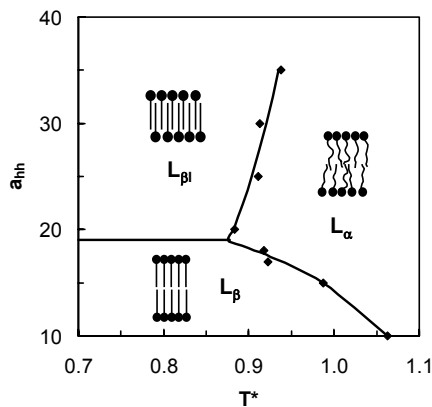


Figure 3.3: Computed phase diagram of the lipid ht_9 as function of head-head repulsion parameter α_{hh} and reduced temperature T^* . At high values of the head-head repulsion parameters the interdigitated phase $L_{\beta I}$ phase is formed, while at low values the non-interdigitated L_β phase is formed. Increasing temperature causes the melting of the bilayer to the L_α phase.

3.3.1 The lipid ht_9

Head-head repulsion $a_{hh} = 35$

In figure 3.4 the average area per lipid A_l and the bilayer thickness, D_{hb} , are plotted as function of temperature. The error bars have been calculated with the block averages method [32, 67]. In all the other plots of the area per lipid or bilayer thickness, we will not include error bars, which, however, have been estimated as $\leq 5\%$.

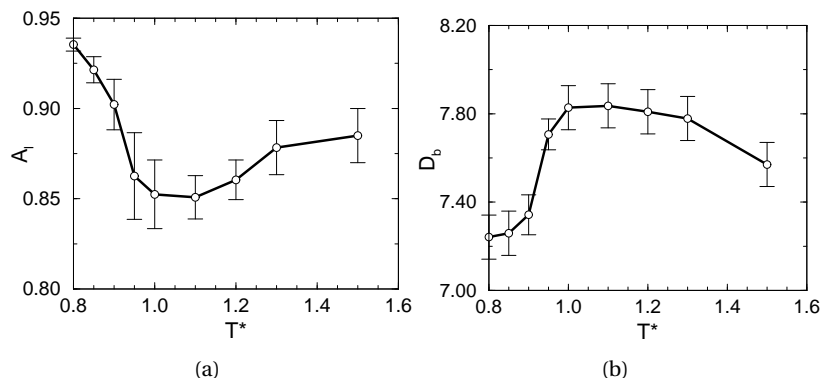


Figure 3.4: Area per lipid A_l and (b) bilayer thickness D_b as function of reduced temperature T^* for lipid type ht_9 .

In both figures 3.4(a) and 3.4(b) we can distinguish two regions: at low temperatures, the area per lipid decreases with increasing temperature and the thickness is increasing, while at high temperatures the area is increasing with increasing temperature, and the thickness is decreasing. At the lowest temperature studied ($T^* = 0.8$) the area is larger than the area at the highest temperature studied ($T^* = 1.5$) while the thickness at $T^* = 0.8$ is smaller than the thickness at $T^* = 1.5$. This different temperature dependence of A_l and D_b suggests that the bilayer undergoes a phase transition. Before discussing this transition in detail we will first characterize the low and the high temperature phases.

To characterize the ordering of the lipids in the bilayer we use the order parameters S_{tail} and S_n . In figure 3.5 the values of both S_{tail} and S_n are plotted as a function of temperature. The high values of S_n at temperatures below $T^* = 0.95$ indicate that the bonds are ordered along the bilayer normal. This order persists even for bonds far from the head-group region, decreasing slightly with increasing temperature. Above $T^* = 0.95$ the values of S_n further decrease with increasing temperature, and the order along the chain is lost.

The overall order of the tails (S_{tail}) shows a similar behavior (figure 3.5(b)). Also here we can distinguish two regions: below $T^* = 0.95$ where S_{tail} has values higher than 0.5 indicating that the chains are ordered along the bilayer normal, and above

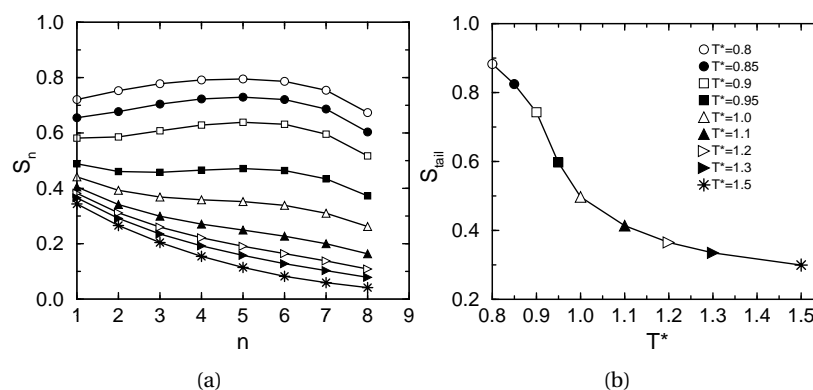


Figure 3.5: (a) Local order parameter S_n and (b) tail order parameter S_{tail} , as function of reduced temperature T^* .

$T^* = 0.95$ where the values of S_{tail} decrease below 0.5, showing an increase in the disorder of the chains.

To further characterize the structure of the bilayer in the low and high temperature regions, we compare in figure 3.6 the in-plane radial distribution function $g(r)$ of the head beads of the lipids at one interface, for two different temperatures: $T^* = 0.8$ and $T^* = 1.5$. At $T^* = 0.8$, the radial distribution function shows more pronounced peaks compared to the $g(r)$ at $T^* = 1.5$, which corresponds to a more structured organization of the lipids head groups in the bilayer plane. The structure in the radial distribution function and the high values of the order parameters for low temperatures, suggest that the low temperature phase is the ordered gel phase, while at high temperatures the bilayer is in the disordered liquid crystalline phase.

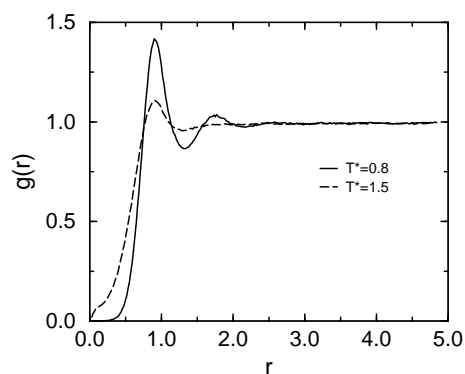


Figure 3.6: Two dimensional radial distribution function $g(r)$ in the bilayer plane for the head groups at $T^* = 0.8$ and $T^* = 1.5$.

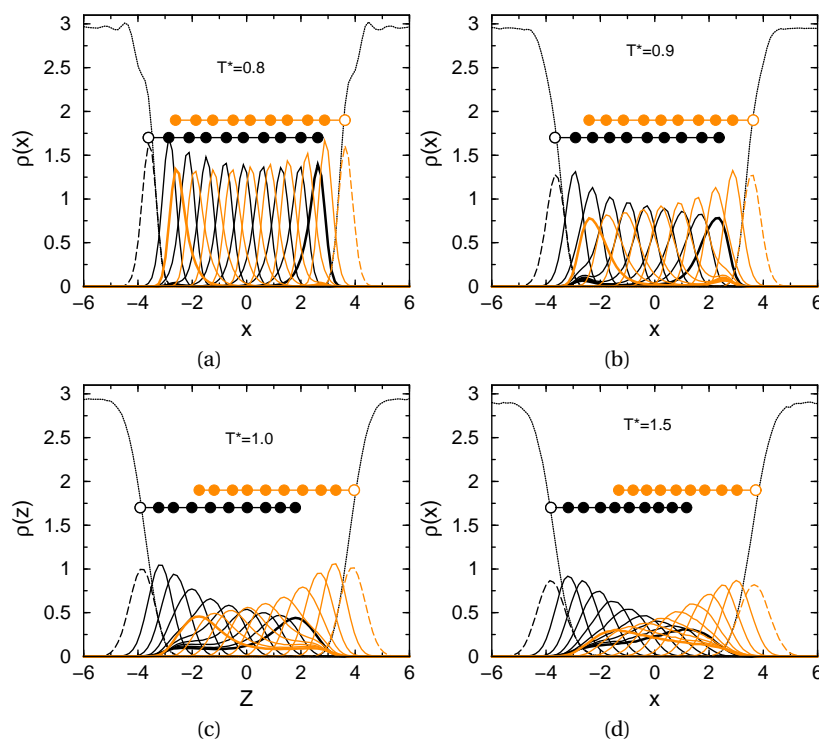


Figure 3.7: Density profiles $\rho(z)$ along the bilayer normal z for different reduced temperatures T^* . Each line is the density profile for a different bead: full lines are the densities of the tail beads, dashed lines are the densities of the head beads, and the thin solid line is the density of water. The black lines correspond to the lipids in one monolayer, while the grey lines correspond to the lipids in the opposite monolayer. The big dots correspond to the maxima in the bead density distributions and illustrate the position of the beads in the bilayer. The full circles correspond to tail beads and the open circles to head beads.

In figure 3.7 we show the density profiles in the direction normal to the bilayer for the system components at different reduced temperatures. Figures 3.7(a) and 3.7(b) correspond to a bilayer in the gel phase, while 3.7(c) and 3.7(d) correspond to a bilayer in the liquid crystalline phase. It is clearly visible that, in the low temperature region, the two monolayers are interdigitated. At $T^* = 0.8$ the overlap extends up to the 8th bead in the tail and the peaks of the density profiles for the lipids tail beads in one monolayer (black full lines) are exactly alternating with the peaks of the opposite monolayer (red full lines), showing an optimal packing of the tails. This structure resembles the experimentally observed interdigitated phase $L_{\beta I}$.

We can now explain the temperature dependence of the area per lipid (figure 3.4). The low temperature phase is the interdigitated gel $L_{\beta I}$. In this phase the ordering

of the chains is the dominating effect. The lipids stretch out in the direction normal to the bilayer, inducing interdigitation. This packing results in a larger average distance between the lipids head groups in each monolayer and in a larger area. In this region an increase of temperature reduces the values of the order parameter (figure 3.5(b)), but along the chain the order persists (figure 3.5(a)). Thus interdigitation is still present, but is decreasing in depth, resulting in an increase of the bilayer thickness and a decrease of the area per lipid. Above the transition temperature, the chains loose the persisting order and are not interdigitated. Only the terminal tail beads overlap, due to thermal disorder. In this temperature region an increase in temperature increases the effective volume occupied by the molecules, but the extent of tail overlap does not depend significantly of temperature. As a result the area per molecule increases while the bilayer thickness decreases.

Head-head repulsion $a_{hh} = 15$

In the previous section we have seen that single tail lipids spontaneously form an interdigitated phase at low temperatures, while the most common organization of (symmetric) phospholipids in membranes is a bilayer formed by two separate monolayers [68]. It is therefore interesting to investigate whether we can adapt the single tail model to reproduce the phase behavior of real membranes, and in particular if we are able to obtain a non-interdigitated gel phase. If the main cause of interdigitation is an increase in the head-groups surface area [65, 66], we can test this mechanism by changing the value of the head-group repulsion parameter, a_{hh} , in our model. Taking as initial condition the interdigitated bilayer at $T^* = 0.85$, we decrease the head-group repulsion parameter from $a_{hh} = 35$ to $a_{hh} = 15$, the latter being the same repulsion parameter as between an hydrophilic bead and a water-bead. Experimentally, changing the head-head interactions corresponds to, for example, adding salt to the system. It is important to recall that, with the zero surface tension scheme, the system can evolve to the optimum area per lipid even if the bilayer undergoes structural rearrangements.

Figure 3.8(a) shows the temperature dependence of the area per lipid for the repulsion parameters $a_{hh} = 35$ and $a_{hh} = 15$. We observe that the behavior in temperature of the area per lipid for the two values of a_{hh} is very different. At low temperatures the area at $a_{hh} = 35$ is almost twice the value of the area at $a_{hh} = 15$. The decrease of the head-group surface area is also shown in figure 3.8(b), where we compare the radial distribution functions of the head groups in the bilayer plane at $T^* = 0.85$ (see also figure 3.9 for snapshots of the two systems). The peaks in the radial distribution function for the system with $a_{hh} = 15$ (solid line) are shifted to the left compared to the system with $a_{hh} = 35$ (dashed line), showing a decrease of the distance between the head groups. This is a strong indication that at low temperature, with the lower repulsion parameter, the bilayer is in the L_β phase.

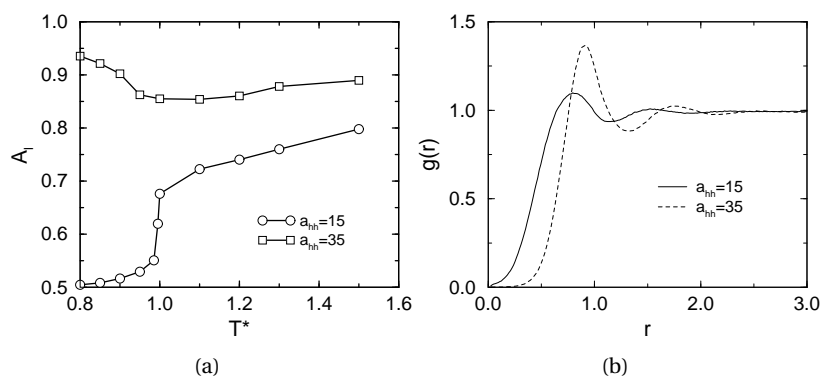


Figure 3.8: Comparison of (a) the area per lipid A_l as function of reduced temperature T^* , and (b) two dimension radial distribution function $g(r)$ in the plane of the bilayer at $T^* = 0.85$, for two different repulsion parameters between the lipid head groups: $a_{hh} = 15$ (circles, solid line) and $a_{hh} = 35$ (squares, dashed line).

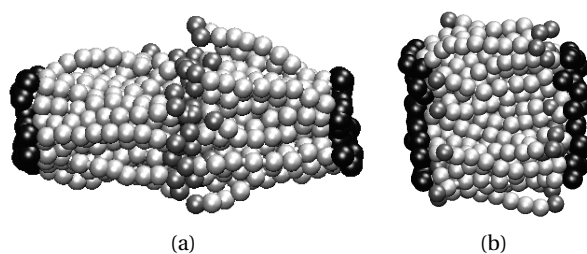


Figure 3.9: Snapshots of the simulations of a bilayer consisting of the lipid ht_9 at $T^* = 0.85$. (a) The non-interdigitated gel phase L_β at $a_{hh} = 15$ and (b) the interdigitated gel phase L_β at $a_{hh} = 35$. Black represents the hydrophilic head group and grey represents the hydrophobic tails.

To further characterize the bilayer structure for $a_{hh} = 15$, we study the order parameters S_n and S_{tail} , which are plotted in figure 3.10. At temperatures $T^* \leq 0.95$ the chains are locally ordered (values of S_n above 0.5), and the order does not decrease significantly going through the hydrophobic core. Also the overall order of the chains S_{tail} is high in this temperature region. Above $T^* = 0.95$ we observe a decrease in both the order parameters. The chains become disordered and the persistence of order along the chain is lost. This trend is analogous to the one observed for $a_{hh} = 35$. In both cases the low temperature region is characterized by the ordering of the chains, while at high temperatures the chains are disordered. However, while for $a_{hh} = 35$ the two monolayers are interdigitated in the ordered phase, for $a_{hh} = 15$ the ordered phase is a bilayer formed by two separated leaflets. This can clearly be seen from the density profiles, which we plot as function of reduced temperature in figure 3.11. This figure shows that the melting of the bilayer results in a broader shape of the den-

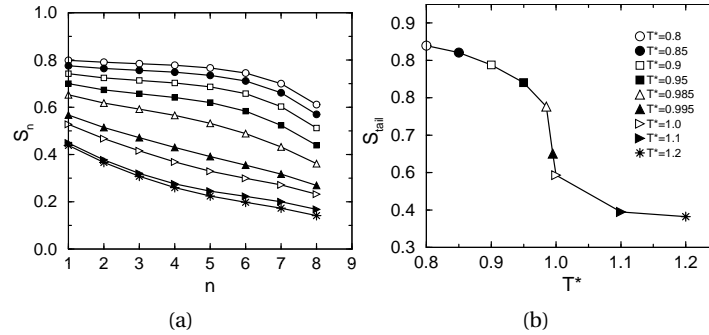


Figure 3.10: (a) Local order parameter S_n and (b) tail order parameter S_{tail} , as function of reduced temperature T^* for a bilayer formed by lipids with $a_{hh} = 15$.

sity profiles. The increase of disorder in the chains (see figure 3.10) results in a partial overlap of the two monolayers. This transition upon heating is also reflected in the trend of the area per lipid with temperature (figure 3.8(a)), which shows a sharp increase between $T^* = 0.95$ and $T^* = 1.0$. We can then conclude that a transition from an ordered to a disordered phase takes place at a temperature $0.95 < T_m < 1.0$.

We have shown that the bilayer structure in the low temperature region depends on the repulsion between the lipid head groups. By tuning this parameter, we can obtain both the gel phase L_β and the interdigitated gel phase $L_{\beta I}$. Experimentally, both in the liquid crystalline phase [69] and in the gel phase [70], a monotonic increase of the area per lipid is observed when the temperature is increased. This is caused by an increase in the disorder of the tails [69]. For the low repulsion parameter of $a_{hh} = 15$ we reproduce the experimental observed trends. It is worth mentioning that, in most cases, in the gel phase the phospholipid chains are tilted with respect to the bilayer normal [9]. While for single tail lipids we do not observe any tilt, we will see in the next chapter that the double tail lipids are tilted in the gel phase ($L_{\beta'}$ phase).

Phase behavior as a function of head-head repulsion

It is now interesting to do a more systematic study of these phase transitions for a range of repulsion parameters. The phase transitions we consider are:

1. transition from interdigitated gel to gel ($L_{\beta I} \rightarrow L_\beta$)
2. transition from interdigitated gel to liquid crystalline ($L_{\beta I} \rightarrow L_\alpha$)
3. transition from gel to liquid crystalline ($L_\beta \rightarrow L_\alpha$).

As we have shown, the first transition is induced by a decrease in the repulsion parameter a_{hh} , while the latter ones are temperature dependent.

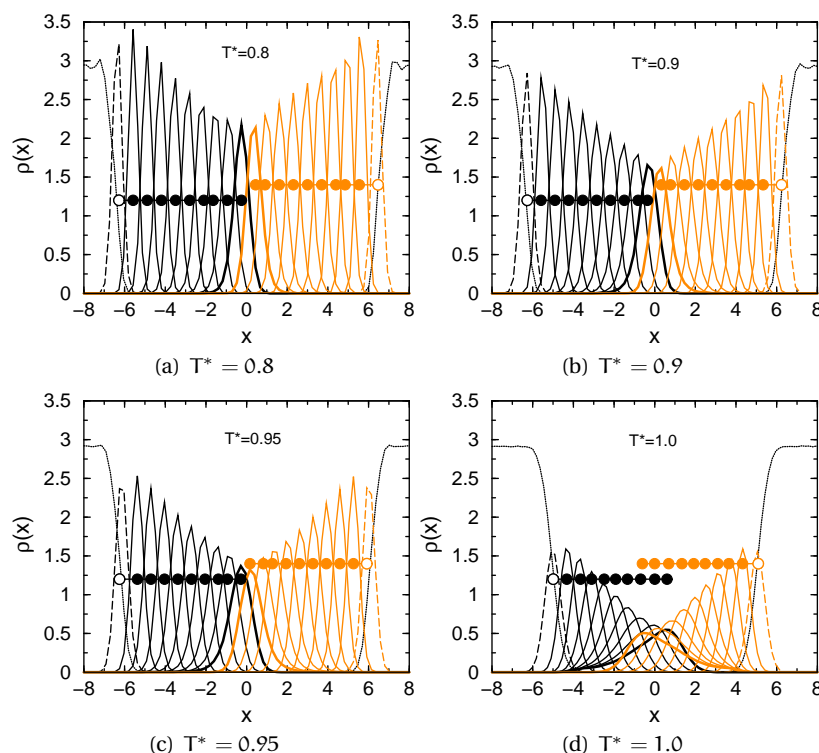


Figure 3.11: Density profiles as function of temperature for a bilayer formed by lipids with $a_{hh} = 15$ (see also the caption to figure 3.7)

We use three quantities to distinguish among the different phases: the area per lipid A_l , the extent of tail overlap D_{overlap} , and the ordering of the tails S_{tail} . By studying the behavior of these quantities as function of temperature and head-head repulsion parameter we can determine the phase diagram of ht_9 as shown in figure 3.3.

In figure 3.12 we plot the area per lipid A_l , the extent of tail overlap D_{overlap} , and the chain order parameter S_{tail} as function of temperature and head-head repulsion parameter. For repulsion parameters $a_{hh} \leq 18$, the low temperature phase is the bilayer gel L_β phase, while for repulsion parameters $a_{hh} > 18$, the low temperature phase is the interdigitated gel $L_{\beta I}$.

By increasing temperature all bilayers melt from an ordered into a disordered phase. For bilayers in the L_β phase, the area per molecule and chain overlap increase upon melting, while for bilayers in the $L_{\beta I}$ phase the area per molecule and chain overlap decrease.

The curves in figure 3.12(c) show that the transition from an ordered phase to a disordered one is very gradual. Much larger systems might be required to observe

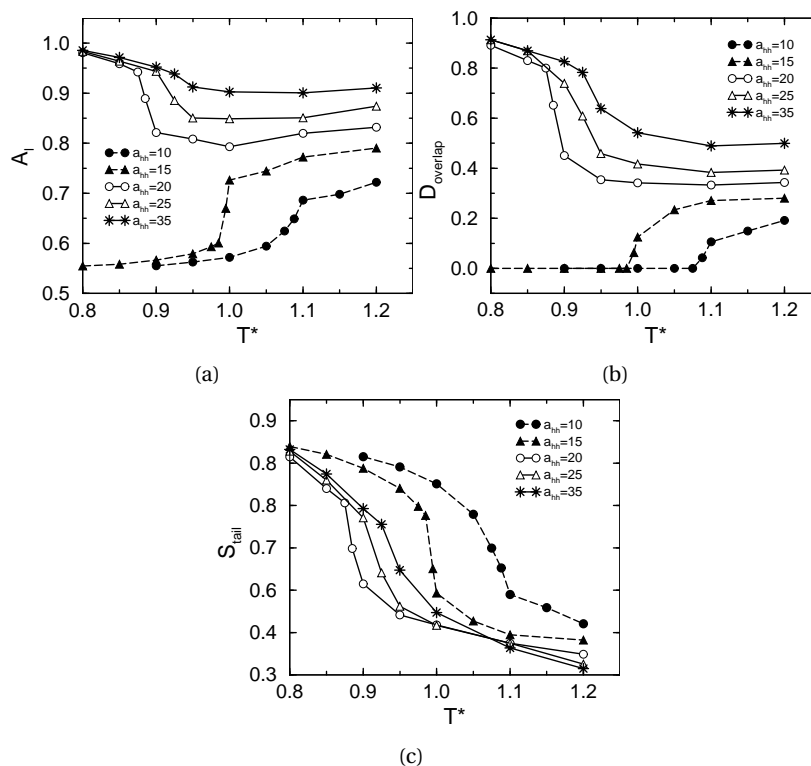


Figure 3.12: (a) Area per lipid A_l , (b) extent of chain overlap D_{overlap} , and (c) tail order parameter S_{tail} as function of reduced temperature T^* for different repulsion parameters $a_{h,h}$. Dashed curves show a transition from the L_β to the L_α phase, solid curves show the transition from the $L_{\beta I}$ to the L_α phase.

a sharp transition in these quasi two-dimensional systems. This gradual transition makes it difficult to determine the exact location of the phase boundaries and therefore we used the inflection point as our definition of the phase boundary. The temperature at which the chains get disordered is the same as the temperature of the inflection point in A_l and D_{overlap} . We define as the main transition temperature T_m the value of temperature at the inflection point of the shown curves. T_m is higher for bilayers in the L_β phase than for bilayers in the $L_{\beta I}$ phase. This is in agreement with experimental results [65].

3.3.2 Phase behavior as a function of tail length

Besides investigating the effect of changing the head-head repulsion parameter, it is also interesting to vary the tail length of the lipid. A similar analysis, as was presented for the lipid ht_9 , has been carried out for lipid types ht_6 , ht_7 , and ht_8 (see figure 3.13).

Depending on the repulsion parameter we obtain two gel phases $L_{\beta I}$ and L_{β} for all tail lengths. For high head-head repulsion the system can gain energy by adding water particles in between the heads. As a result the distance between the head groups increases and the interdigitated phase is stabilized. For low values of a_{hh} the head groups expel water and the stable phase is the non-interdigitated phase. In between we find a_{hh}^* for which the transition from $L_{\beta I}$ to L_{β} occurs. The difference between the two phases is that in the $L_{\beta I}$ phase the tail ends are in direct contact with water, whereas in the L_{β} phase the tail ends face each other. Therefore, the critical value a_{hh}^* to induce interdigitation is higher than the value of a_{hw} .

We observe hysteresis if we change a_{hh} at a constant temperature: the bilayer can be both in the L_{β} or in the $L_{\beta I}$ phase, depending on the initial dimension of the area. The range of a_{hh} , in which hysteresis occurs, increases with decreasing temperature (see figure 3.14). This suggests that the transition L_{β} to $L_{\beta I}$ is a first order transition. In the phase diagrams of figure 3.13 we define the phase found during decreasing temperature at a constant head-head repulsion parameter as the stable phase.

As we increase the tail length the gel phases are stabilized and the transition shifts to higher temperatures. The effect of increasing the head-head repulsion on the gel to liquid crystalline transition temperature is much more pronounced for the $L_{\beta} \rightarrow L_{\alpha}$ compared to $L_{\beta I} \rightarrow L_{\alpha}$. This can be understood from the fact that in the interdigitated phase the average distance between the heads is already much larger compared to the non-interdigitated phase, and a further increase in this distance does not have a dramatic effect on the stability of the gel phase.

For lipids ht_8 and ht_9 the $L_{\beta I}$ phase occurs at slightly lower repulsion parameters than for lipids ht_6 and ht_7 . This is consistent with experimental results [66]. Since the interdigitated phase is more closely packed than the non-interdigitated phase, the vanderWaals energy is greater. This energy gain is proportional to the number of carbon atoms in the phospholipid chain and thus interdigitation becomes energetically more favorable for longer chains. Also in our simulations we observe that the interdigitated phase is more compact and hence a_{hh}^* decreases slightly with increasing tail length.

It is interesting to compare these results with the experimental data [71]. Misquitta and Caffrey systematically investigate the phase diagrams of monoacylglycerols, a single-tail lipid, and show a similar tail length dependence for the $L_{\beta} \rightarrow L_{\alpha}$ transition. Interestingly, for a similar model of a double-tail lipid we do not observe the formation of an interdigitated phase (see chapter 5). This corresponds to the experimental observation that for the most common double-tail lipids the interdigitated phase does not form spontaneously, but should be induced by the addition of, for example, alcohol [72] (see chapter 6).

The effect of adding salt on the gel to liquid crystalline transition has been studied

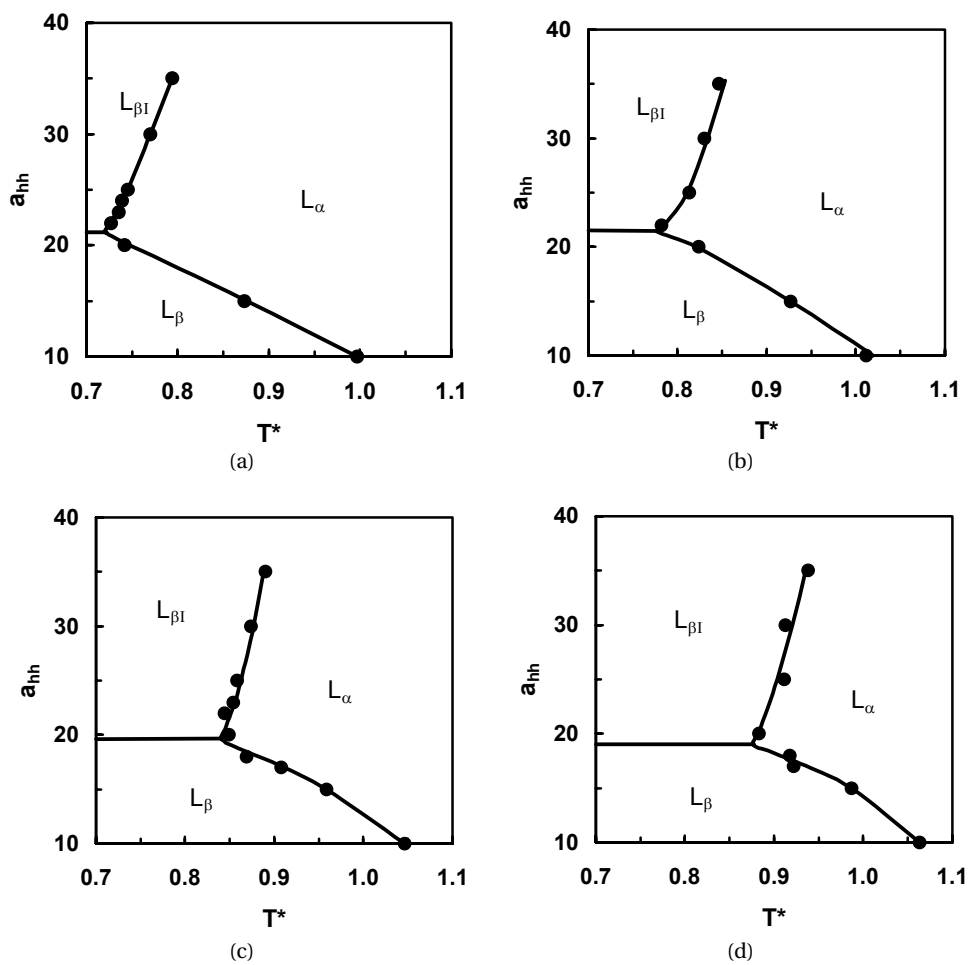


Figure 3.13: Phase diagrams as a function of the head-head repulsion parameter a_{hh} and reduced temperature T^* for lipids of different chain lengths: (a) ht_6 (b) ht_7 (c) ht_8 , and (d) ht_9 .

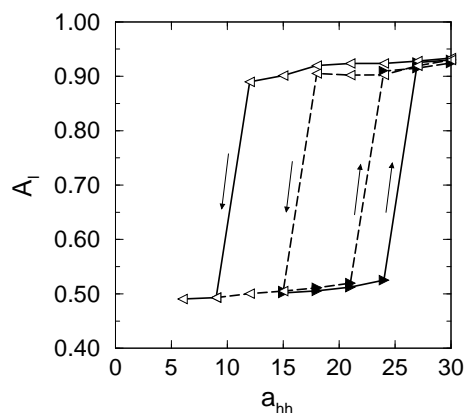


Figure 3.14: Hysteresis curves for the area per lipid, A_l of the lipid type ht_8 , as function of the head-head repulsion parameter a_{hh} at constant temperature $T^* = 0.75$ (solid line) and $T^* = 0.8$ (dashed line). Configurations of both phases L_β (at $a_{hh} = 6$) and $L_{\beta I}$ (at $a_{hh} = 30$) are taken as initial conditions, and a_{hh} is slowly increased or decreased respectively.

for double-tail lipids [73] and recently for single-tail lipids [74]. These studies show that adding so-called kosmotropic salts increases the $L_\beta \rightarrow L_\alpha$ transition temperature, while chaotropic salts decrease this transition temperature. Similar effects have been observed for nonionic single-tail lipids [75]. Takahashi *et al.* [74] explain these observations by assuming that kosmotropes tend to be excluded from the interfacial region and hence reduce the amount of interfacial water, while chaotropic salts have the inverse effects, *i.e.* are adsorbed at the interfacial region and increase the amount of interfacial water. In our model a similar effect can be achieved by changing the head-head interactions; increasing or decreasing a_{hh} corresponds to adding chaotropes or kosmotropes, respectively. Our simulations show that decreasing the head-head repulsion stabilizes the L_β phase, which corresponds to the case that water is excluded from the interface. Adding chaotropic salts has the reverse effect: it increases the head-head repulsion and stabilizes the L_α phase. Our simulations show that at sufficiently high head-head repulsion the interdigitated phase ($L_{\beta I}$) is stable. This suggests that it experimentally might be possible to induce the $L_\beta \rightarrow L_{\beta I}$ phase transition by adding chaotropic salts to the systems.

3.4 Conclusions

In this chapter, we performed simulations on the most simple representation of a phospholipid. The model consists of a single hydrophilic head bead connected to one tail of hydrophobic beads, which can vary in length. Using the area per lipid, the hydrophobic thickness, the order parameter, and the extent of chain overlap, we are

able to characterize various bilayer phases.

The simulations showed that different stable phases are obtained for a wide range of temperatures. We characterized the low temperature phase as a gel phase, and we reproduced the main order/disorder phase transition from a gel to a liquid crystalline phase. This transition temperature to the L_α phase increases with increasing tail length, as was also found experimentally.

In bilayers consisting of single-tail lipids, only the non-interdigitated L_β phase and the fluid L_α phase are observed. However, experiments show that if chaotropic salts are added to the system, the distance between the head groups is increased, stabilizing the L_α phase. We show that at high enough head-head repulsion the L_α phase is indeed stabilized and that the low temperature phase is the interdigitated $L_{\beta I}$ phase. This suggests that it is possible to induce an interdigitated phase in bilayers of monotail lipids by adding chaotropic salts to the system.

From our results, we can conclude that a model consisting of a head bead connected to a single tail does not describe the phase behavior of a double-tail lipid correctly. The single-tail lipids spontaneously form a low temperature interdigitated phase for high enough values of the repulsion parameter between head groups. Experimentally, this phase is observed in bilayers consisting of double-tail lipids, but should be induced by adding salt to the system. By lowering the value of the head-head repulsion the low-temperature phase is the L_β phase. In this phase the tails are ordered parallel to the bilayer normal, while for most common double-tail phospholipids the hydrocarbon tails show a tilt with respect to the bilayer normal (the L_β'). An option to obtain the correct phase behavior is to make the model more complex by adding the detail of, for instance, two hydrophobic tails to a hydrophilic head group.

IV

Coarse graining a phospholipid

Abstract

In this chapter we show how a coarse-grained model of a phospholipid can be developed and we study the parameter sets applied to the formation of a coarse-grained DiMyristoylPhosphatidylCholine (DMPC) bilayer. We refine our model to a model comprising a head group of three hydrophilic beads, to which two hydrophobic tails are connected. From results obtained with Molecular Dynamic simulations on a single lipid in water, a bond-bending potential between three subsequent beads was added. Using a bead volume of 90 \AA^3 , we reproduce the experimental values of the area per lipid and the hydrophobic thickness. There is no linear relation between the repulsion parameter a_{ij} and the level of coarse graining. The key factor in the formation of a lipid bilayer is the difference between the water-water and the water-hydrophobic tail repulsion parameters.

4.1 Introduction

Atomistic Molecular Dynamics (MD) simulations become computationally more accessible because of the increased capacity of computers. However, it is still a problem to bridge the gap between the time and length scales of MD simulations and the experimental observations. Therefore, many researchers have been interested in the question of how to coarse grain a phospholipid [16, 18, 22, 55, 76]. Designing a mesoscopic model of a phospholipid is important since such a model allows us to investigate the phase behavior and the equilibrium properties on longer time and length-scales than can be reached by atomistic simulations. The main advantage of mesoscopic simulations lies in the fact that the CPU time required for a simulation is lowered with 4 to 5 orders of magnitude.

A commonly used model is a coarse-grained MD simulation, where the interactions between the particles are defined by a Lennard-Jones type of potential [16–18]. Another option is to use Dissipative Particle Dynamics (DPD) with a soft repulsive force as the conservative force. The parameters to tune in such a mesoscopic simulation are few and due to the soft potential the main advantage of DPD is the efficiency gained compared to atomistic simulations. The main disadvantage of these soft repulsion potentials is, like any mesoscopic model, the translation of, for example, temperature and the length to real units.

If we compare the different repulsion parameters that are used in the literature [22–24, 43, 47–50], we see large differences and in most cases the intramolecular interactions are simple springs between DPD particles. In this chapter we study which factors are important in a mesoscopic model to reproduce the correct chain-length dependence of the area per lipid of a phospholipid bilayer. In chapter 3 we showed that a model, consisting of one hydrophilic head group bead and a single tail of hydrophobic beads, does not reproduce the correct phase behavior of a double tail lipid bilayer and thus we refine the model in this chapter. We investigate the influence of the level of coarse graining, *i.e.* how many atoms are represented by a single DPD bead, and the choice of repulsion parameters. We compare two models that differ in the number of water molecules representing a single DPD particle and, additionally, we apply different sets of parameters. We develop our model by using all-atom MD simulations on a single lipid in water to obtain the missing intramolecular parameters of our mesoscopic model.

In this study we will focus on the formation of a bilayer of DiMyristoylPhosphatidylCholine (DMPC) in the fluid or L_α phase and we will compare some structural properties of these bilayers with experiments and with MD simulations. In section 4.2 we describe the details of the MD simulations. In section 4.3 we discuss various models and parameter sets used by other groups applying DPD on amphiphilic

systems and we present our models. In section 4.4 we show the density profiles computed with DPD simulations and we compare these with the profiles obtained with MD simulations and with experimental values.

4.2 Computational details

Molecular Dynamics (MD) simulations on an all-atom model of lipids and water were carried out to develop and test our mesoscopic model. For the development we used a single lipid in water and for the test a full bilayer. These MD simulations were carried out using the DLPOLY package [77]. An all-atom model was employed to describe the interactions between atoms using the potential energy parameter set PARM27 from the CHARMM package [78]. The TIP3P water model [79] was used in all simulations. Bonds involving hydrogen were held fixed with the SHAKE algorithm [80]. Electrostatic interactions were computed using the Smooth Particle Mesh Ewald method [81]. Our simulations were performed in the NVT ensemble [82], *i.e.* with constant temperature, volume, and number of particles. The equations of motion were solved using the Verlet Leapfrog integration algorithm [83] and simulations were run with periodic boundary conditions in all directions. All the simulations were performed using a cutoff radius of 12 Å for the vanderWaals terms.

To simulate a single lipid in water, a lipid was equilibrated in vacuum. After this short equilibration, we added water to the system and let the system equilibrate, using the NPT ensemble. After this equilibration, we collected 20 independent starting configurations. For each configuration we performed NVT simulations at 300 K for 1 ns, with time step $\Delta t = 0.002$ ps, to obtain good statistics.

To simulate a lipid bilayer, we performed the following procedure. Initially, a single lipid molecule stretched along its longer axis was pre-equilibrated in vacuum. We built a complete membrane by placing the lipids on a 6×6 grid with hydrophilic head groups forming the outer side of the membrane and the aliphatic chains the inner side. The size of the grid is set such to get an area per lipid equal to the experimental value of 63 \AA^2 . The second layer of the membrane has been built by mirroring twice the initial lipid layer with respect to both the mid plane of the membrane and a perpendicular plane to conserve the chirality of the molecule. The dry membrane was equilibrated during a few hundred time steps. Subsequently, the box was filled by adding water molecules. The resulting simulation box of dimension $47.6 \times 47.6 \times L_z$, with $L_z \approx 65 \text{ \AA}$, contained 2×36 lipid molecules, and more than 2,000 molecules of water, in total approximately 15,000 atoms. The complete system was equilibrated for 100,000 steps, with a timestep of 2 fs at a temperature of 317.5 K. During equilibration, a density profile and energy convergence of the system have been monitored. The resulting density profile is in very good agreement with the profiles reported earlier [15, 61].

For the DPD simulations we used the procedure described in chapter 2.

4.3 Parameter sets

In DPD we have to choose the repulsion parameters such that the simulations yield the experimental obtained values. In this section, we first summarize the method of Groot and coworkers [22, 57], in which the repulsion parameters are coupled to the Flory-Huggins χ -parameter. Then we give an overview of the parameter sets used by different researchers who studied the (phase) behavior of surfactants and phospholipids. On the basis of these parameters we define the sets used to perform the simulations in this chapter.

Groot and Rabone published a data set, in which the compressibility of water is reproduced for a repulsion parameter $a_{ww} = 78$ at a reduced temperature of $T^* = 1$, a mapping factor of $N_m = 3$, and the particle density $\rho = 3$ [22]. To obtain the repulsion parameter of water at a different mapping factor, one can use:

$$a_{ii} = 78k_B T \times N_m / \rho \quad (4.1)$$

To obtain the repulsion parameters for interactions between different types of beads, mutual solubilities of polymers in water can be used, expressed by the Flory-Huggins χ -parameters, which represent the excess free energy of mixing two species. There is a direct relationship between the Flory-Huggins χ -parameter and the excess repulsion Δa_{ij} [22, 57].

$$\chi = (0.231 \pm 0.001) \Delta a_{ij} \quad \text{if } \rho = 3 \quad (4.2)$$

a_{ij} can then be calculated with

$$a_{ij} = a_{ww} + \Delta a_{ij} \quad (4.3)$$

For most systems the Flory-Huggins χ -parameters are tabulated and equations 4.1 to 4.3 can be used to obtain the repulsion parameters. However, Flory-Huggins χ -parameters are determined for uncharged polymers, while phospholipids contain charged units.

With the mapping of three water molecules on one bead ($N_m = 3$), Groot and Rabone created the model of a phospholipid, depicted in figure 4.1. Using this mapping factor, one DPD-bead represents a volume of 90 \AA^3 . This volume also corresponds with the volume occupied by three methylene groups. The division of the lipid head group in three particles is estimated. Using the Flory-Huggins χ -parame-

ters, Groot and Rabone obtained the set of parameters for this system as shown in table 4.1.

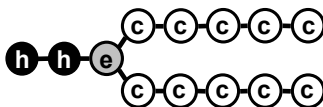


Figure 4.1: The coarse graining of a phospholipid used by Groot and Rabone [22], in which c represents a hydrophobic tail bead, e the ester linkage and h the hydrophilic head bead.

a_{ij}	w	c	e	h
w	78	104	79.3	79.3 (75.8)
c	104	78	86.7	104
e	79.3	86.7	78	79.3
h	79.3 (75.8)	104	79.3	78 (86.7)

Table 4.1: Parameter sets used by Groot and Rabone [22]. In this set the head groups are regarded as water with respect to the ester linkage and the hydrocarbon tails. In this approximation the head group is regarded as an ester group. For the values between brackets the charges of the head group are taken into account, leading to a reduced repulsion with water and an increased repulsion mutually.²

One can also compare parameters used for ionic surfactants to obtain parameters for phospholipids. Table 4.2 shows the parameter set for ionic surfactants used by Groot [50]. In this set of parameters a different mapping is used: one water molecule is mapped onto a single DPD particle. For this mapping the compressibility of water is reproduced using $a_{ww} = 25$ for $\rho = 3$ (see equation 4.1). a_{hw} is lower compared to a_{ww} to mimic the hydration of a charged head group, and the increased value of a_{hh} represents the repulsion between charged head groups. The values of a_{ij} , describing the hydrophobic interactions of the tail beads, are not based on the Flory-Huggins parameters, but chosen to study the formation of micelles.

a_{ij}	w	t	h
w	25	80	15
t	80	15	80
h	15	80	35

Table 4.2: Parameterset of Groot used for ionic surfactants [50]

²Groot and Rabone find that despite these different values, the density profiles are almost equal. Only the area per lipid changes from 62 \AA^2 to 66.8 \AA^2 if the charge of the head group is taken into account. Both values of the area per lipid are within the experimental range [64].

Shillcock and Lipowsky [84] investigated different models for a phospholipid with Dissipative Particle Dynamics. They used a different parameter set in which on average a single tail bead represents three or four methyl groups. They suggest that the most simple model of a phospholipid contains one hydrophilic head bead with a single chain of hydrophobic segments. In this approach the single head bead represents the complete head group of a phospholipid. In a refinement of the model, the hydrophilic part contains more beads and the hydrophobic part contains two tails, varying in length. These tails are connected to two different beads of the head group. If the tails are connected to the same head bead no lamellar phase is found with this parameter set. Shillcock and Lipowsky also use a large angle bending potential to avoid interdigitation between the monolayers.

a_{ij}	w	t	h
w	25	50	35
t	50	25	75
h	35	75	25

Table 4.3: Parameter set of Shillcock and Lipowsky [84]

Ryjkina *et al.* [48] use DPD simulations to compute the phase behavior of non-ionic surfactants. In their model the bead density equals 5 and therefore they divide the a_{ww} parameter by 5 to reproduce the compressibility of water at this particular density (see equation 4.1). One molecule of DDAO (dodecyldimethylamine) is translated to a model which consists of one hydrophilic and one hydrophobic bead.

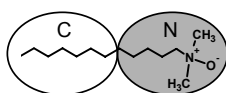


Figure 4.2: Atomistic and DPD model of DDAO

a_{ij}	w	c	n
w	15	80	0
c	80	15	78
n	0	78	15

Table 4.4: Parameter set of Ryjkina *et al.*

Clearly, this short overview illustrates that there is no unique set of mesoscopic parameters to describe phospholipid systems. Groot and Rabone [22] developed a systematic method to relate the repulsion parameters to the experimental system. This method implies that it is possible to translate parameters when a different level of coarse graining is applied. To investigate the sensitivity of the results on the details of the model, we define two independent sets of parameters. A third set is created by recalculating one set of parameters using equations 4.1 and 4.2. We apply these parameter sets on two mesoscopic models, which differ in the level of coarse graining.

These different parameter sets are listed in table 4.5. Parameter set A is based on the simulations performed by Groot and Rabone [22], with exclusion from a separate

parameter for the glycerol linkage in the simulations. Parameter set B is based on the parameters used by Groot on calculations on surfactants [50]. We reduced the tail-tail interaction to avoid a very high density in the hydrophobic core. We obtained parameter set C from the repulsion parameters of Groot and Rabone [22]. By using equations 4.1 and 4.2, we obtain the parameters for a bead volume of 30 \AA^3 .

A	w	t	h	B	w	t	h	C	w	t	h
w	25	80	15	w	78	104	75.8	w	25	34	24
t	80	25	80	t	104	78	104	t	34	25	34
h	15	80	35	h	75.8	104	86.7	h	24	34	29

Table 4.5: Parameter sets used in our simulations. Parameter set A is based on the parameter set used by Groot for ionic surfactants [50] (see table 4.2). Parameter sets B and C are derived from the set used by Groot and Rabone [22] for bilayers (see table 4.1).

4.3.1 Coarse-grained models

In this section, we present the two models used in the simulations. The volume per bead in model I is 30 \AA^3 (corresponding with the mapping factor $N_m = 1$), while the bead volume of model II is 90 \AA^3 ($N_m = 3$). In this section we discuss how we obtained a coarse-grained model of the phospholipid DiMyristoyl-PhosphatidylCholine (DMPC). We show how the bond-bending potentials of the various angles are obtained from MD simulations. While these are results for a single tail length, it is very easy to change the lengths of the hydrophobic tails by adding or removing beads and their corresponding bond-bending potential.

Model I: $N_m = 1$

In the literature one can find applications with a mapping factor $N_m = 1$ [50], which corresponds to a coarse-grained level that is almost identical to an united atom model. One may wonder whether the use of the soft repulsion model is appropriate for this level of coarse-graining. To address this question, we created a model at this level of coarse-graining and we developed the model by defining additional intramolecular interactions between the beads. At the mapping factor $N_m = 1$, we obtain the mapping shown in figure 4.3. To obtain this model we divide the DMPC in equal volumes of 30 \AA^3 , using the phospholipid component volumes determined by Armen *et al.* [85]. Two consecutive beads are connected by harmonic springs with spring constant $k_r = 100.0$ and equilibrium distance $r_0 = 0.7$. To control the flexibility of the tails we add a harmonic bond-bending potential with bending constant k_ϕ and equilibrium angle ϕ_0 .

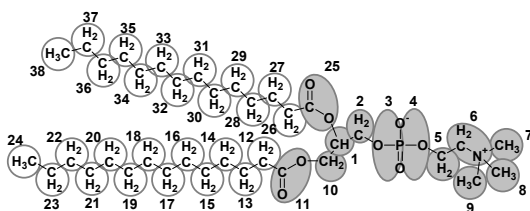


Figure 4.3: The atomistic representation of DMPC and its corresponding coarse-grained model with a bead volume of 30 \AA^3 (model I). White indicates a hydrophobic bead and grey indicates a hydrophilic bead.

Based on the method developed by Tschöpp *et al.* [86], we obtained the values of κ_ϕ and ϕ_0 by measuring the angular distribution function

$$P(\phi) = C \exp[-\beta(U(\phi))] \quad (4.4)$$

from all-atom MD simulations of a single phospholipid in water. This distribution is calculated using the center of mass of the cluster of atoms representing one bead. The parameters of κ_ϕ and ϕ_0 were found by a quadratic fit of the data according to the relation:

$$\frac{1}{2}\beta\kappa(\phi - \phi_0)^2 = -\ln P(\phi) \quad (4.5)$$

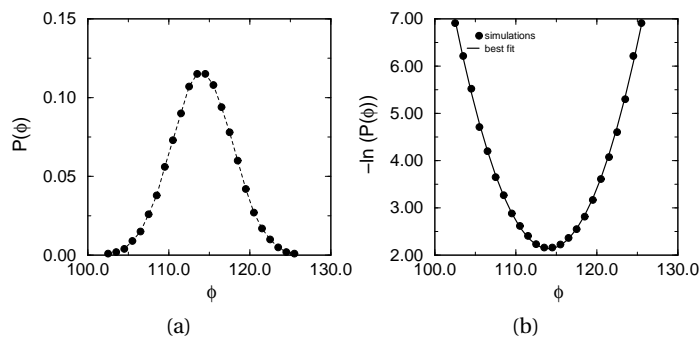


Figure 4.4: Distribution (a) and fitting procedure (b) for the bond-bending potential of the angle between three subsequent beads in the tail ($\phi_{i,i+1,i+2}$).

In figure 4.4 the distribution of the angle ϕ , obtained from MD, and the curve fitting of the data are shown for the angle between three consecutive beads in the hydrocarbon chain. In table 4.6 the values of the bond bending potentials are listed. The angle bending potentials of the angles in the tails are very well defined, which is to be expected, since the mapping of these hydrocarbon tails is equal to the united atom model. However, in the head group region, we cannot use the united atom

approach and we find much more flexible angles. For some angles we observe a large distribution of the angles, which indicates a very flexible angle. For these angles we do not use a bond-bending potential.

Preliminary results showed that the resulting density profile of a bilayer consisting of these lipids does not resemble the density profile computed from MD simulations (results not shown). Therefore, we sought to improve the model by inserting additional angle-bending constants in the tails in which an angle is set between three non-consecutive beads $\phi_{i,i+2,i+4}$ (e.g. $\phi_{14-16-18}$, $\phi_{31-33-35}$). With the mapping procedure we found $k_\phi = 3.5$ and $\phi_0 = 180^\circ$ for these angles.

ϕ	k_ϕ	ϕ_0
\angle_{1-2-3}	3.1	125°
\angle_{2-3-4}	4.3	127°
\angle_{3-4-5}	4.4	124°
\angle_{4-5-6}	1.3	131°
\angle_{2-1-10}	25	113°
$\angle_{1-10-11}$	9	143°
$\angle_{1-25-26}$	24	140°
$\angle_{10-11-12}$	23	140°
type A	22	115°

Table 4.6: Parameters of model I. The angles between three consecutive beads in the tails (beads 11 to 24 and beads 25 to 38) are of type A. The remaining angles are very flexible and therefore a bond-bending potential is not used.

Model II: $N_m = 3$

If we use a mapping in which three water molecules are represented by a single DPD bead, we obtain the representation shown in figure 4.5. Again using the volumes determined by Armen *et al.* [85], the mapping of the lipid using a bead volume of 90 \AA^3 results in a model consisting of three hydrophilic head beads and two tails, each consisting of five hydrophobic tail beads. The same values for the spring constant and the equilibrium distance between two consecutive beads as in model I are used ($k_r = 100.0$ and $r_0 = 0.7$).

To obtain the values k_ϕ and ϕ_0 we followed the same procedure as for model I. However, due to the larger volume per bead and thus the higher number of atoms represented by one bead, the distribution of some angles is multimodal (see figure 4.6). To keep the simple harmonic potential, we repeated the MD simulations on a bilayer of DMPC to confirm that the selected equilibrium angle is the most abundant. The most abundant equilibrium angle ϕ_0 is used in subsequent simulations. In this way we obtained the values of k_ϕ and ϕ_0 listed in table 4.7. The simulations show that the head group is completely flexible, and that the tails exhibit some order. Due to the larger volume per bead, a broader angle distribution is found for all angles

compared to the results found for the angles of model I. As a result the values of k_ϕ are lower.

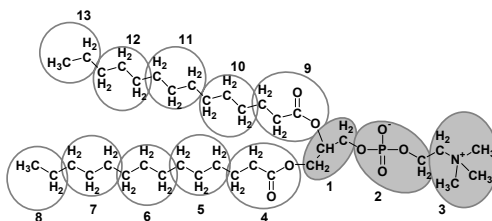


Figure 4.5: The atomistic representation of DMPC and its corresponding coarse-grained model (model II). White indicates a hydrophobic bead and grey indicates a hydrophilic bead.

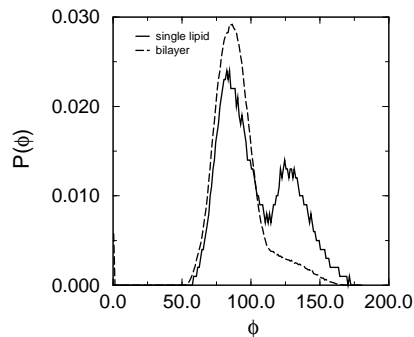


Figure 4.6: Distribution of the angle ϕ_{4-1-9} obtained with MD-simulations of a single lipid in water and of a bilayer of DMPC.

$\phi_{0,A}$	180°
$k_{\phi_{0,A}}$	6
$\phi_{0,B}$	90°
$k_{\phi_{0,B}}$	3

Table 4.7: Parameters of model II. The angles ϕ_{4-5-6} , ϕ_{5-6-7} , ϕ_{6-7-8} , $\phi_{9-10-11}$, $\phi_{10-11-12}$, and $\phi_{11-12-13}$ are of type A and ϕ_{4-1-9} is of type B. The remaining angles are not set, meaning that the head group is completely flexible.

4.4 Results and Discussion

In this section we compare the results from MD simulations with results of DPD simulations for the two models and the parameter sets defined in table 4.5. The quantities to compare are the area per lipid A_L , the hydrophobic thickness D_c of the bilayer,

and the bilayer thickness D_b (see chapter 2, section 2.6 for a detailed description). These quantities can also be obtained experimentally by X-ray and neutron diffraction studies, and volumetric measurements (see for instance ref [63]). We also compare density profiles in the direction of the bilayer normal.

To compare the density profiles of the MD simulations with those of the DPD simulations it is necessary to obtain a density profile from the MD simulations in which the atoms are clustered in one particle. By dividing the simulation box in small slabs of equal volume and using the centers of mass of the representation of DMPC in beads (figures 4.3 and 4.5), we obtain a bead-like density profile of the MD-simulations.

A typical DPD simulation required 100,000 cycles of which 10,000 cycles were needed for equilibration. Per cycle it is chosen with a probability of 70% whether to perform 50 DPD time steps or to make an attempt to change the area of the box.

4.4.1 Model I: bead volume 30 \AA^3

We used DPD to compute the properties of a bilayer of DMPC in water with model I (30 \AA^3 bead size) and parameter set A. Starting from a random configuration of 200 lipids in 16200 water beads at a temperature $T^* = 1.0$ a bilayer was formed. Applying the zero surface tension scheme showed that this bilayer was stable.

Figure 4.7(a) shows the density profiles of the MD-simulation, in which the atoms are translated to the corresponding beads, and of the DPD-simulation (figure 4.7(c)). The snapshots of the bilayer show that in the MD-simulation the final beads are located near the midplane of the bilayer (figure 4.7(b)), while in the DPD simulation the terminal beads are more spread throughout the hydrophobic region (figure 4.7(d)). This is also reflected in the curves representing the CH_3 -group; whereas in the MD density profile this curve is a narrow peak around the bilayer midplane, the curve in the DPD density profile is almost constant across the hydrophobic core. The curves representing the CH_2 -groups support this conclusion. In the MD density profile we observe a clear minimum at the bilayer midplane, while this minimum is absent in the DPD density profile.

The curve representing the ester linkage obtained with the DPD simulation is in good agreement with the curve obtained with the MD simulation. In both profiles the peaks of these curves are located in the water and also surrounded by the hydrophobic core of the bilayer. The fact that in DPD the COO is not completely within the hydrophobic core, while this is the case in the MD simulation, is due to the strong repulsion between the hydrophobic and hydrophilic particles in the DPD simulations.

A remarkable difference can be observed from the curves representing the beads of the head group. The density profile of the MD simulation shows two 'Gaussian' curves for the choline group and phosphate group, which are overlapping and near

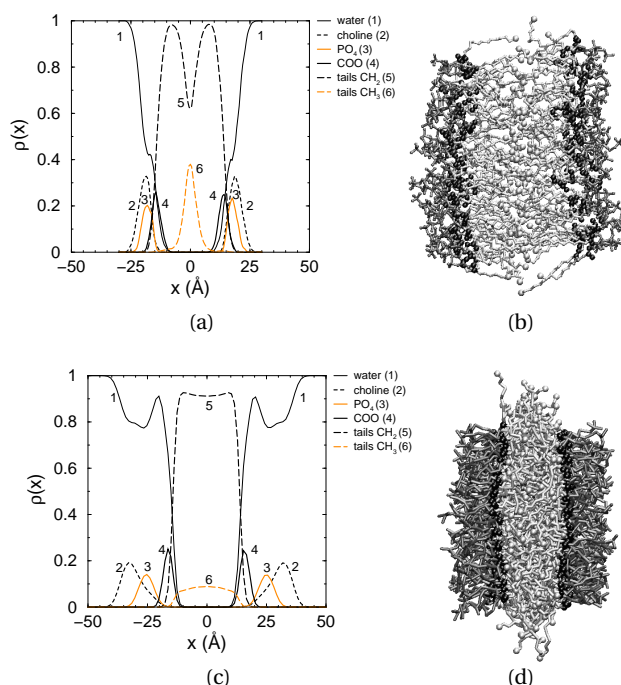


Figure 4.7: Density profiles (a) and (c) and snapshots (b) and (d) of a bilayer of DMPC in water computed from MD simulations using the centers of mass as defined in figure 4.3 and DPD, using model I, respectively. In the density profiles (a) and (c) choline represents the sum of beads 6, 7, 8, and 9, PO_4 is the sum of beads 3 and 4, COO the sum of beads 11 and 25, the terminal CH_3 the sum of beads 24 and 38, and CH_2 the sum of the remaining hydrophobic beads (see figure 4.3). In (b) and (d) dark grey represents the head groups, the black spheres represent the ester groups, and light grey represents the hydrocarbon tails, of which the tail ends are indicated by a sphere.

the interface. The density profile of the DPD simulations shows that the head group is much more hydrated: the density of water is higher and the head group is more stretched, leading to a clear separation of the beads representing the choline and the phosphate group. Where in the MD simulations the hydrophobic region has the largest contribution to the bilayer thickness, in the DPD simulations the contributions of the hydrophilic part and the hydrophobic part are almost equal, *i.e.* in DPD the hydrophilic tendency of the head is overrepresented.

Quantitatively the results from the simulations approach the experimentally observed values. We find for the area per lipid and the hydrophobic thickness 55 \AA^2 and 32 \AA , respectively, while experimentally 60 \AA^2 and 25.6 \AA is found. [69]

It is interesting to create a new parameter set by recalculating parameter set B, created for a bead volume of 90 \AA^3 , to obtain a set for bead volume 30 \AA^3 . With the

resulting parameter set C we performed simulations on 200 lipids in water. Starting from a random configuration, no bilayer was formed. Most lipids assemble in a cluster, with water included in the hydrophobic core. Even if we take a bilayer as the initial configuration and perform the zero surface tension simulations the bilayer breaks up in a cluster of lipids, also containing water in the hydrophobic core and free lipids in the water phase.

4.4.2 Model II: bead volume 90 \AA^3

With model II we performed simulations on 800 lipids with on average 10000 water particles using parameter sets A and B. Figure 4.8 shows the density profiles of the resulting bilayers. Figure 4.8(a) shows the profile using the results of the MD simulations, and figures 4.8(b) and 4.8(c) shows the profiles of bilayers computed from DPD simulations using parameter sets A and B, respectively.

In all profiles the glycerol linkage (bead 1 in model II, see figure 4.5) is located at the interface and the head groups are pointing into the water. The main difference in the density profiles obtained with the DPD simulations is that with parameter set A (figure 4.8(b)) the peaks are somewhat higher and narrower than with parameter set B (figure 4.8(c)). On the whole, however, the density profiles obtained with both parameter sets are in good agreement with the density profile obtained with the MD simulation. The terminal beads of the tails are located around the bilayer midplane and are on average on the midplane of the bilayer. This is also reflected in the curve representing the CH_2 groups of the tails, which shows a minimum at the bilayer midplane. The glycerol linkage, which is the bead connecting the two tails (bead nr 1 in figure 4.5), forms the separation between the hydrophobic core and the water plus head groups. Both the curve of the density of the tail beads and the curve of the density of water cover this peak. Finally, the head groups point into the water and are clearly separated from the hydrophobic core.

The difference between the profiles is the height of the peaks: with MD simulations the peaks are higher and narrower than with DPD simulations. The same difference can be noticed comparing the density profiles of the DPD simulations with parameter sets A and B. This indicates that the bilayer obtained with MD simulations is more ordered than the bilayer obtained with DPD simulations, parameter set A giving a more ordered bilayer than parameter set B.

Quantitatively, both parameter sets A and B give the same results for the area per lipid and the hydrophobic thickness. In our simulations we find at $\gamma = 0$, $A_l = 67 \text{ \AA}^2$ and $D_c = 29 \text{ \AA}$, which are both within the experimental range.

Comparing the results from model I with model II shows that a higher level of coarse graining leads to a better correspondence between MD and DPD simulations. It is necessary to coarse grain a phospholipid to a higher level than a level in which

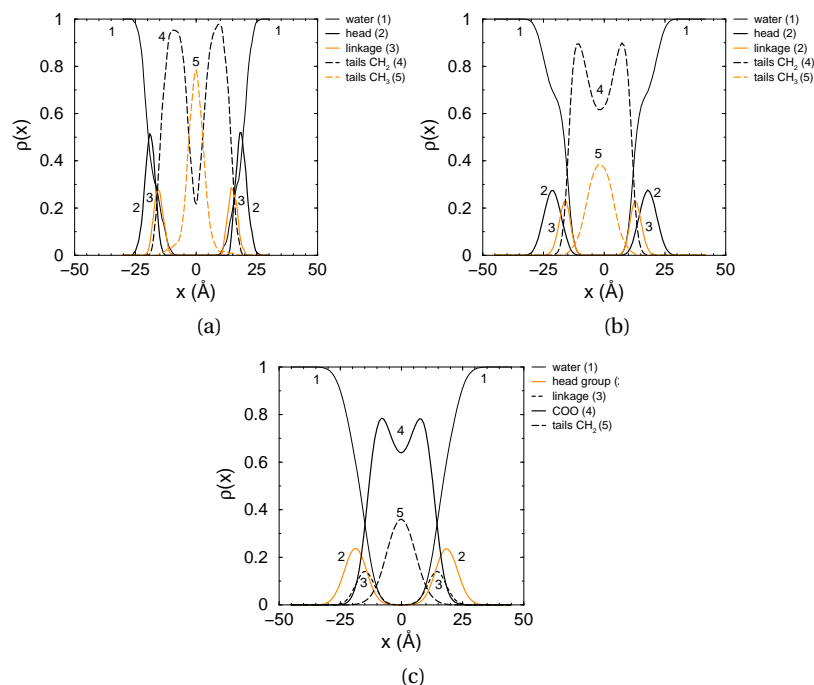


Figure 4.8: Density profiles of a bilayer computed from MD simulations using the centers of mass as defined in figure 4.5 (a), and of a bilayer formed by lipids coarse grained according to model II obtained from DPD simulations using parameter set A (b) and B (c)

one particle represents only one water molecule. The reason is that in DPD each particle represents a cluster of atoms. The soft interactions in DPD allow these particles to overlap. If the particle size approaches a united-atom model size, as in model I, overlap of the particles is no longer realistic and soft potentials can no longer be used.

Using a higher mapping factor N_m , in which one DPD particle represents three water molecules or methylene groups, it is possible that particles do overlap. At this level a soft potential can be applied. This is clear from the density profiles; using a higher level of coarse graining gives the doubly peaked curve for the CH_2 -group and a distribution of the tail ends around the mid plane of the bilayer, as was found both experimentally and by MD simulations.

4.4.3 Changing temperature and lipid topology

In the previous sections we discussed results obtained at a reduced temperature $T^* = 1.0$. At this temperature the bilayer is in the liquid crystalline or L_α phase, also called the liquid phase. We showed in the previous section that results obtained from model

II agreed well with MD and experimental results. In this section we study the behavior of model II at a lower temperature. Experimentally, it is observed that the low temperature phase is the gel or $L_{\beta'}$ phase. In this phase the tails are ordered and show a collective tilt with respect to the bilayer normal. The head groups and the water surrounding the head groups are still fluid. Further we discuss briefly what is happening if the topology of the coarse-grained model changes by varying the length of the hydrophobic tails.

Changing temperature

Figure 4.9(a) shows a bilayer consisting of model II lipids at a temperature of $T^* = 0.3$. From this snapshot it is clear that at this low temperature the bilayer is much more ordered than at temperature $T^* = 1.0$. The tails are straightened and ordered and show a tilt with respect to the bilayer normal. In figure 4.9(b) we show the two dimensional radial distribution functions of various particles in the plane of the bilayer. These curves show that the hydrophobic region is a very structured lipid. Due to the ordering of the tails the head groups are more localized, but the radial distribution functions of the beads in the head group show that the bilayer as a whole and the surrounding water are still fluid. This allows us to apply the zero surface tension scheme.

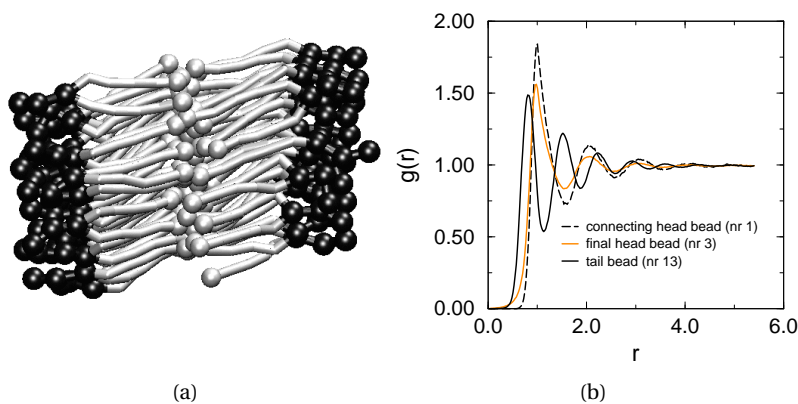


Figure 4.9: (a) Snapshot of a DPD bilayer at $T^* = 0.3$ and (b) the two dimensional radial distribution functions of the final head bead, the bead connecting the two tails and a tail bead (bead 3, 1, and 13 in figure 4.5 respectively) in the plane of the bilayer. In (a) black represents the hydrophilic head group and grey the hydrophobic tails. The terminal beads of the tail are depicted by a grey sphere.

The phase found at this temperature resembles very well the experimentally observed $L_{\beta'}$ phase. Experimentally a tilt angle of $\theta = 32^\circ$ [87, 88] is observed, while we find a tilt angle of $\theta = 27^\circ$ for parameter set A and $\theta = 18^\circ$ for parameter set B. For

the area per lipid we find $A_l = 46.6 \text{ \AA}^2$ and $A_l = 43.4 \text{ \AA}^2$ for parameter sets A and B, respectively, while the experimental value is $A_l = 47.2 \text{ \AA}^2$ [88]. The hydrophobic thickness deviates significantly from the experimental value of $D_c = 30.3 \text{ \AA}$ [88]; for parameter set A we find $D_c = 43.4 \text{ \AA}$ and for B $D_c = 45.5 \text{ \AA}$. The two parameter sets lead to a different temperature at which the transition from the L_α to the $L_{\beta'}$ phase takes place. For parameter set A the transition temperature is found at $T^* = 0.35$, while for parameter set B a value of $T^* = 0.65$ is found.

Changing lipid topology

There are several ways to change the topology of the coarse grained lipid. One is to vary the length of the hydrophobic tails by adding or removing a tail bead. Simulations at $T^* = 1.0$ show that at zero surface tension the area per lipid is constant with increasing tail length from 4 to 7 beads. The hydrophobic thickness increases linearly with increasing tail length, both experimentally and in our simulations [69, 89].

Experimentally it is found that at the melting temperature the area per lipid as a function of tail length is constant [89]. However, the experimental data show large fluctuations in the area per lipid. A detailed study at a fixed temperature above the melting temperature, shows that the area per lipid decreases slightly, going from a tail length of 14 to a tail length of 18 carbons [69]. This decrease is attributed to the larger inter chain vanderWaals interactions among the longer tails. In figure 4.10 we plotted the area per lipid in \AA^2 as a function of number of carbons in the tails of both the experimental and the computed values. Using the mapping factor $N_m = 3$ and parameter set A, we found that with fully flexible tails (*i.e.* no bending potentials) the area per lipid actually rose with increasing tail length. After introduction of bending potentials the area per surfactant is constant within the error ($\Delta A_s/A_s = 5\%$), in agreement with the experimental results. The observed decrease in area per surfactant by Petrache *et al.* [69] is too small to allow for a detailed comparison with our mesoscopic model.

4.4.4 Driving forces in the formation of a bilayer

By comparing simulations with the three different parameter sets (see table 4.5) we are able to pinpoint the repulsion parameters that are important in the self-assembly of a bilayer. In this section we discuss the choice of the repulsion parameters combined with the level of coarse graining.

To obtain a bilayer with DPD, we must have a phospholipid with clear hydrophobic and hydrophilic parts. The hydrophilic part sticks into the water phase, while the hydrophobic tails shield the core from the water particles. The parameter determining this shielding is a_{wt} . Too low a value for this parameter and water penetrates the

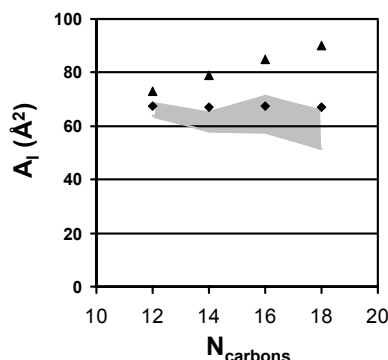


Figure 4.10: Comparison of the experimental and computed values of the area per surfactant as a function of tail length. The computed values are represented by the black symbols and are calculated at a temperature $T^* = 1.0$. At this temperature, all bilayers are in the fluid L_α phase. The triangles are the values obtained with fully flexible model and the diamonds represent the values obtained with the model with additional bond-bending potentials. The grey area indicates the range of the experimentally obtained values [69, 89–93].

core. As a result, no bilayer is formed as one saw from the simulations on model I, parameter set C (see section 4.4.1). In section 4.3 we assumed by combining equations 4.1 and 4.3 that a_{ii} can be calculated for every combination of N_m and ρ . The above results indicate, however, that one set of parameters cannot be translated straightforwardly into the other using these equations. Since the hydrophobic core of the cluster contains water and lipids can diffuse into the bulk water, it can be concluded that the repulsion between water and the hydrophobic tail segments a_{wt} is too low. This shows that the choice of parameters depends on the coarse graining level of the lipid in a more complex way than just a linear relation.

However, the scale to which water will penetrate the hydrophobic core depends not solely on the size of a_{wt} , but also on the interactions between the water particles themselves. Thus we expect that a large difference between a_{ww} and a_{wt} will favor the formation of a bilayer, while relatively low values of this difference allow for free mixing of water particles and tail beads. This is indeed borne out by the results presented in sections 4.4.1 and 4.4.2. For parameter sets A and B where $|a_{ww} - a_{wt}| = 55$ and $|a_{ww} - a_{wt}| = 26$ respectively, a bilayer was formed, while for parameter set A with $|a_{ww} - a_{wt}| = 9$ a bilayer could not form.

Another important parameter that can influence the stability of the bilayer is a_{hw} , which determines the hydration of the head group. As was indicated by Groot and Rabone [22] the Flory-Huggins χ -parameter is not known for the head groups. They compare two parameter sets, in which the head group-water interaction is changed, resulting in a change in area per lipid but equal density profiles. For model II and parameter set A we changed a_{hw} from 15 to 25. The main effect is on the area per lipid;

for $a_{hw} = 15 A_l = 67 \text{ \AA}^2$, while for $a_{hw} = 25 A_l = 63 \text{ \AA}^2$, which is both within the experimental range. Increasing this repulsion parameter to even higher values seems not a logical choice, since both the phosphate group and the nitrogen are charged units in the head group. This charge will result in the hydration of the head group, which can be translated in DPD by a lower value of a_{hw} compared to a_{ww} .

Also the results from model II indicate that the difference between a_{ww} and a_{wt} is of importance. Both for parameter set A and B a stable bilayer is formed and within the accuracy of our data the area per lipid A_l is equal.

4.5 Conclusions

In this work, we compared the results from DPD simulations on coarse-grained models of a phospholipid with atomistic MD simulations. We created two mesoscopic models of DMPC, which differ in their level of coarse graining. Model I has a mapping factor of $N_m = 1$ with a volume of 30 \AA^3 per bead and model II has a mapping factor of $N_m = 3$ with a volume of 90 \AA^3 . We found that we could correctly reproduce tail length dependency of both area per lipid and hydrocarbon core thickness, if we include bond-bending potentials in our model. We used results from MD simulations to obtain the bending constants and equilibrium angles.

This work shows that DPD is a powerful method to study the self-assembly of the lipids in a bilayer. It can be used to obtain qualitative dependence on temperature and length of the hydrophobic tail if a DPD beads represents a sphere with a volume of 90 \AA^3 . At the reference temperature of $T^* = 1.0$, where the bilayer is in the fluid L_α phase, the resulting density profiles of the MD and DPD simulations are in good agreement. At this temperature we can also reproduce the experimental values of area per lipid and the hydrophobic thickness. Lowering the temperature gives us the experimentally observed L_β' phase, in which the tails are ordered and show a tilt with respect to the bilayer normal. Using a lower value of the mapping factor is not useful, because the soft repulsive potential used in DPD allows the beads to overlap, while overlap is not realistic in an (almost) atomic system.

The results obtained with model I show that it is not possible to recalculate one parameter set into another one, if at the same time the level of coarse graining is changed. The assumption that a_{ii} can be calculated for every combination of N_m and ρ is too simple: the choice of the parameters depends not only on the level of coarse graining of the lipid. Also, a minimum difference between water-water and the water-hydrophobic tail repulsion parameters is needed if a lipid bilayer is to be formed. If the difference between this parameters is too small, the hydrophilic and the hydrophobic particles will not be completely separated and other structures than a bilayer are observed.

V

Phase behavior of double tail lipids

Abstract

In this chapter we investigate the phase behavior of double-tail lipids, as a function of temperature, head group interaction and tail length. At low values of the head-head repulsion parameter a_{hh} , the bilayer undergoes with increasing temperature the transitions from the subgel phase L_c via the flat gel phase L_β to the fluid phase L_α . For higher values of a_{hh} the transition from the L_c to the L_α phase occurs via the tilted gel phase $L_{\beta'}$ and the rippled phase $P_{\beta'}$. The occurrence of the $L_{\beta'}$ phase depends on tail length. We find that the rippled structure ($P_{\beta'}$) occurs if the head groups are sufficiently surrounded by water and that the ripple is a coexistence between the L_c or $L_{\beta'}$ phase and the L_α phase. The anomalous swelling, observed at the $P_{\beta'} \rightarrow L_\alpha$ transition, is not directly related to the rippled phase, but a consequence of conformational changes of the tails.

5.1 Introduction

A phospholipid bilayer knows many phases, depending on temperature, pressure and hydration, and on its structural properties, such as the length of the hydrocarbon tails and the composition of the head group¹ (see figure 5.1). For the most common phospholipids, the low temperature phase is the subgel L_c , in which the hydrocarbon tails are highly ordered and show a tilt with respect to the bilayer [9]. Upon heating the subgel transforms to a lamellar gel phase. Dependent on the structural composition of the lipid head group, the gel phase is the L_β phase (for example, for phosphatidylethanolamines or PE's) or the $L_{\beta'}$ phase (for example, for phosphatidylcholines or PC's). In these gel phases the bilayer is more hydrated than in the L_c phase and the hydrocarbon tails still show a high order, but less than in the L_c phase. In the L_β phase the tails are ordered parallel to the bilayer normal, while in the $L_{\beta'}$ phase the tails show a tilt angle with respect to the bilayer normal. At higher temperature the gel phase undergoes a transition to the L_α phase, which is also called the liquid crystalline or fluid phase; the tails are disordered and do not show any tilt. This L_α phase is physiologically the most important phase.

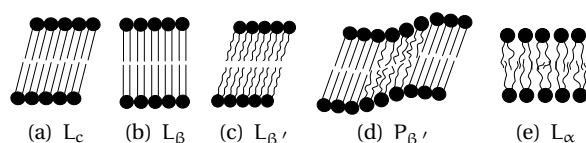


Figure 5.1: Schematical drawings of the various bilayer phases. The characteristics of these phases are explained in the text. The filled circles represent the hydrophilic head group of a phospholipid and the lines represent the hydrophobic tails.

For some lipids the transition from the ordered gel phase to the disordered liquid crystalline phase occurs in two steps. First a transition from the gel phase to the rippled phase $P_{\beta'}$ takes place (*i.e.* the pretransition). This transition is followed by the melting of the bilayer from the $P_{\beta'}$ to the L_α phase, which is called the main transition. The rippled phase is characterized by a long-wavelength rippling of the bilayer and an (anomalous) swelling of the membrane. The hydrophobic chains are ordered and there is a preferred tilt angle with respect to the bilayer normal. The temperature interval between the pretransition and the main transition decreases with increasing chain length. For chains containing more than 20 carbon atoms the pretransition is not observed. It is assumed that this transition disappears completely or that the temperature interval between the pretransition and the main transition is too small to be observed [95]. The rippled phase is only observed in bilayers containing PC's, of which the low temperature phase is the $L_{\beta'}$. Phosphatidylethanolamines (PE's) and glucolipids, of which the low temperature phase is the untilted L_β , do not display a

¹for a review, see refs. [9] and [94]

pretransition ([96] and references therein).

This rippled phase has attracted the attention of many groups, from the moment it was first observed by Tardieu *et al.* in 1973 [97]. After this first observation, many studies, both theoretically and experimentally, have been addressed to the question how such a corrugated $P_{\beta'}$ phase can exist, while the low temperature gel phase $L_{\beta'}$ and the high temperature fluid phase L_{α} are flat. It is assumed that the shape of the ripple is a asymmetric sawtooth [97–101], but in some models it is also proposed that the ripple is a sinusoidal [28, 96, 102–104]. The logical next question is then how the sawtooth or the sinusoidal can occur. Explanations can be found in variations of the thickness of the bilayer due to changes in tilt angles of the hydrophobic chains [27, 28, 104–108], and coexistence between the fluid L_{α} phase and the gel phase $L_{\beta'}$ [96, 99, 109–113]. Also it is not very clear if the (anomalous) swelling of a membrane is coupled to the formation of the rippled phase [94, 114, 115] and if the rippled phase only exists in multilayers or if it is also present in a single bilayer system [116–118]².

Despite all investigations, an explanation of the formation of the rippled phase at a molecular level is still lacking. We use computer simulations to study the phase behavior of phospholipid bilayers. Simulations allow us to investigate the bilayer at a molecular level, which is not always possible experimentally. We use a combined technique of Dissipative Particle Dynamics (DPD) and Monte Carlo as was described in chapter 2. This scheme, in which we impose the bilayer to adopt a tensionless configuration, allows us to observe directly phase transitions in which the area per lipid changes.

The phase behavior of membranes depends on the structural properties of the phospholipid. Therefore, we study the phase behavior as a function of tail length and head group interaction. Here we apply our mesoscopic model developed in chapter 4 to a model consisting of three hydrophilic beads and two hydrophobic tails. The resulting phase diagrams are presented in section 5.3. We will show that we can reproduce the various phases of the phospholipid bilayer, dependent on temperature and head-head interaction. While for the shortest lipid studied the $L_{\beta'}$ phase is not present, this phase appears for longer tails and its stability increases with increasing tail length. We show that the anomalous swelling is not directly related to the formation of the rippled phase and finally, we discuss the structure of the ripple. We conclude that the key factor in the formation of the rippled phase is a frustration of the surface area of the head group with the packing of the hydrophobic tails.

²See section 5.5.3 for a discussion on the structure of the ripple.

5.2 Computational details

In this investigation we consider lipids with three head segments and two tails with variable length (see figure 5.2). As we described in chapter 4, our model with a tail length of five beads corresponds to the phospholipid DMPC. Two consecutive beads are connected by harmonic springs with spring constant $k_r = 100.0$ and $r_0 = 0.7$. To control the chain flexibility, we added a bond-bending potential between three consecutive beads in the tails with bending constant $k_\phi = 6.0$ and equilibrium angle $\phi_0 = 180^\circ$. An additional bond-bending potential is applied between the vectors connecting the tails to the head group, with $k_\phi = 3$ and $\phi_0 = 90^\circ$.

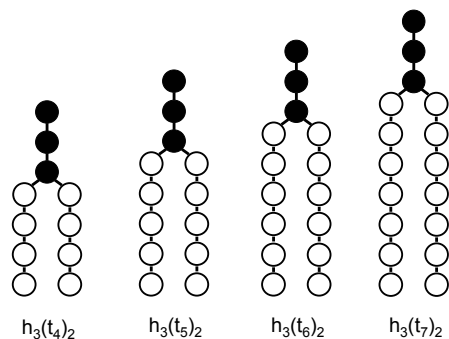


Figure 5.2: Models of the lipids used in this study with their nomenclature; the black particles represent the head beads and the white particles the tail beads.

The hydrophilic and hydrophobic interactions of the particles are described using soft repulsive interactions: $\mathbf{F}_{ij}^C = \alpha_{ij}(1 - r_{ij}/r_c)\hat{\mathbf{r}}_{ij}$. The values of α_{ij} used are $\alpha_{ww} = \alpha_{tt} = 25$, $\alpha_{ht} = \alpha_{wt} = 80$, and $\alpha_{hw} = 15$. The value of the repulsion parameter α_{ww} is taken such that the DPD water-like particles reproduce the compressibility of water. The interactions of the hydrophilic and hydrophobic particles are based on the Flory-Huggins solubility parameters (see chapter 2 for more details.) In addition, we vary the head-head α_{hh} interaction parameter to study the effect of changing the interactions between the head groups of a lipid. Experimentally, the head-head interactions can be changed by, for example, modifying the chemical nature of the head group or adding salt to the system.

Simulations were performed on a bilayer containing 800 lipids. 8000-15000 water particles are added to ensure that a bilayer does not have any interaction with its periodic image. After the formation of the bilayer, by applying DPD steps only, we allowed the bilayer to adopt a tensionless configuration by applying both DPD and Monte Carlo, in which the area of the bilayer is changed. The overall density of the system is $\rho = 3$. A typical simulation required 100,000 cycles of which 20,000 cycles were needed for equilibration. Per cycle it is chosen with a probability of 70%

whether to perform 50 DPD time steps or to make an attempt to change the area of the box.

To characterize the different phases we used the area per lipid, the order of the tails, the tilt angle, and the thickness of the hydrophobic part of the bilayer as order parameters, as was described in section 2.6 of chapter 2.

5.3 The lipid $h_3(t_4)_2$

In this section we discuss the influence of temperature, tail length, and head group repulsion on the phase diagram of double-tail lipids. To facilitate the presentation of our results, we first summarize the computed phase diagram of the lipid $h_3(t_4)_2$, which consists of three hydrophilic head groups and two hydrophobic tails with a length of 4 beads. In the next section we investigate the changes in the phase diagram as a function of the tail length.

We study the phase behavior as a function of temperature and head-head repulsion parameter a_{hh} . We vary the head-head repulsion parameter from $a_{hh} = 10$ to $a_{hh} = 55$. For each value of a_{hh} we study the temperature behavior of the bilayer by cooling down the system in steps of $\Delta T = 0.05$. The resulting phase diagram of the lipid $h_3(t_4)_2$ is given in figure 5.3. In these simulations we observe the low temperature L_c phase and the high temperature L_α phase. For low values of a_{hh} we find that the transition from the L_c phase to the L_α phase takes place via the L_β phase, in which the tails are ordered, but are not tilted with respect to the bilayer normal. At high head-head repulsion ($a_{hh} > 25$) the transition $L_c \rightarrow L_\alpha$ occurs via the rippled phase P_β .

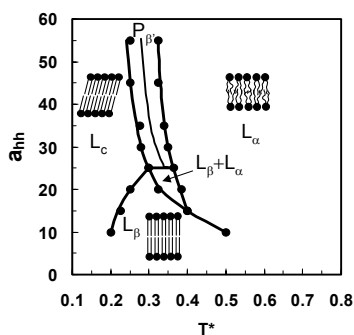


Figure 5.3: Phase diagram of $h_3(t_4)_2$ as a function of reduced temperature T^* and head-head repulsion parameter a_{hh} . In the narrow region between the L_c phase and the L_α phase we find the rippled phase. The thin line corresponds with the condition of 50%-50% of both phases.

5.3.1 Phase behavior as a function of temperature and head group interaction

Figure 5.4 shows the area per lipid, the thickness of the hydrophobic core and the tail order parameter as a function of temperature for various head-head repulsion parameters. At the low temperature extreme ($T^* < 0.2$) the area per lipid is small and the hydrophobic thickness is large. This indicates that the lipids are tightly packed, which is reflected in the order parameter. The high value of S_{tail} at low temperatures indicates that the tails are ordered. This tail order parameter does not reach the value of 1 (ordering parallel to the bilayer normal), due to an average tilt angle with respect to the bilayer normal of about $\theta = 25^\circ$, except for $a_{\text{hh}} = 10$ where $\theta = 15^\circ$. At $T^* > 0.6$ a gradual increase of A_l and decrease of D_c is observed. At these high temperatures the order of the tail is lost. For the intermediate temperatures we observe a more complex temperature dependence.

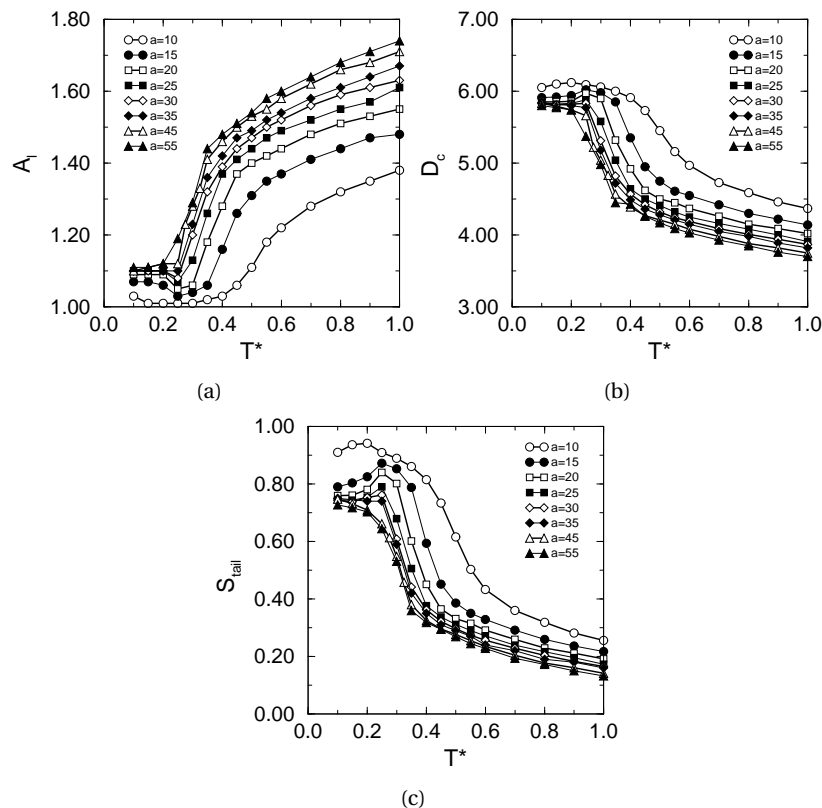


Figure 5.4: (a) Area per lipid A_l , (b) hydrophobic thickness D_c , and (c) tail order parameter S_{tail} as a function of temperature T^* at and head-head repulsion parameter a_{hh} .

In figure 5.5 we plotted the density profiles in the direction of the bilayer normal for both temperatures, taking $a_{\text{hh}} = 35$ as an example. At high temperature ($T^* = 1.0$)

the different tail segments have a low order, reflected in the broad distribution peaks and overlap of the two monolayers, due to disorder of the tails, is observed. This phase corresponds with the fluid L_α phase. At a temperature of $T^* = 0.25$ the peaks are narrow, indicating a high order, and the two monolayers are completely separated. At this temperature the bilayer is in the L_c phase. Due to the high organization of the tails, the head groups are quite ordered as well and thus the density of water is locally increased. The bulk water (depicted by the thin dashed line) is in the fluid phase. Lowering the temperature even further to $T^* = 0.1$ results in complete freezing of the tails and at this temperature also the water starts to freeze.

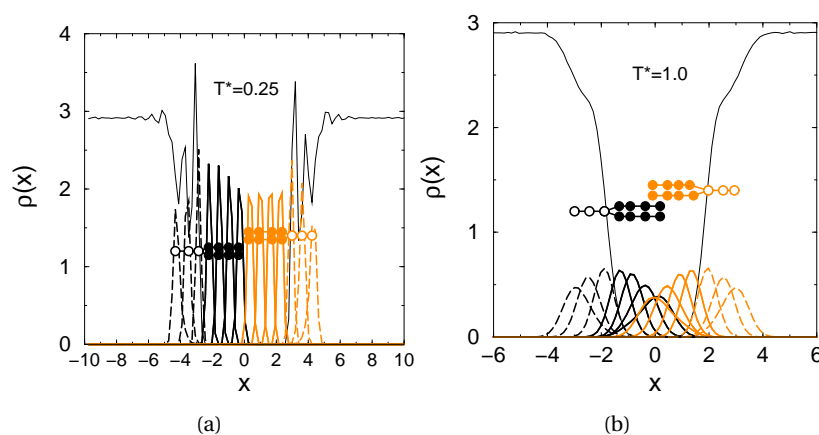


Figure 5.5: Density profiles $\rho(x)$ along the bilayer normal x for temperatures (a) $T^* = 0.25$ and (b) $T^* = 1.0$. Each line is the density profile for a different bead: full lines are the densities of the tail beads, dashed lines correspond to the head beads and the thin solid line is the density of water, while the colors black and grey represent the lipids of the two monolayers. The dots correspond with the x position of the maximum density, illustrating the positions of the beads in the bilayer.

The main trends in the curves of the area per lipid, the hydrophobic thickness, and the order parameter can now be explained. At low temperatures the packing of the tails is the dominating effect: the order in the tails is high and the tails stretch out, which results in a large value for the thickness of the hydrophobic core and a small area per lipid. To minimize contributions to the total energy of both head group and tail-interactions, the tails are tilted with respect to the bilayer normal. With increasing temperature the tails lose their order and the collective tilt, and the bilayer becomes fluid. Due to this increasing disorder the area per lipid increases and the hydrophobic thickness decreases.

Till now, we concentrated on the two extreme temperature regions, but a distinction can be made between the phase transition at low head-head repulsion ($a_{hh} \leq$

25) and high head-head repulsion parameters ($a_{hh} > 25$). For $a_{hh} < 15$ the system gains energy if a water particle, which is hydrating a head particle, is replaced by another head particle, while for higher repulsion parameters the system gains energy by surrounding the head groups with water.

For every value of a_{hh} the tails are in the L_c phase at the lowest temperatures. At low a_{hh} , for which the water particles are expelled from the head group region, we observe that at $T^* > 0.2$ the area per lipid decreases slightly and the thickness increases. At the same time, the order parameter increases. Investigating the tilt angles in these systems shows that at the lowest temperature a collective tilt is present, but with slightly increasing temperature the tilt angle disappears. The disappearance of the tilt angle explains the increase in the order parameters, since this order parameter is calculated with respect to the bilayer normal. In this temperature region, the tails are still ordered and due to the strong head-head interactions the system will form the flat gel phase L_β . For $a_{hh} > 25$ we do not observe the formation of the L_β phase. At these values of the head-head repulsion the most favorable configuration of the heads is to be surrounded by water and as a result the tails will optimally pack in a tilted configuration.

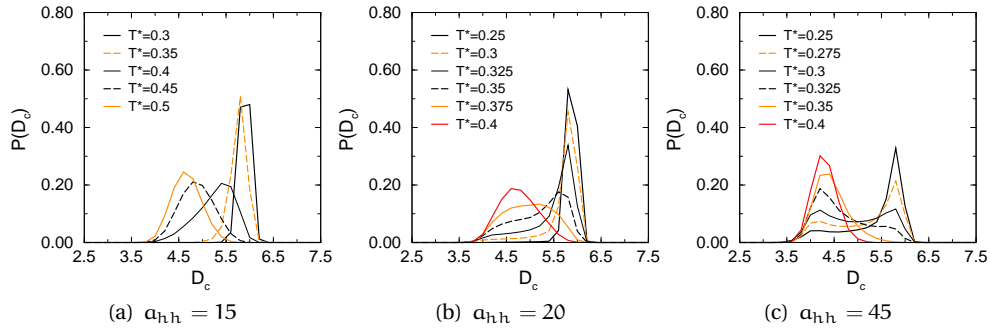


Figure 5.6: Distribution of thicknesses in the bilayer at different temperatures near the transition to the L_α phase for three repulsion parameters: (a) $a_{hh} = 15$, (b) $a_{hh} = 20$, and (c) $a_{hh} = 45$.

We investigated the temperature region in which the phase transition occurs more accurately by computing a thickness profile of the bilayer. In figure 5.6 we plotted the distribution of the thickness as function of temperature for three different repulsion parameters. We observe that the transition to the L_α phase occurs via a narrow region, except for the lowest head-head repulsion parameters of $a_{hh} \leq 15$, where the transition takes place at once.

For values of $a_{hh} > 25$ the distribution near the transition temperature shows a double peak. The low value corresponds with the thickness of the L_α phase and the high value with the thickness of the L_c phase, indicating that there is a coexistence

between the two phases. If we simulate exactly at the point, where the bilayer consists of 50% L_c and 50% L_α , we find the contourplot depicted in figure 5.7(a). This contourplot shows the thickness of the bilayer as a function of the position in the yz plane. The thick and thin parts of the bilayer alternate, leading to a striped structure. This structure closely resembles the rippled phase $P_{\beta'}$, as can also be seen in figure 5.7(b). We further investigated this structure and we found that in the thick part the two monolayers are separated and that in the thin arm the end segments of the tails overlap. Computing the tail order parameters of the lipids in the thick and in the thin part, gives that the tails in the thick part of the bilayer are more ordered than the tails in the thin part of the bilayer. Furthermore, the tails in the thick part of the ripple have a tilt angle with respect to the bilayer normal, whereas in the thin part this tilt angle has disappeared. The average orientation of this tilt is parallel to the direction of the ripple. All these results point out that the rippled phase is a coexistence between the ordered L_c phase and the disordered L_α phase.

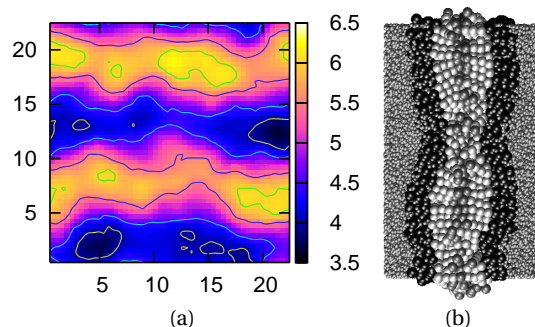


Figure 5.7: Structure of the rippled phase with $\alpha_{hh} = 45$ and $T^* = 0.3$. At this temperature we obtain exactly equal amounts of the L_c and the L_α phase. The contourplot (a) shows the thickness of the bilayer as a function of the position in the yz plane where the colors indicate the hydrophobic thickness. (b) is a side view of the bilayer, in which the head groups are colored black, the tails are grey. The darker color grey is used to indicate the end segments of the tails. The water particles are depicted by smaller spheres.

For $\alpha_{hh} = 20-25$ we do not observe the double peak in the distribution of the thickness near the transition to the fluid L_α phase. With increasing temperature the distribution of the thicknesses shifts from the thickness corresponding to the L_β phase to the thickness observed in the L_α phase and all thickness in between these two extremes. In figure 5.8 the corresponding contourplots are given. At $T^* = 0.325$ we observe the formation of domains of the L_α phase comparable to the domain formation at higher repulsion parameters. With increasing the temperature we observe the melting of the bilayer into the L_α phase, but this transition is very gradual, as can be seen from figures 5.8(b) and (c). We did not find any indication of the formation of a rippled phase.

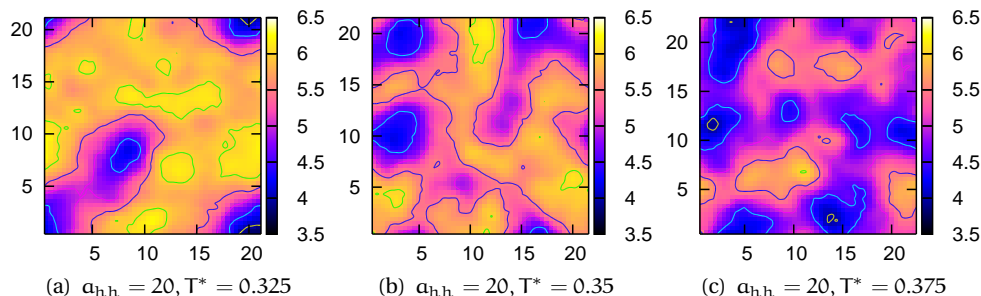


Figure 5.8: Contourplots of the bilayer at the head-head repulsion $\alpha_{hh} = 20$ at temperatures of (a) $T^* = 0.325$, (b) $T^* = 0.35$, and (c) $T^* = 0.375$. The colors indicate the hydrophobic thickness of the bilayer.

With these results we are now able to create the phase diagram of the lipid $h_3(t_4)_2$ (see figure 5.3). Depending on the head-group interactions the transition from the low temperature phase L_c to the fluid phase L_α occurs via two different routes. The stability of the L_c phase is determined by the tails, which pack optimally in a tilted configuration. However, the configuration of the head groups can be far from optimal, depending on the head-head interactions. At low values of α_{hh} water is expelled from the head group region and due to the strong interactions between head groups the L_β phase is formed, in which the area per lipid is small, the tails are ordered but no tilt is present. The transition from this phase to the L_α phase occurs gradually. For high values of α_{hh} it is favorable to surround the head groups with water and the tilt will not disappear. Instead the transition $L_c \rightarrow L_\alpha$ will occur via the rippled phase $P_{\beta'}$. This rippled structure becomes more stable with increasing hydration of the head group.

5.3.2 The rippled phase

To study the formation of the ripple in more detail, we computed the contourplots of the bilayer at different temperatures near the temperature where we find the ripple (*i.e.* at the point where we have 50% of the L_c phase and 50% of the L_α phase) (see figure 5.9). At the temperature of $T^* = 0.275$ the bilayer is mainly in the L_c phase, but domains of the L_α phase are formed. At a temperature of $T^* = 0.325$ we observe that the bilayer is in the L_α phase, containing domains of the L_c phase. At both temperatures, these domains are stable and do not fuse into one large domain and the typical rippled structure is not formed.

The rippled structure is more stable with increasing head-head repulsion parameter. At $\alpha_{hh} = 35$ we find the rippled structure only at the temperature where we have 50% of the L_c phase and 50% of the L_α phase. However, at a repulsion parameter

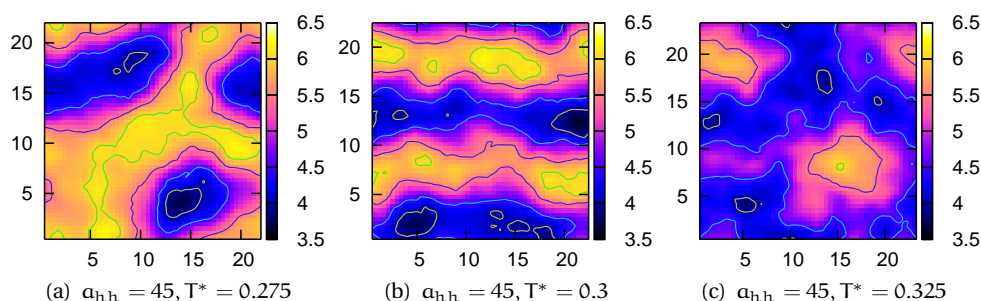


Figure 5.9: Contourplots of the bilayer at the head-head repulsion $\alpha_{hh} = 45$ at temperatures of (a) $T^* = 0.275$, (b) $T^* = 0.3$, and (c) $T^* = 0.325$. The colors indicate the hydrophobic thickness of the bilayer.

of $\alpha_{hh} = 55$ we find that this structure is stable at a temperature range of $\Delta T^* = 0.05$ around this temperature. A second effect of increasing the head-head repulsion parameter is on the distance between two ripples. At higher repulsion parameters the head group is more hydrated, which leads to slightly higher value of the tilt angle in the $L_{\beta'}$ phase. As a result, the period of the rippled phase increases slightly with increasing repulsion parameter.

We performed several simulations to test whether the rippled structure that we observe is really a stable phase, or that this structure is induced by the way the simulations are performed. In all simulations we cooled down the system from $T^* = 1.0$ to $T^* = 0.1$ in steps of $\Delta T = 0.05$. If the rippled phase is the stable phase, it should also be formed if we heat the system up. For $\alpha_{hh} = 45$, at which the rippled phase is observed at $T^* = 0.3$ (see figure 5.9(b)), we decreased the temperature from $T^* = 0.325$ to $T^* = 0.3$ and increased the temperature from $T^* = 0.275$ to $T^* = 0.3$. In both cases the rippled structure is observed at $T^* = 0.3$, while at the lower and the higher temperature no ripple was observed.

We also performed some simulations to test the influence of the system size. For $\alpha_{hh} = 45$, we find the rippled structure in a system containing 800 lipids (figure 5.9(b)). In this system, two “ripples” are observed. Increasing the system size to 1800 lipids, should give the formation of three ripples. However, we find that only two ripples are formed. If we double this system to 6400 lipids, we indeed observe the formation of four ripples.

For $\alpha_{hh} = 55$, we observed that the ripple was formed diagonally in the yz -plane of the simulation box (figure 5.10(a)). Since we apply periodic boundary conditions in all three directions, one might wonder if this is a rippled phase or just the formation of two domains. Increasing the system size to 1800 lipids shows that in this case the striped structure is again formed parallel to the y -axis of the system (figure 5.10(b)), indicating that the rippled phase is the stable phase. Also, in this case,

multiplying the system by two leads to a doubling of the number of ripples.

These results show that in the system of 800 lipids, there can be some friction in the distance between the ripples. Increasing the system size leads to the formation of a rippled phase, in which the distance between the ripples is optimal. Once optimized this period of the ripple, there is a linear relation between the system size and the number of ripples. The period of the ripple is very characteristic and depends on the tilt angle of the hydrocarbon tails.

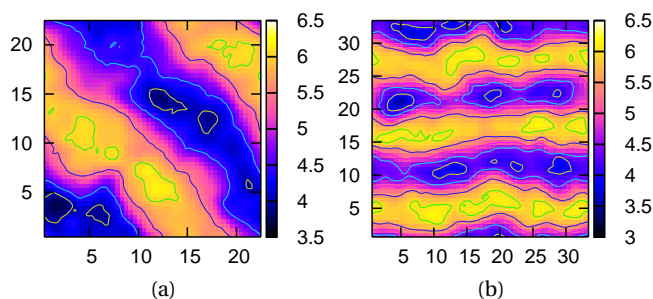


Figure 5.10: Contourplots at the head-head repulsion $\alpha_{hh} = 55$ at temperature $T^* = 0.275$ of (a) a bilayer consisting of 800 lipids and (b) a bilayer consisting of 1800 lipids.

In summary, we observe that the transition from the ordered gel phase to the disordered fluid phase occurs via a coexistence region. For low values of the head-head repulsion parameter ($\alpha_{hh} \leq 25$), there is a coexistence region of the L_β and the L_α phase, in which domains are formed. These domains grow with increasing temperature until the bilayer is completely fluid. Contrary to this behavior, we do not find domain formation for the high values of α_{hh} ($\alpha_{hh} > 25$). The coexistence between the $L_{\beta'}$ phase and the L_α phase leads to the rippled phase $P_{\beta'}$. The period of this ripple depends on the tilt angle of the hydrophobic tails.

5.4 Influence of tail length

Now that we have determined the phase diagram of the shortest lipid, it is interesting to investigate how this diagram changes with increasing tail length. We performed simulations on model lipids with tail lengths increasing up to 7 beads in the tail. The resulting phase diagrams are presented in figure 5.11. We included the phase diagram of $h_3(t_4)_2$ for comparison.

In all phase diagrams we find the phases observed for the shortest model $h_3(t_4)_2$. However, with increasing tail length we observe the appearance of a third phase, the $L_{\beta'}$ phase. This $L_{\beta'}$ phase is characterized by less order in the tails than in the L_c

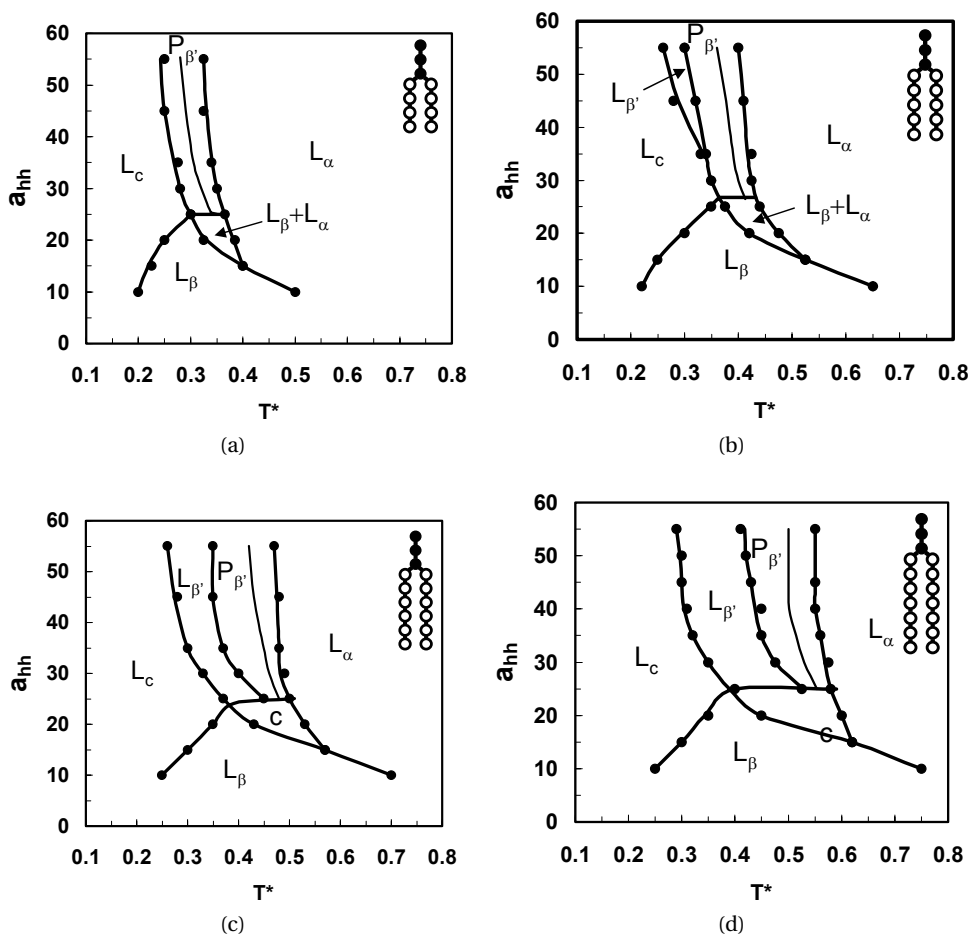


Figure 5.11: Phase diagrams of model lipids as a function of head-head repulsion and reduced temperature: (a) $h_3(t_4)_2$, (b) $h_3(t_5)_2$, (c) $h_3(t_6)_2$, (d) $h_3(t_7)_2$. In (c) and (d) **c** denotes a coexistence region, of which the exact structure was difficult to determine. A description of this phase can be found in the text.

phase, a collective tilt with respect to the bilayer normal and no overlap of the two sheets of the bilayer. The temperature- and a_{hh} stability depends on tail length: the $L_{\beta'}$ is more stable if the tails are longer. The appearance of the $L_{\beta'}$ phase is in agreement with experimental data of the phase behavior. For DLPC (DiLauroylPC, 12 carbons per tail) the $L_{\beta'}$ phase is not observed, while this phase becomes more stable if the tail length is increased from 14 to 20 carbons per tail [9, 94].

With increasing tail length the temperature at which the main transition occurs increases, in agreement with experimental observations. This shift in melting temperature is most significant for the $L_{\beta'} \rightarrow L_{\alpha}$ transition, the $L_{\beta'} \rightarrow P_{\beta'}$ transition, and from the transition of the $L_{\beta} - L_{\alpha}$ coexistence region to the pure L_{α} phase. The transition from the L_c phase to the $L_{\beta'}$ is at an almost constant temperature independent of tail length. Thus the increased stability of this phase with increasing tail length is caused by the higher $L_{\beta'} \rightarrow P_{\beta'}$ transition temperature.

The temperature region, in which the $P_{\beta'}$ phase is the stable phase, does not depend on tail length. However, we find an increase of the period of the ripple with increasing tail length. Using a system containing 800 lipids, we observed that with increasing tail length the rippled structure was not formed parallel to the y - or z -axis of the system, but diagonally, as was also observed with the lipid $h_3(t_8)_2$ at $a_{hh} = 55$. By adapting the system size to a maximum of 3200 lipids, the rippled phase was formed for all tail lengths with an increasing period going from 4 to 8 beads in the tail.

For the two longest models studied, it is difficult to determine the structure of the bilayer in the coexistence region at the low head-head repulsion parameters ($a_{hh} < 25$). This coexistence region (denoted with c in the phase diagrams of figure 5.11(c) and (d)) seems to be a coexistence between the L_{β} , the $L_{\beta'}$ phase and the L_{α} phase. With increasing temperatures the average tilt angle first decreases, indicating the $L_c \rightarrow L_{\beta}$ transition. At the second transition the tilt angle again increases till the transition to the L_{α} phase occurs, where no tilt angle is observed. The rippled structure was never observed at these low repulsion parameters.

5.5 Discussion

In this section, we compare the results from our simulations with the experimental data. First, we will discuss the phase diagram as a function of temperature and tail length of the lipids. Then we pay attention to the anomalous swelling, which is observed near the main transition $P_{\beta'} \rightarrow L_{\alpha}$, and, finally, we discuss the structure of the rippled phase.

5.5.1 Phase behavior as a function of temperature and tail length

In figure 5.12 we plotted the transition temperatures as a function of tail length for the typical head-head interaction used by Groot [50], $\alpha_{hh} = 35$. The low temperature phase is the highly ordered L_c phase and at high temperatures the L_α phase is the stable phase. With increasing temperatures the transition $L_c \rightarrow L_\alpha$ goes through different phases, dependent on tail length. For the shortest tail length ($N=4$) no $L_{\beta'}$ phase is observed and the transition holds $L_c \rightarrow P_{\beta'} \rightarrow L_\alpha$. For longer tails the $L_{\beta'}$ phase is observed in between the L_c and $P_{\beta'}$ phase. Qualitatively, this phase diagram nicely resembles the experimental phase diagrams [119, 120]. The temperatures of the $L_{\beta'} \rightarrow P_{\beta'}$ and the $P_{\beta'} \rightarrow L_\alpha$ transition increase with increasing tail length. The $L_{\beta'}$ phase is not observed for the shortest lipid, but for longer tail lengths the stability of this phase increases with increasing tail length. The only difference is that we find a constant temperature region in which the rippled phase is stable, independent of tail length, while experimentally this region decreases and finally disappears with increasing tail length.

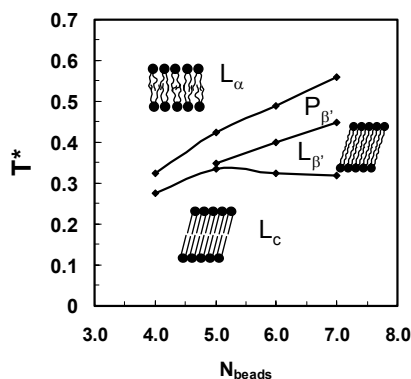


Figure 5.12: Transition temperatures as a function of tail length for the head-head repulsion parameter $\alpha_{hh} = 35$.

We can translate the reduced temperatures to the real temperatures, by, for example, taking the temperatures of the pretransition $L_{\beta'} \rightarrow P_{\beta'}$ and the main transition $P_{\beta'} \rightarrow L_\alpha$ of the phospholipid DMPC as reference points. As was discussed in chapter 4, DMPC corresponds with the model lipid $h_3(t_5)_2$. If we take $T^* = 0.35$ and $T_{exp} = 15.3^\circ\text{C}$ for the pretransition temperature and $T^* = 0.425$ and $T_{exp} = 24.0^\circ\text{C}$ for the main transition, we obtain the linear relation $T_{exp} = 116 \times T^* - 25.3$. This relation leads to large discrepancies from the experimental values for the pre- and main transitions of the other lipids. As an example, we take a model lipid with a tail length of 7 beads. This mesoscopic model corresponds with the phospholipid DAPC, containing 20 carbons in the hydrocarbon chains. From our simulations, we find $T^* = 0.56$

for the main transition $P_{\beta'} \rightarrow L_{\alpha'}$, which corresponds with $T_{\text{exp}} = 40^\circ\text{C}$. However, the main transition of DAPC is experimentally determined at $T_{\text{exp}} = 64^\circ\text{C}$ [10].

At this point, it is important to recall that the parameters have been tuned to reproduce the compressibility of water and the Flory-Huggins solubilities at ambient conditions. The DPD model is too simple to expect that, once these parameters have been fitted at a given temperature, one would, for example, reproduce the compressibility of water at other temperatures. This gives, however, a temperature dependent parameter which would make the interpretation of our results more complex. Therefore, we do not expect a quantitative agreement.

5.5.2 Anomalous swelling

One of the main questions in the phase behavior of PC's is the observed anomalous swelling (non linear increase of the lamellar repeat distance with temperature) near a phase transition. For long times this swelling was considered to be a key factor in the formation of the rippled phase. However, it is not clear what causes this anomalous swelling [94, 114].

Experimental work and theories suggest that the swelling could be caused by increased interactions between bilayers due to changes in the Helfrich undulation forces [121–126]. Approaching the transition temperature T_m , the bilayer has a reduced bending rigidity and as a result the fluctuations of the bilayer increase. Due to these increased bilayer fluctuations the steric repulsion between bilayers increases. As a result the thickness of the water layer in between two bilayers becomes larger, which causes the anomalous swelling [62, 125]. Another explanation is that the anomalous swelling is mainly caused by an increase of the thickness of the hydrocarbon region [62, 114]. Near the transition temperature the hydrocarbon chains show a critically straightening. In most papers a coupling is made between the various explanations: due to a straightening of the tails, the fluctuations of the bilayer increase, which finally results in the anomalous swelling.

In a recent paper, Mason *et al.* [115] showed that the anomalous swelling is not coupled to the formation of the rippled phase $P_{\beta'}$. By successively adding methyl groups to DiMyristoylPhosphatidylEthanolamine (DMPE, no methyl groups attached to the terminal nitrogen) to form DMPC (three methyl groups attached) it is observed that anomalous swelling occurs in the case of mmDMPE (monomethyl-DMPE) and dmDMPE (dimethyl-DMPE), while bilayers of these phospholipids undergo a transition into the flat gel phase (L_{β}) rather than into the rippled phase.

In our simulations we calculated the contribution of the hydrophobic thickness (D_c) and the thickness of the head group region (D_h) to the swelling for $h_3(t_5)_2$ for different repulsion parameters. Figure 5.13(a) shows the hydrophobic thickness and the bilayer thickness D_b as a function of temperature and in figure 5.13(b) the thick-

ness of the head group region is plotted. We observe a large increase of the hydrophobic thickness, which may be responsible for the swelling of the bilayer.

The behavior of the hydrophobic thickness is closely related to the phase behavior of the bilayer (see figure 5.11(b)). For the lowest repulsion parameter ($a_{hh} = 10$), we observe upon decreasing temperature the transitions $L_\alpha \rightarrow L_\beta \rightarrow L_c$. Decreasing the temperature in the L_α phase results in an increased ordering of the chains and in the L_β phase the chains are ordered and do not show a tilt. Further decrease of the temperature gives the L_c phase and because of the tilt, the hydrophobic thickness is smaller, which explains the maximum in the curve. This maximum is not present in the curve for the bilayer thickness D_b . Figure 5.13(b) shows that for $a_{hh} = 10$ decreasing the temperature straightens the heads and, in particular, in the L_c phase this increase in the thickness of the head region completely compensates the decrease of the hydrophobic thickness.

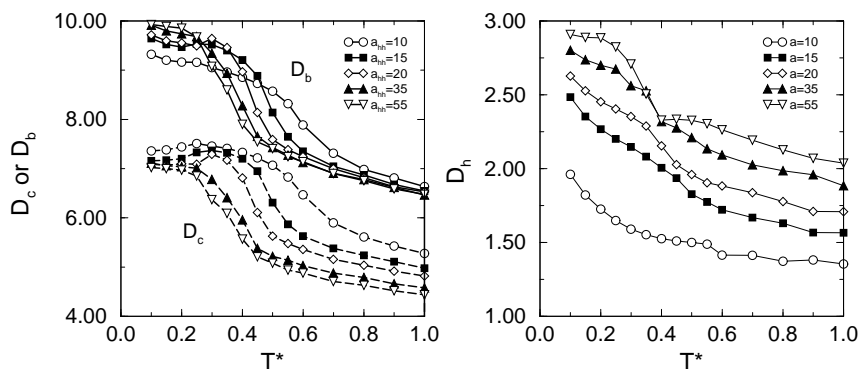


Figure 5.13: (a) Bilayer thickness (D_b)(solid lines), thickness of the hydrophobic region (D_c)(dashed lines), and (b) thickness of the head group region (D_h) as a function of temperature for various head-head repulsion parameters of the $h_3(t_5)_2$ lipids.

For higher values of a_{hh} , but still for $a_{hh} \leq 25$, the main trend is equal to the trend observed for $a_{hh} = 10$. Figure 5.11(b) shows that the temperature range, for which the L_β phase is stable, decreases. Hence, the increase of the hydrophobic thickness in the L_β phase occurs in a much narrower temperature interval and therefore gives a sharp increase of D_c . For $a_{hh} = 20$, the decrease of D_c in the L_c phase is not completely compensated by the increase of the thickness of the head groups (D_h , see figure 5.13(b)) and for this head-group interaction, we observe a decrease of the bilayer thickness.

For $a_{hh} > 25$, for which the ripples phase $P_{\beta'}$ is observed, we find a strong increase of the hydrophobic thickness associated to the $L_\alpha \rightarrow P_{\beta'}$ transition. We also observe a discontinuous increase in the thickness of the head group region, located at the point where the $L_\alpha \rightarrow P_{\beta'}$ transition occurs. Ordering of the tails and the head

groups occurs simultaneously. Due to the strong hydration of the head groups at high a_{hh} the head groups will stretch into the water phase, such that each segment is surrounded by water. This larger increase in D_h causes the change in order of the curves representing the bilayer thickness in the low temperature region.

For all values of a_{hh} the increase of the bilayer thickness is mainly a consequence of the increase of the hydrophobic thickness. For $a_{hh} > 25$ the larger increase of the bilayer thickness is caused by a relatively larger contribution of the thickness of the head group region.

We observe for the model lipid $h_3(t_5)_2$, which corresponds to the phospholipid DMPC (see chapter 4), that increasing a_{hh} from a very low value to a value above the triple point results in similar swelling curves to the curves obtained by increasing the size of the head group by adding successively methyl groups to form DMPC from DMPE [115]. Increasing the number of methyl groups in the head groups corresponds with increasing the repulsion between the lipid head groups, since the steric hindrance increases with increasing number of methyl groups and the ionic interactions decrease as the head group is larger. For DMPE, which corresponds to a lipid with head-head repulsion parameter $a_{hh} = 10$, the hydrophobic thickness increases gradually at the transition $L_\alpha \rightarrow L_\beta$. The swelling curves of mmDMPE and dmDMPE, corresponding with $a_{hh} = 15$ and $a_{hh} = 20$, respectively, show a maximum near the main transition. The maximum in bilayer thickness for dmDMPE is sharper than for mmDMPE [115]. In our simulations, we show that the occurrence of this maximum is due to an increase of the hydrophobic thickness, caused by the formation of the L_β phase. Since the stability of this L_β phase decreases with increasing head-head repulsion, the maximum becomes sharper until the triple point is reached at $a_{hh} = 25$. For the PC lipids, corresponding with the high values of a_{hh} ($a_{hh} > 25$), the experimentally obtained curves show a sharp maximum at the main transition for the shorter chain lengths. For the longer tail lengths, this maximum disappears [124, 126]. We observe a large increase of the bilayer thickness for all lipid tail lengths, caused by a simultaneously increase of the hydrocarbon thickness and the thickness of the head group region. We do not observe a maximum in the curve for the shorter lipids.

Only for DMPC, which is above the triple point a rippled phase is observed, which reinforces the conclusion of Mason *et al.* [115] that the anomalous swelling of mmDMPE, and dmDMPE is not related to the rippled phase. Our simulations show that in all cases the (anomalous) swelling is the consequence of changes of the conformation of the hydrocarbon tails. Of course, experiments are often performed on multiple layers and changing the temperature may also change the amount of water in between the layers. Also, the electrostatic interactions between the lipid head groups can play a crucial role in the swelling of the bilayer [123, 127]. These effects are not included in our simulations.

5.5.3 Structure of the rippled phase

One of the main questions in the phase diagram of a phospholipid bilayer is the existence of the rippled phase, since this corrugated phase lies between the two flat phases $L_{\beta'}$ and L_{α} . Besides much experimental work, a lot of theoretical and modeling studies are devoted to the nature of the rippled phase. Different approaches are used to model the rippled phase. Macroscopic theories regard the bilayer as a whole and explanations can thus be found in the elasticity and the curvature of the membrane [27, 28, 97, 102, 109, 118, 122]. Microscopic theories explain the existence of the rippled phase in terms of the packing properties of individual molecules [96, 99, 104, 110]. In these studies the formation of the ripple is often attributed to a packing competition between the lipid head groups and the hydrocarbon chains. Also a combination of these two approaches is possible: it is proposed that competition exists between macroscopic curvature and microscopic properties of the bilayer [103, 107, 113]. A third approach is the approach in which interbilayer interactions are taken into account in the formation of the ripple [104].

The general picture of the rippled phase is that the shape is an asymmetric sawtooth, with a difference in thickness between the long and the short arm [97–101]. However, there are also studies in which the shape of the ripple is sinusoidal [28, 96, 102–104]. The wavelength of the ripples is in the range of 120 - 160 Å if a bilayer is heated from the $L_{\beta'}$ phase. This wavelength increases with increasing length of the hydrocarbon tails [98, 99, 128, 129]. In this section we compare the results of our simulations with some of the experimental and theoretical studies on the structure of the rippled phase. We do not pay attention to the sawtooth or sinusoidal shape of the ripple, since much larger systems are needed to observe the typical sawtooth.

In most experimental work, the sample is not a unilamellar system but a multilayer. It is assumed that the ripples occur due to bilayer-bilayer interactions, which are mediated by the lipid head groups. In an AFM study on supported double DPPC-bilayers on mica Fang and Yang [116] detected the existence of a ripple structure in the upper bilayer of the double-bilayer regions only. This indicates that the bilayer-bilayer interaction might be responsible for the formation of the ripple structures. However, also in unilamellar systems the pretransition is found. Mason *et al.* [117] argue that in the AFM study the undulations are suppressed by the substrate and they provide evidence that the rippled phase exists in large unilamellar vesicles of DPPC. Another study by Takeda *et al.* [118] shows that the ripple structure appears in a system if the thickness of the water layer between the lipid bilayers is increased by the addition of salt, indicating that the ripple originates mainly in the intralayer interactions. In these unilamellar systems the transition is broader and less separated from the main transition [28, 130].

All our simulations are performed on a single bilayer and we observe the rippled phase in all systems, provided that $a_{hh} > 25$. Although we apply periodic boundary

conditions in all three directions, there is no bilayer-bilayer interaction. We impose that the thickness of the water layer between two bilayers is at least $4r_c$ to guarantee that two periodic images do not have any interactions in the x -direction. To test whether the results change if the bilayers do interact, we performed simulations on a multilayer system at $a_{hh} = 35$ in the temperature range $T^* = 0.1$ to $T^* = 0.7$. These simulations gave the same results as were obtained for a single bilayer, indicating that interbilayer interactions are not the key factor in the formation of a rippled structure.

It is difficult to determine directly the structure of the two arms of the ripple, which differ in thickness, experimentally [64]. For example, Sun *et al.* [99] assume that the X-ray diffraction patterns are best fitted with a model in which the asymmetry of the bilayer height profile is the dominant feature. The major side of the ripple is similar to the $L_{\beta'}$ phase, while the minor side may be more the fluid L_{α} phase. The formation of the ripple due to the coexistence between these two phases is also proposed in many other experimental and theoretical studies [96, 109–113]. However, since it was found that in the $P_{\beta'}$ phase the chains are mainly frozen in an all-trans configuration [108], the explanation of coexistence is less probable and the difference in the existence of the ripple is attributed to a change in tilt angle and/or elastic properties [27, 28, 104–107]. Sengupta *et al.* [107] conclude that the asymmetry of the ripple is not caused by an asymmetry of the height profile, but that the difference in the bilayer thickness is the primary feature. In this model the height profile is symmetric and the differences in the thickness are attributed to a mean tilt of the hydrocarbon chains.

Our simulations show that the thickness in the two parts of the ripple is different, due to coexistence of the L_c or $L_{\beta'}$ phase and the L_{α} phase. In the thick part (L_c or $L_{\beta'}$), the tails have a preferred tilt, while in the thin part (L_{α}) this tilt has disappeared. The contribution of the L_{α} phase in the $P_{\beta'}$ phase increases with increasing temperature (see figures 5.6 and 5.9), and at the condition of 50%-50% of both phases (L_c or $L_{\beta'}$ and L_{α}) we find a structure that is similar to the rippled structure. This indicates that both the pretransition and main transition are caused by the same effect of chain melting [96]. In the case of coexistence, the chains are not frozen in an all-trans conformation as was proposed by Cameron [108]. However, spectroscopic [111] and diffusion studies [131] have shown the existence of a significant fraction of disordered chains, supporting the presence of the L_{α} phase.

A surprising aspect of the rippled phase is that, unlike ordinary coexistence, the system does not minimize the total interfacial area formed by the two phases. Our simulations show that the head-head interaction is a key factor in the formation of the ripple: if $a_{hh} < 25$ we do not observe the rippled phase. For $a_{hh} > 25$ the system can gain energy if more head groups are exposed to water. In the coexistence region the head-group water contact area is locally increased (see figure 5.14), hence by in-

creasing the number of interfaces the system can lower its energy. We also observe this tendency to increase the head-group water contact area, if we perform simulations in the region where there is coexistence of the two phases, but not at the condition of 50%-50% $L_{\beta'}$ – L_{α} . We observe that at different ratios of $L_{\beta'}$ – L_{α} more than one domain of one phase in the dominating phase is formed (see figure 5.9). In this way, the number of head groups exposed to water is larger than if only one domain is formed.

Obviously, the system can lower its energy by increasing the number of interfaces in the rippled structure. The total number of interfaces, however, will be limited by the repulsive forces between the ripples. The origin of this force is the elastic energy, which tends to minimize the curvature of the interface between the thick and thin parts. This aspect will depend on the tail length; the longer the tails, the larger the thickness that has to be crossed. This explains why we observe that the period of the ripple increases with tail length. Within the thick part of the ripple, the average orientation of the tilt is parallel to the direction of the ripple, which is an important factor in stabilizing a linear interface.

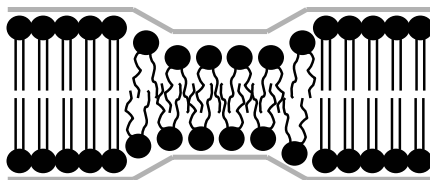


Figure 5.14: Schematic figure of the rippled phase. Because of the coexistence between the thick (L_c or $L_{\beta'}$) and thin (L_{α}) phases, the system can lower its energy by increasing the number of interfaces. In this way the total water head-group area is increased at the interfacial region.

It is interesting to compare these results with the continuum Landau theory of Lubensky and MacKintosh [28], in which a rippled phase occurs due to the coupling of molecular tilt to the membrane curvature if the longitudinal elastic constant is negative. Our results show that the microscopic origin of this negative constant is the surface area of the heads, which is not compatible with the lateral density of the tails. This confirms the reasoning by Carlson and Sethna [104]. They argue that the packing competition between the head groups and chains is the essential feature for two reasons. First, the ripple does not occur in bilayers consisting of phospholipids with smaller head groups and second, the pretransition temperature increases as the hydrocarbon chain length is increased, which suggests that the attraction between the chains is important.

5.6 Conclusions

In this investigation, we studied the phase behavior of phospholipid bilayer, and especially the formation of the rippled phase, as a function of temperature, head group interactions, and tail length. The formation of the rippled phase, its relation with anomalous swelling of these membranes, and the structure of the ripple observed about 30 years ago has attracted the attention of many researches. Many different theories have been put forward to explain the formation of this phase, but a molecular explanation is still lacking. Therefore, we perform computer simulation on a mesoscopic model of a lipid, that consists of a head group of three hydrophilic beads and two hydrophobic tails varying in length from 4 to 7 beads.

We showed that we can reproduce the experimentally observed phases. At low temperatures the L_c phase is stable, in which the tails are highly ordered and show a tilt with respect to the bilayer normal. Increasing temperature leads to the melting of the bilayer, which goes through different phases, dependent on the head group interactions. For low values of the head-head repulsion parameters, the head groups want to expel water and as a consequence the transition to the fluid L_α phase takes place via the flat gel phase L_β , in which the tilt has disappeared. For high values of the head-head repulsion parameter, we find a coexistence region of the gel phase and the fluid phase. We observe the rippled structure ($P_{\beta'}$) in a narrow region around the line where we have approximately 50% L_c or $L_{\beta'}$ phase and 50% L_α phase. For longer tails, this phase is preceded by the $L_{\beta'}$ phase. The stability of this phase increases with increasing tail length.

A key factor in the understanding of the rippled phase, is a frustration induced by the optimal surface area of the heads which is not compatible with the optimal lateral density of the tails. For high values of a_{hh} the system can gain energy if more head groups are exposed to water and therefore, at the condition of 50-50% material of both phases, the space filling problem leads to a striped solution. Taking into account the curvature constrain, the period of the ripple increases with increasing tail length. The anomalous swelling, observed at the $P_{\beta'} \rightarrow L_\alpha$, is caused by conformational changes of the lipid tails, but is not directly related to the rippled phase.

VI

Induced interdigitation

Abstract

In this chapter, we study the induced interdigitation of bilayers consisting of double-tail lipids by adding an additional hydrophobic bead to the head group or by adding model alcohols to the bilayer. In both situations interdigitation is induced by the increased head group surface area, which leads to the formation of voids in the hydrophobic core. Since voids in the bilayer core are energetically unfavorable, the interdigitated phase is formed, in which the lipid tails of one monolayer interpenetrate the opposing layer, filling up the voids. With the additional bead we find that an increased steric hindrance plays the crucial role in increasing this area and that an increased head-head repulsion facilitates the formation of the interdigitated phase. In the case of adding alcohol, we reproduce the experimental observations, but at much lower concentrations at the interface than predicted experimentally. The transition from a non-interdigitated to an interdigitated phase, via a coexistence region, depends on the length of the alcohol, the concentration, and temperature.

6.1 Introduction

In chapter 3 we showed that a bilayer, consisting of monotail lipids, can spontaneously form the interdigitated $L_{\beta 1}$ phase. Interdigitation does not occur in bilayers of symmetrical chain phospholipids, but has to be induced. Examples of factors that can induce interdigitation are changes in the environment, like in the hydrostatic pressure or in the pH of the solution [65], or by adding small amphiphilic molecules, like alcohols [132–134], or anesthetics [135] (see ref. 72 for a review). Besides changes in the environment, interdigitation can also be induced by changes in the molecular structure of the lipid, for example by introducing an ester-linkage in the head group of the phospholipids [136, 137]. In this chapter, we study the effect of such a linkage and the addition of alcohol to the bilayer.

Lipid bilayers, consisting of lipids with an additional hydrophobic group in the head group, show the spontaneous formation of a fully interdigitated bilayer in the low temperature region [136, 137]. One way to obtain these lipids (for example 1,2-Diacyl-P-O-ethyl-phosphatidylcholines) from the zwitterionic PC lipids is to add a (hydrophobic) ethyl group at the P-O in the head-group region. The esterification of this group leads to the formation of cationic lipids, that play an important role in the delivery of DNA to eukaryotic cells. The interdigitation in these bilayers is induced by two effects: charge repulsion of the cationic head groups and steric hindrance in the head group region caused by the presence of the ethyl group. Lewis *et al.* [136] found that converting the zwitterionic head group into a positively charged head group by esterification is of main importance for inducing interdigitation and that the steric hindrance facilitates the interdigitation.

Short-chain alcohols (methanol through heptanol) are also known to induce interdigitation. In the first instance it was found that these alcohols have two different effects on the transition from the low temperature gel phase to the high temperature fluid phase, dependent on concentration [138]. At low concentrations of alcohol, the main transition temperature shifts to a lower temperature, while at high concentrations this transition temperature shifts to a higher temperature compared to a pure lipid bilayer. This effect was called the “biphasic effect”. One year later, Simon and McIntosh [66] observe in their study the formation of the interdigitated phase at high concentrations of alcohol, which explains the biphasic effect. At low concentrations of alcohol the disorder of the lipid tails increases, leading to a lower transition temperature. At high concentrations the more tightly packed interdigitated phase is formed, resulting in an increase of the transition temperature.

Interdigitation can be understood if we consider the addition of alcohol molecules to the bilayer. The alcohol molecules replace the interfacial water molecules: the OH group binds to the phosphate group of the lipid head group and the hydrophobic

tail sticks into the hydrophobic core of the bilayer. Since the OH-group binds to the phosphate moiety of the lipid head group [139], lateral space is created between the head groups, leading to voids in the hydrophobic core. These voids are energetically unfavorable and thus the system will minimize the energy by the formation of an interdigitated phase. By interdigitation the system gains energy due to the stronger vanderWaals interaction [66, 140, 141] in the interdigitated phase compared to the non-interdigitated phase and due to an entropy gain by replacing the highly ordered water molecules at the interface by alcohol molecules [66, 133, 142]. Since the tail ends of the alcohol molecules shield the tail ends of the lipids from the interfacial water, the energy cost in the formation of the interdigitated phase is minimized.

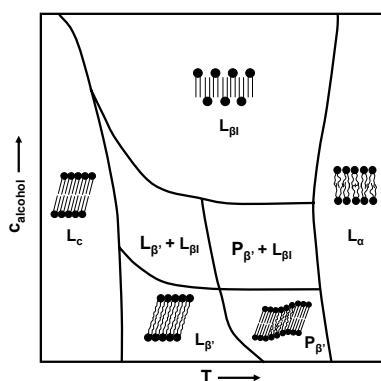


Figure 6.1: Schematic representation of the phase diagram of a PC/alcohol mixture as a function of the concentration alcohol and temperature [140, 143–145]. The various phases are schematically drawn and are explained in the text.

Phase diagrams of various lipids and alcohols are constructed [140, 143–145] (see figure 6.1 for a schematic sketch of an experimental phase diagram). At high temperatures the fluid L_α phase is stable. At low temperatures, various structures are found, dependent on temperature and alcohol concentration. At low concentrations, we find the transition from the highly ordered subgel or L_c phase via the gel phase $L_{\beta'}$ to the rippled phase $P_{\beta'}$. In all these phases the tails have a tilt with respect to the bilayer normal. At high concentrations of alcohol the rippled phase disappears, and the interdigitated phase $L_{\beta I}$ is formed, in which the tails do not show a tilt. In between these extremes a coexistence region is observed between the rippled phase or the gel phase and the interdigitated phase.

The addition of alcohol has a larger effect on the pretransition $L_{\beta'} \rightarrow P_{\beta'}$ than on the main transition $P_{\beta'} \rightarrow L_\alpha$. At low concentrations of alcohol this transition is shifted to lower temperatures and after the critical concentration $c_{L_{\beta I}}$ (the concentration at which interdigitation is complete) the rippled phase disappears [146]. Questions in the formation of the interdigitated phase which are still not (completely)

solved are the distribution of the alcohols in the bilayer, the exact molecular structure of the alcohol-induced interdigitated phase, and the concentration of alcohol in the lipid bilayer at which interdigitation occurs.

In this chapter, we investigate whether, similar to experiments, we can induce interdigitation in our mesoscopic model by adding a model ester-linkage to the lipid head group or by the addition of small amphiphilic molecules. In experiments it is not always possible to isolate a single cause and effect relation. Therefore, we use computer simulations to investigate the different factors that can play the crucial role in the induction of the interdigitated phase.

6.2 Computational details

In this investigation we consider a basic lipid consisting of a head group with three hydrophilic segments and two tails with variable length (see figure 6.2). Two consecutive beads are connected by harmonic springs with spring constant $k_r = 100.0$ and $r_0 = 0.7$. To control the chain flexibility, we added a bond-bending potential between three consecutive beads in the tails with bending constant $k_\theta = 6.0$ and equilibrium angle $\theta_0 = 180^\circ$. An additional bond-bending potential is applied between the vectors connecting the tails to the head group, with $k_r = 3$ and $\theta_0 = 90^\circ$. The hydrophilic and hydrophobic interactions of the different particles are described using the soft repulsive interactions: $F_{ij}^C = a_{ij}(1 - r_{ij}/r_c)\hat{\mathbf{r}}_{ij}$. The values of a_{ij} used in the simulations are $a_{ww} = a_{tt} = 25$, $a_{hh} = 35$, $a_{ht} = a_{wt} = 80$, and $a_{hw} = 15$ (see chapter 2 for more details).

To investigate the effect of adding an ethylgroup to the phosphate group of the lipid head group, we attached an additional hydrophobic bead to the second bead (h_2) of the head group (see figure 6.2(a)). We study two different tail lengths and to investigate the influence of the interaction between the lipid head groups, we vary a_{hh} from 5 to 55.

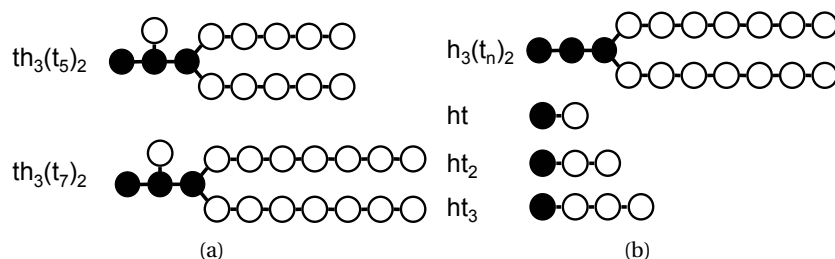


Figure 6.2: Models used in the simulations with their nomenclature: (a) models of lipids with an additional hydrophobic bead to the head group and (b) models used in the lipid/alcohols system (n denotes the number of hydrophobic beads in the tails).

The model of the alcohols consists of one hydrophilic head bead and a tail that varies in length from one to three hydrophobic beads (see figure 6.2(b)). Using the mapping procedure in which 1 DPD particle represents a volume of 90 \AA^3 , the alcohols methanol through pentanol correspond with the coarse-grained models ht and ht₂ and hexanol and heptanol corresponds with the model ht₃. The bond-bending potential with $k_\theta = 6.0$ and $\theta_0 = 180^\circ$ was also applied between three consecutive beads of these alcohols.

The system was initialized by placing 200 phospholipids randomly in a simulation box. In the case of the addition of alcohol to the system, the model alcohols were placed together with the lipids, varying in number from 20 to 200. 3200 - 6700 water particles were added to ensure that a bilayer does not have any interaction with its periodic image. At a temperature of $T^* = 1.0$ a bilayer was formed, using DPD steps only. After the formation of the bilayer we allowed the bilayer to adopt a tensionless configuration by applying both DPD and Monte Carlo, in which the area of the bilayer is changed. We then slowly cooled the system from $T^* = 1.0$ to $T^* = 0.1$. A typical simulation required 100,000 cycles of which 20,000 cycles were needed for equilibration. Per cycle it is chosen with a probability of 70% whether to perform 50 DPD time steps or to make an attempt to change the area of the box.

6.3 Effect of an additional bead in the head group

In our simulations we are able to investigate the influence of an increased repulsion between the head groups and the presence of the ethylgroup separately. In a bilayer of monotail lipids, interdigitation was induced by increasing the repulsion between the head groups. For double-tail lipids we have shown in chapter 5 that even at the highest repulsion parameter applied ($a_{hh} = 55$), the low-temperature phase is the non-interdigitated gel phase. However, the addition of an additional hydrophobic bead to the head group of the lipid, does lead to the formation of the interdigitated phase. In figure 6.3 a snapshot of a patch of the bilayer and the corresponding density profile for th₃(t₅)₂ lipids with $a_{hh} = 55$ at $T^* = 0.25$ are shown.

The effect of the additional bead is twofold: it causes an increase in the distance between the head groups and it changes the conformation of the head group. The additional hydrophobic bead sticks into the hydrophobic core, facing the tails of the lipids in the opposite monolayer (see figure 6.3(a)), and forcing the second head bead to the interface. Since the additional head bead is located at the same depth in the bilayer as the first bead in the tail, given a tail length of 5 beads, interdigitation occurs up to four tail beads, as can be seen from the density profile (figure 6.3(b)).

To analyze the effect of the repulsion parameter (which could, for example, mimic the charge on the head group or changing the salt concentration) and the tail length on the stability of this interdigitated gel, we compared the lipid types th₃(t₅)₂ and th₃(t₇)₂ with head-head repulsion parameters varying from $a_{hh} = 5$ to $a_{hh} = 55$. In

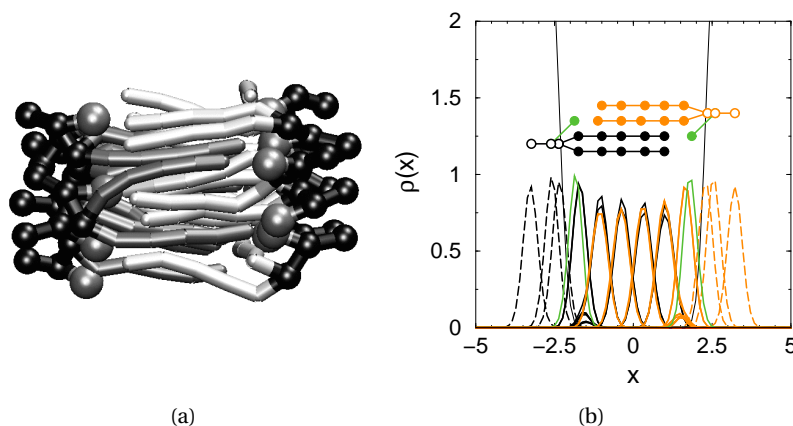


Figure 6.3: (a) Snapshot and (b) density profile of $th_3(t_5)_2$ lipids at $T^* = 0.25$. The additional hydrophobic bead is depicted as a larger grey sphere in (a) and the lipid tails in one monolayer are darker grey to distinguish them from the tails of the opposite monolayer.

figure 6.4 the corresponding phase diagrams are shown.

At the lowest repulsion parameter $a_{hh} < 7$, the lipids demix; inverted micelles are formed within the hydrophobic core of the bilayer. In the case of $th_3(t_5)_2$ (figure 6.4(a)) the bilayer is in the liquid crystalline phase at temperatures $T^* > 0.5$ for $a_{hh} > 7$. At low temperatures different phases can be observed, as a function of a_{hh} . For the large head-head repulsion, the system gains energy if water molecules hydrate the lipid heads, and for $a_{hh} > 30$ this hydration is sufficient to stabilize the interdigitated phase. For $a_{hh} < 30$ we observe coexistence between the interdigitated phase $L_{\beta I}$ and the tilted phase $L_{\beta'}$.

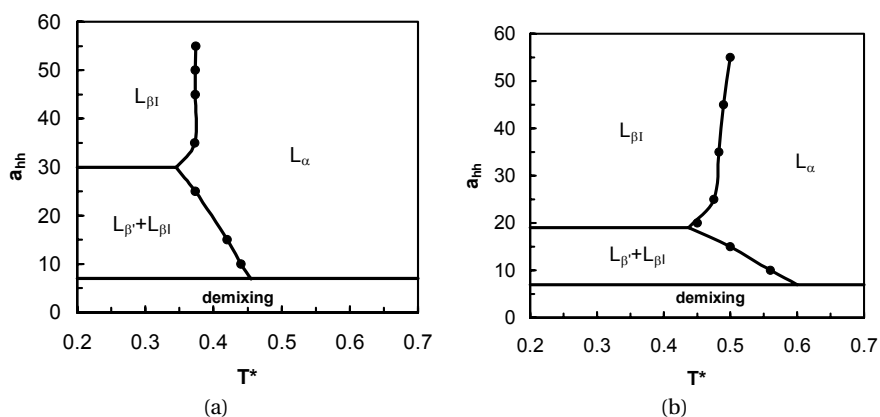


Figure 6.4: Phase diagrams for a bilayer consisting of (a) $th_3(t_5)_2$ lipids and (b) $th_3(t_7)_2$ lipids.

The effect of increasing the head-head repulsion on the gel to liquid crystalline transition temperature is much more pronounced for the $L_{\beta'} \rightarrow L_{\alpha}$ compared to $L_{\beta'} + L_{\beta I} \rightarrow L_{\alpha}$. This can be understood from the fact that in the completely interdigitated phase the average distance between the heads is larger than in the non-interdigitated part of the coexistence region. A further increase in this distance does not have a significant effect on the stability of the interdigitated gel phase.

Increasing the tail length from 5 to 7 beads in the tails, leads to the phase diagram depicted in figure 6.4(b). Similar to the single-tail lipids, increasing the tail length stabilizes the gel phases and hence shifts the melting transition to higher temperatures. Also, the coexistence region between the interdigitated and non-interdigitated phase is smaller. Because of the larger tail-tail interactions, the unfavorable contacts of the tail ends with water in the interdigitated phase, are less important and therefore a lower head-head repulsion is required to stabilize this phase for the longer tails. The critical value α_{hh}^* to induce complete interdigitation is decreased from $\alpha_{hh}^* = 30$ for $th_3(t_5)_2$ to $\alpha_{hh}^* = 19$ for $th_3(t_7)_2$.

If we now compare these phase diagrams with the phase diagrams of the monotail lipids (see figure 3.13, chapter 3) we observe some noticeable differences. Firstly, we do not observe the demixing for the single tail lipids at the very low values of α_{hh} . By adding the hydrophobic bead in the head group, the head group becomes more soluble in the hydrophobic core of the bilayer, resulting in the demixing of the bilayer. Secondly, for the monotail lipids, we do not find a region in which there is coexistence between the L_{β} and the $L_{\beta I}$ phase. And thirdly, the critical value α_{hh}^* is much lower for the monotail lipid with a tail length of 7 beads in the tail, than for the double tail lipid of the same length. For the double-tail lipids in the interdigitated phase, both tail ends are in contact with the water phase, which needs to be compensated by a higher energy gain from the adsorption of water particles in the head-group region, *i.e.* α_{hh}^* is higher compared to single-tail lipids. The additional hydrophobic head bead however, partially shields these tail ends and therefore the increase is not a factor of two. Striking is that the tail length dependence is much more pronounced in these systems, which is a consequence of the tilted configuration these molecules have in the $L_{\beta'}$ phase.

The explanation for the formation of the interdigitated phase can be found in the larger area per lipid, like in the case of the monotail lipids. In figure 6.5 we compare for the lipid $th_3(t_5)_2$ the two dimensional radial distribution function of the head-bead connecting the two tails (h_1) for lipids with and without the extra head bead (at $T^* = 0.25$ and $\alpha_{hh} = 55$).

The bilayer of $h_3(t_5)_2$ lipids is more “solid-like” than the bilayer of $th_3(t_5)_2$ lipids. Due to the interdigitation, in the second case the head groups have a larger surface area. Also the location of the peaks in both cases is different. For both lipids the

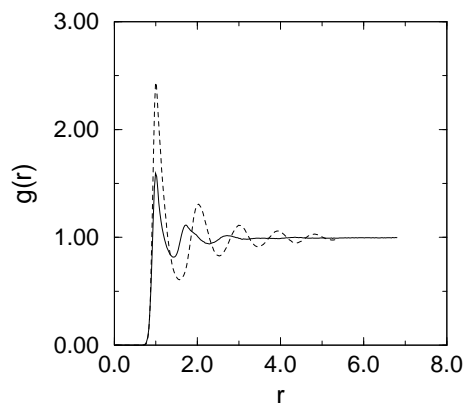


Figure 6.5: Two-dimensional radial distribution function of the head bead connecting the two tails of $th_3(t_5)_2$ (solid line) and $h_3(t_5)_2$ (dashed line) lipids at $T^* = 0.25$.

first peaks are located at the same distance, but the peak for $th_3(t_5)_2$ is considerably lower than the peak of $h_3(t_5)_2$. The second peak for $th_3(t_5)_2$ is shifted to the left, compared to $h_3(t_5)_2$. The additional hydrophobic bead is located between two head groups which are at the distance of the second peak in $g(r)$. Thus this second peak for $th_3(t_5)_2$ indeed corresponds to nearest neighbors which are at a larger distance, due to the presence of the extra bead in the head, while for $h_3(t_5)_2$ it really corresponds to next-nearest neighbors.

From these results we can conclude that interdigitation induced by addition of an ester-linkage in the phospholipid head-group region is mainly due to an increase of the head-group surface area. This larger area is due to: 1. steric hindrance of an extra group in the head group and 2. increase in head-group repulsion. We have shown that the steric hindrance plays the crucial role in inducing interdigitation and isn't just facilitating the interdigitation [136]. The additional hydrophobic segment penetrates into the hydrophobic core, increasing the interface area, and it faces the tails of the opposite monolayer, screening them from the surrounding water. The increased repulsion between the head groups alone is not sufficient to induce interdigitation, but only facilitates the formation of a complete interdigitated phase.

6.4 Induced interdigitation by alcohols

In this section we discuss the influence of the addition of small amphiphilic molecules, like alcohols, to a phospholipid bilayer. We will focus on the phase diagram of the lipid $h_3(t_7)_2$ with different model alcohols as a function of temperature and the concentration of alcohol at the interface and we shortly describe the influence

of changing the tail length of the lipid. We compare our results with the experimental results on lipid/alcohol mixtures, since these systems are investigated the most extensively.

6.4.1 Phase behavior

In our simulations we observe that at high temperatures the bilayer is in the L_α phase. With decreasing temperatures, different phases are formed, depending on the concentration of alcohol in the bilayer (N_{alc}). In figure 6.6 snapshots are shown of the various low temperature phases of the lipid $h_3(t_7)_2$ at three concentrations of the model alcohol ht_2 . At low alcohol concentrations (figure 6.6(a)), we find the non-interdigitated (sub)gel phase L_c as the low temperature phase. The alcohols are homogeneously distributed at the interface, but the concentration is too low to induce interdigitation. Experimentally, it is observed that in this region of the phase diagram the tilt angle of the lipid tails increases to a maximum of 50° [144, 147] to compensate the additional space between the tails. We do not observe an increase in the tilt angle: the average tilt angle is constant (26°) with increasing number of alcohols from 0 to 30. At high alcohol concentrations the interdigitated gel $L_{\beta I}$ is formed, in which the lipid tails do not have a tilt with respect to the bilayer normal. The tails of the lipids of one monolayer are fully interpenetrated into the opposing layer and the tail ends are facing the tail end of the alcohol (see figure 6.6(c)). In between these two extremes we find that there is coexistence between the interdigitated and non-interdigitated phase (figure 6.6(b)). The alcohols are mainly located in the interdigitated part of the bilayer.

To study the influence of the tail length and concentration of alcohol in more detail, we calculated the phase diagrams of $h_3(t_7)_2$ with the model alcohols ht , ht_2 , and ht_3 . In figure 6.7 these phase diagrams are plotted as a function of temperature and the ratio $N_{\text{alc}}/N_{\text{lipid}}$. The phase diagrams nicely resemble the experimental phase diagram (see figure 6.1). The high-temperature phase in all cases is the L_α phase. The low-temperature phase is, dependent on alcohol concentration, the L_β phase, the $L_{\beta I}$ phase, or a coexistence between these two phases. We observe that the length of the alcohol molecule had little influence on the $L_{\beta I} \rightarrow L_\alpha$ transition, but the shorter the alcohol, the more stable $L_{\beta I}$ phase. At lower temperatures the concentration of alcohol required to obtain the fully interdigitated phase increases, which is in agreement with the experimental observations of Nambi *et al.* [143].

We also observe the biphasic effect on the main transition from the gel phases ($L_{\beta'}$, $L_{\beta'} + L_{\beta'}$, or $L_{\beta I}$) to the fluid L_α phase in our simulations: at a low fraction alcohols/lipids, the transition temperature shifts to a lower temperature. Increasing the number of alcohols leads to an increasing melting temperature. If interdigitation is complete, the melting temperature is almost constant. Comparing the different chain lengths of the alcohols shows that the transition from the fully interdigitated

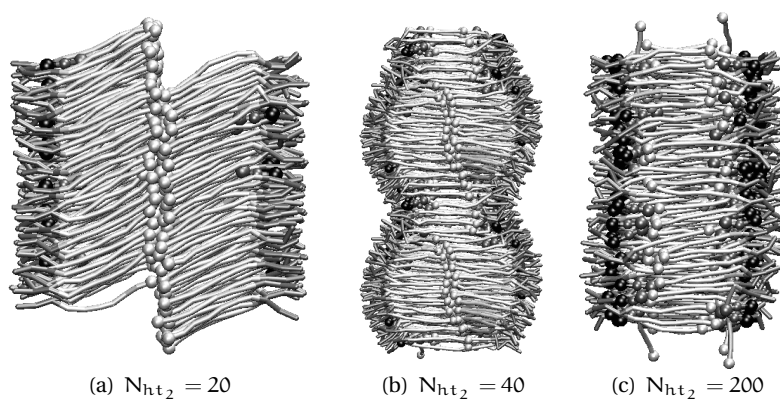


Figure 6.6: Snapshots of a bilayer consisting of the lipid $h_3(t_7)_2$ with various concentrations of the model alcohol ht_2 at $T^* = 0.25$. The bonds represent the lipids, with the darker color grey indicating the hydrophilic head group. The bonds and spheres representation indicates the alcohol molecules, where the black sphere is the hydrophilic head group. The terminal beads of both the lipid and the alcohol are depicted by a larger sphere. In (b) the system is depicted twice, so that the coexistence is illustrated more clearly

phase to the fluid phase slightly decreases with increasing chain length. Experimentally, this transition temperature is difficult to locate, since large hysteresis of this main transition was noted [144, 148–150]. In a pure lipid bilayer, that corresponds with $N_{\text{alc}}/N_{\text{lipid}} = 0$, we observed the rippled phase $P_{\beta'}$ (see chapter 5). Much larger system are required than the one studied in this chapter, to study the affect of alcohol in the stability of this phase. Therefore, we did not investigate this part of the phase diagram in detail.

Experimentally, a coexistence region between the non-interdigitated gel phase or the rippled phase and the interdigitated $L_{\beta I}$ is observed, if the concentration of alcohol is increased at a constant temperature [140, 144, 145]. Nagel *et al.* [147] observed the coexistence of the $L_{\beta'}$ and $L_{\beta I}$ phase in a DPPC/ethanol system. Mou *et al.* [151] assume that this coexistence can occur due to an inhomogeneous distribution of the alcohol in the bilayer. If the ethanol molecules could aggregate to certain regions, the local ethanol concentration in certain areas is increased to above the critical value, so that a mosaic pattern of interdigitation can be formed. Even at very low alcohol concentrations, very narrow domains of the interdigitated phase are formed [151]. Our simulations confirm that the alcohol molecules are indeed inhomogeneously distributed in the lipid bilayer. We find that, at a constant temperature, in the observed coexistence region the molefraction of alcohols in the interdigitated phase is constant. The molefraction of alcohols in the non-interdigitated part increases with increasing number of alcohols. This explains the experimentally observed coexistence region: at a fixed temperature, the part of the bilayer, which is interdigitated, increases and the non-interdigitated part decreases with increasing alcohol concen-

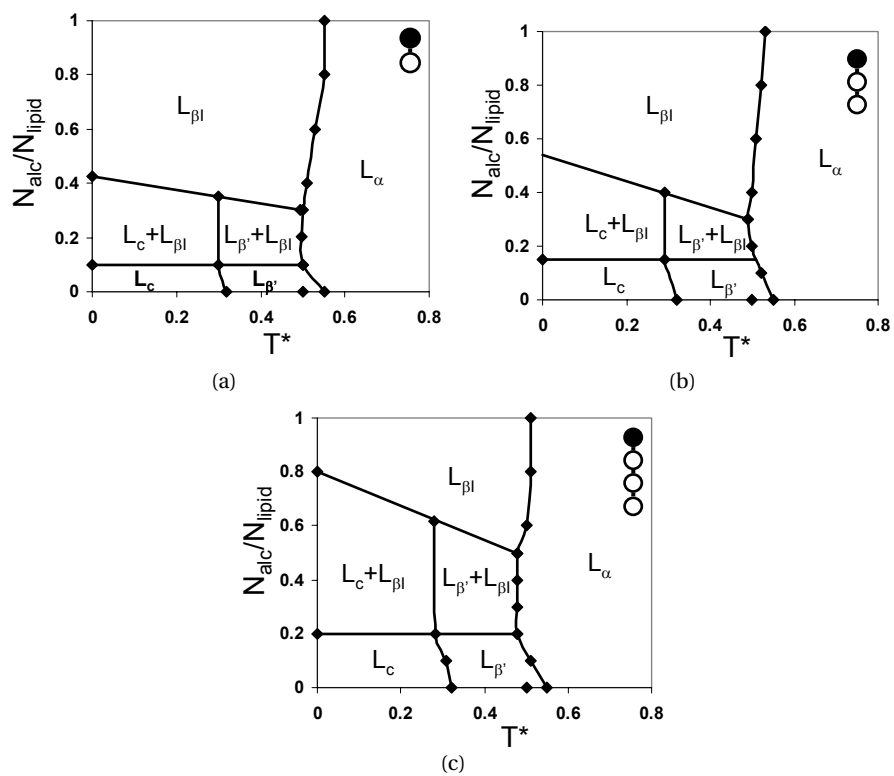


Figure 6.7: Phase diagrams of the lipid $h_3(t_7)_2$ with the model alcohols ht (a), ht_2 (b), and ht_3 (c). The dot at $N_{alc}/N_{lipid} = 0$ indicates the transition from the gel phase $L_{\beta'}$ to the rippled phase $P_{\beta'}$, as was observed in chapter 5. For the definition of the various phases, see figure 6.1.

tration.

All experimental investigations study the interdigitation as a function of the concentration of alcohol in the bulk. The critical concentration at which interdigitation is complete ($c_{L_{\beta 1}}$) decreases with increasing length of the alcohol [138, 142, 145]. However, the concentration in bulk is not necessarily equal to the concentration of alcohol in the lipid bilayer. To relate the concentration of alcohol in bulk with the concentration of alcohol in the bilayer, the membrane-buffer or partition coefficient K_p is often used. K_p describes the ratio of the solute concentration in the bulk water and in the lipid bilayer and its value increases with increasing chain length of the alcohol, caused by the hydrophobic effect [142, 152, 153]. Experimentally, the distribution of alcohol between water and lipid vesicles can be determined and it is assumed that this distribution is equal to K_p in a lipid bilayer. There is little consensus in the literature whether this procedure yields a reliable estimate of the alcohol concentration in the bilayer [154–158]. For example, it is assumed that the structure of the vesicle bilayer is representative for the bilayer phases, while depending on the temperature an alcohol molecule has a different affinity for the different phases in the order $L_{\beta 1}$ (or L_{α}) > L_{α} (or $L_{\beta 1}$) > $P_{\beta'}$ > $L_{\beta'}$ [142, 143, 145, 159], which is not taken into account.

Using computer simulations, we impose a number of alcohols in the bilayer. Comparing the phase diagrams of $h_3(t_7)_2$ with three different alcohols shows that there is little difference between the concentration of alcohols of ht and ht₂ needed to obtain the fully interdigitated phase $L_{\beta 1}$, but that the concentration of the alcohol ht₃ is higher¹. These results are in agreement with the conclusions of Rowe and Campion [142]. They found, using the bilayer partition coefficient, that up to pentanol the concentration of alcohol in the bilayer is almost constant, but that for hexanol and heptanol higher concentrations are needed.

6.4.2 Structure of the interdigitated phase

The structure of the interdigitated phase is still not well known. Adachi *et al.* [134] proposed a model in which the terminal methyl group of the alcohol faces a terminal methyl group of a lipid chain (see figure 6.8). The assumption is based on the observation that the membrane thickness increases by about 0.08 nm per one methylene unit in both the alcohol molecules and the phospholipids. This distance of 0.1 nm is the length of one CH₂-unit in the stretched chain of an alkane [160]. The small difference might be due to fluctuations in the hydrophobic chains. Furthermore, Adachi *et al.* [134] show that two alcohol molecules can occupy a volume surrounded by the PC

¹We observe that for the alcohols ht₂ and ht₃ all alcohols are at the interface, independent of the number of alcohols. For the alcohol ht we observe that at the highest number used, some alcohols diffuse into the bulk water forming micelles. This is consistent with the experimentally observed values of K_p , that indicates that adsorption of the alcohols at the interface is due to the hydrophobic effect.

head groups of one layer. From this it follows that the number of alcohol molecules should be twice as high as the number of lipids in the bilayer. Given the concentrations in the experimental procedure to determine the concentration at the interface, it is of interest to use simulations to investigate this interpretation of the experimental data in detail.

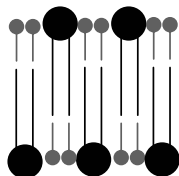


Figure 6.8: Proposed model of the interdigitated phase by alcohols [134], in which every tail end of a phospholipid is facing the tail end of an alcohol. Black molecules represent the phospholipids and grey molecules the alcohols.

In our simulations we calculated the hydrophobic thickness D_c for combinations of the lipids $h_3(t_6)_2$ through $h_3(t_8)_2$ with the alcohols ht through ht_3 (see figure 6.9). All combinations lead to a linear relation between D_c and the total number of beads. We compare this trend with half the hydrophobic thickness of a pure lipid bilayer, varying the tail length of the lipid from 5 to 8. We observe that the slope of the best fits of these two data sets are almost the same, which is in agreement with the experimentally obtained results [134, 161]. Based on this dependence of the hydrophobic thickness on the total number of beads, Adachi *et al.* [134] proposed the model depicted in figure 6.8, in which the alcohol:lipid ratio equals 2:1. However, our simulations show the same dependence, but at much lower concentrations. In figure 6.9, only the results for the ratio $N_{\text{alc}}/N_{\text{lipid}} = 1 : 1$ are given, but the same graph is obtained for lower alcohol concentrations, provided that this concentration is sufficient to induce the fully interdigitated $L_{\beta I}$ phase.

We observe that the fully interdigitated phase occurs at much lower number of alcohols than twice the number of lipids. Interdigitation can be induced at much lower concentrations in the lipid bilayer than proposed in ref. [134]. This can be explained by taking into account an energy balance between the non-interdigitated and interdigitated phase. By the incorporation of alcohols at the membrane interface, voids are created in the hydrophobic core, which are energetically unfavorable (see figure 6.10, left picture). The more alcohol, the higher the energy of the membrane. In the interdigitated phase the tail ends of the lipid are in contact with the interfacial water (see figure 6.10, right picture). Adding alcohol reduces these energetically unfavorable interactions and hence increasing the alcohol concentration decreases the energy of the membrane. Clearly at the 2 : 1 ratio, the energy of the interdigitated phase will be lowest, but at much lower alcohol concentrations the energy can already be lower compared to the $L_{\beta'}$ phase.

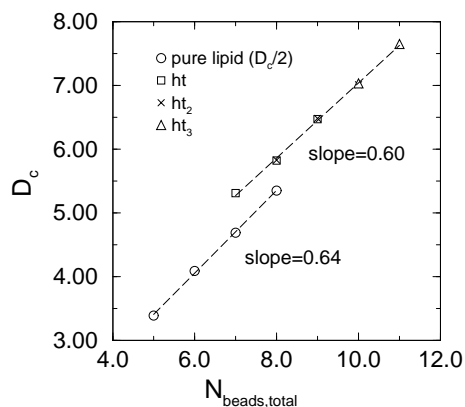


Figure 6.9: Thickness of the hydrophobic core D_c as a function of the total number of beads of the lipid and the alcohol. The length of alcohol tails ranges from 1 to 3, and the length of the lipid tails from 6 to 8 beads. The hydrophobic thickness of the pure lipid bilayer is divided by two to get a corresponding chain length dependence as in the interdigitated phase. All thicknesses are measured at a fully interdigitated bilayer, in which the ratio $N_{\text{alc}}/N_{\text{lipid}} = 1 : 1$. The dashed lines are the best fits of the pure lipid system and the mixtures of lipids and alcohols.

To use this model quantitatively, one would need to take entropy effects into account as well, but this model does rationalize why we observe in our simulations already an interdigitated phase at much lower alcohol concentrations. For the model alcohol ht, our simulations show that the interdigitated phase is formed at a ratio alcohol:lipid $\approx 1:2$ instead 2:1 as proposed by Adachi *et al.* [134]. We also observed that the hydrophobic tail of the alcohol has rotationally more freedom than the lipid tails, meaning that more than one phospholipid tail can be shielded from water by one alcohol molecule.

With this model, we can also understand the dependence on alcohol length of the

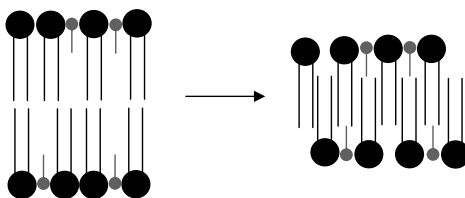


Figure 6.10: Schematical drawing of the formation of the interdigitated phase. Black molecules represent the phospholipids and grey molecules the alcohols. At a ratio lipid:alcohol $\approx 2:1$, the interdigitated phase will be energetically more favorable than the non-interdigitated phase with voids between the hydrophobic tails, even if some of the tail ends are facing the interfacial water.

stability of the $L_{\beta I}$ phase. The longer the alcohol, the smaller the voids in the alcohol saturated $L_{\beta'}$ phase (see figure 6.11). The addition of a longer alcohol molecule perturbs the bilayer in the $L_{\beta'}$ phase to a lesser extent compared to a smaller one. For the interdigitated phase, however, figure 6.9 shows that a longer alcohol results in a thicker hydrophobic core. A void in this phase exposes therefore more hydrophobic groups of the lipids to the water phase compared to the shorter alcohols. These combined effects explain, why the longer the tail length of the alcohol, the more alcohol is needed to stabilize the $L_{\beta I}$ phase. Similarly, we can understand why a higher concentration of alcohol is needed before the L_c phase is destabilized by a longer alcohol.

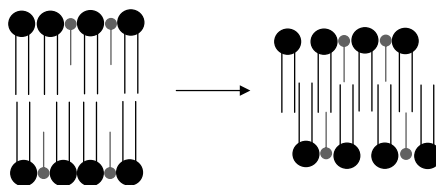


Figure 6.11: Schematical drawing of the formation of the interdigitated phase. With increasing tail length of the alcohol the voids become smaller in the $L_{\beta'}$ phase, while in the interdigitated phase the part of the lipid tails exposed to water becomes larger.

We also investigated the effect of increasing the chain length of the lipid. Experimentally, it was found that lower concentrations of alcohol are needed to obtain the fully interdigitated $L_{\beta I}$ phase [138, 143, 162] and a coexistence region between an interdigitated and non-interdigitated phase was observed for most lipids [144]. There is no consensus in the literature whether a coexistence exists for the longest lipids. We performed simulations on bilayers consisting of $h_3(t_6)_2$ and $h_3(t_8)_2$ lipids, with alcohols varying in length from 1 to 3 beads in the tail. The obtained phase diagrams are similar to the ones depicted in figure 6.7. We find coexistence regions for each lipid-alcohol combination, which is in agreement with the results of Vierl *et al.* [144]. The size of the coexistence region decreases with increasing tail length of the phospholipid, because the concentration of alcohol to obtain the fully interdigitated phase decreases, while the alcohol concentration needed to destabilize the L_c and the $L_{\beta'}$ phase is independent of the alcohol concentration. The energy cost of exposing the tail ends to water becomes less important with increasing tail length, and therefore, the interdigitated phase is stabilized.

6.4.3 Longer chain alcohols

Experiments show that interdigitation only occurs in mixtures of lipids with alcohols up to heptanol. Longer chain lengths of the alcohol, thus from octanol, do not

induce the interdigitated phase. The explanation of these observations is that the energy cost of creating lateral space in the head group region, leading to the formation of voids in the hydrophobic core, is balanced by the increased disorder in the lower part of the tails [133, 145, 163]. We performed some simulations on the lipid $h_3(t_8)_2$ with the alcohols ht to ht_4 . For alcohols ht to ht_3 , we find similar phase diagrams as shown in figure 6.7; increasing the length of the alcohol requires a higher alcohol concentration to stabilize the interdigitated phase. For ht_4 , however, we do not find an interdigitated phase, but the structure shown in figure 6.12. In this structure we observe the coexistence of the L_c (or $L_{\beta'}$) phase with a new phase of which the hydrophobic thickness is approximately twice the hydrophobic length of the alcohol. In chapter 3, we have shown that single-tail lipids, to which our model alcohol molecules resemble, can form a stable bilayer for sufficiently long tails. For these long-chain alcohols, the interdigitated phase has to compete with an alcohol rich L_{β} or L_{α} phase.

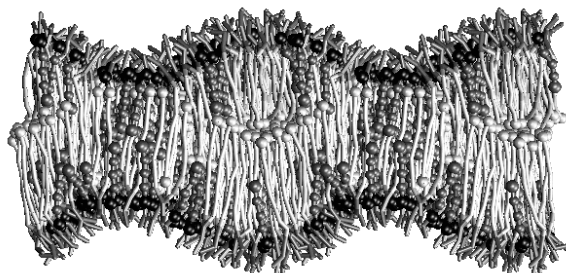


Figure 6.12: Snapshot of a bilayer containing 200 lipids $h_3(t_8)_2$ and 200 alcohols ht_4 . The bonds represent the lipids, with the darker color grey indicating the hydrophilic head group. The bonds and spheres representation indicates the alcohol molecules, where the black sphere is the hydrophilic head group. The terminal beads of both the lipid and the alcohol are depicted by a larger sphere. The system is depicted twice to show the phase separation more clearly.

Experimentally, it is observed that with the longer tail alcohols the $L_{\beta'}$ and the L_c are stabilized [142]. A phase separation, like we find in our simulations, is not observed. At this point, it is important to note that we did not optimize the parameters of our model to reproduce the properties of an alcohol: we used the same head and tail interactions as for our lipids and for the longer chain lengths these molecules resemble the single tail lipids, that are studied in chapter 3. In the literature, it is known that a mixture of two lipids does phase separate in a lipid bilayer. The mixing of, for instance, lipids with different tail lengths, leads to the formation of domains with the shorter lipid and domains containing the longer lipid [164, 165]. Since our model alcohols with tail lengths ≥ 4 self assemble in a bilayer, our observations agree

with the observations of a mixture of two bilayer lipids. Since we only investigated a small system, we cannot distinguish the formation of domains from an ordinary phase transition; it would be interesting to investigate this phase separation with larger systems.

6.5 Conclusions

We studied the induced interdigitation of a bilayer consisting of double-tail lipids. In this chapter, interdigitation is induced by changes in the chemical structure of the lipid head group and by adding model alcohols to the bilayer. Since in experiments it is not always possible to isolate a single cause and effect relation, we investigate the different factors that can play the crucial role in the induction of the interdigitated phase.

The main cause of the formation of the interdigitated $L_{\beta I}$ phase is an increase in the lateral area between the lipid head groups. Due to this increase, voids are created in the hydrophobic core of the lipid bilayer. Since voids in the bilayer core are energetically unfavorable, the $L_{\beta'}$ or L_c phases are destabilized. These voids can be filled by molecules of the opposite monolayer. The bilayer will adapt an interdigitated configuration, in which the lipid tails of one monolayer interpenetrate the opposing layer. Increasing the repulsion between the lipid head groups, increasing the lipid tail length, or decreasing the tail length of the alcohol, leads to an increase of the volume of these voids. The larger this volume, the more stable the interdigitated phase.

By adding an additional hydrophobic bead to the hydrophilic head we mimic the esterification of the lipid head group. In experiments, the lipid will then have a net positive charge, which is modeled by increasing the head-head repulsion parameter. The additional bead sticks into the hydrophobic core of the bilayer, causing a change in the conformation of the head group, which leads to an increased area per lipid. An additional effect is that the hydrophobic bead shields the tail ends of the lipid from the (unfavorable) interaction with water. We show that, the additional hydrophobic bead plays the crucial role in the formation of the interdigitated phase and that an increased head-head repulsion only facilitates the phase transition. This conclusion is an alternative interpretation of the experimental results.

The induced interdigitation by adding alcohol to the system is studied by adding model alcohols with varying lengths to the bilayer. The advantage of performing computer simulations to this system is that we can directly impose the concentration of alcohol in the bilayer, which is not possible experimentally. At low concentrations of alcohol the non-interdigitated gel phase is formed and at high concentrations the fully interdigitated phase is the stable phase. In between we find a co-

existence region between the interdigitated and non-interdigitated phase, in which the alcohol molecules are inhomogeneously distributed between these two phases. We show that the interdigitated phase is formed at a lipid:alcohol ratio of about 2:1, which is significantly lower than was proposed in the literature. At this ratio the formation of the interdigitated phase is energetically more favorable than a non-interdigitated structure with (energetically unfavorable) voids in the hydrophobic core, even if some of the lipid tail ends are exposed to the interfacial water.

References

- [1] Mathews, C. K.; van Holde, K. E. *Biochemistry*; The Benjamin/Cummings Publishing Company, Inc.: California, 1990.
- [2] Stryer, L. *Biochemistry*; W.H. Freeman and Company: New York, 1995.
- [3] Singer, S. J.; Nicolson, G. L. *Science* **1972**, *175*, 720–731.
- [4] Cullis, P. R.; de Kruijff, B. *Biochim. Biophys. Acta* **1979**, *559*, 399–420.
- [5] Israelachvili, J.; Marcelja, S.; Horn, R. G. *Q. Rev. Biophys.* **1980**, *13*, 121–200.
- [6] Israelachvili, J. *Intermolecular & surface forces*; Academic Press: San Diego, CA, 1997.
- [7] Damodaran, K. V.; Merz Jr., K. M. *Biophys. J.* **1994**, *66*, 1076–1087.
- [8] Alberts, B.; Johnson, A.; Lewis, J.; Raff, M.; Roberts, K.; Walter, P. *Molecular Biology of the cell*; Garland Science: New York, 2002.
- [9] Koynova, R.; Caffrey, M. *Biochim. Biophys. Acta* **1998**, *1376*, 91–145.
- [10] Gennis, R. B. *Biomembranes. Molecular Structure and Function*; Springer-Verlag: New York, 1989.
- [11] Cantor, R. S. *J. Phys. Chem. B* **1997**, *101*, 1723–1725.
- [12] Merz Jr, K. M.; Roux, B. *Biological membranes: a molecular perspective from computation and experiment*; Birkhäuser: Berlin, 1996.
- [13] Bandyopadhyay, S.; Tarek, M.; Klein, M. L. *J. Phys. Chem. B* **1999**, *103*, 10075–10080.
- [14] Marrink, S. J.; Lindahl, E.; Edholm, O.; Mark, A. E. *J. Am. Chem. Soc.* **2001**, *123*, 8638–8639.
- [15] Moore, P. B.; Lopez, C. F.; Klein, M. L. *Biophys. J.* **2001**, *81*, 2484–2494.
- [16] Goetz, R.; Lipowsky, R. *J. Chem. Phys.* **1998**, *108*, 7397–7409.
- [17] Shelley, J. C.; Shelley, M. Y.; Reeder, R. C.; Bandyopadhyay, S.; Moore, P. B.; Klein, M. L. *J. Phys. Chem. B* **2001**, *105*, 9785–9792.
- [18] Shelley, J. C.; Shelley, M. Y.; Reeder, R. C.; Bandyopadhyay, S.; Klein, M. L. *J. Phys. Chem. B* **2001**, *105*, 4464–4470.
- [19] Saiz, L.; Klein, M. L. *Acc. Chem. Res.* **2002**, *35*, 482–489.
- [20] Lopez, C. F.; Moore, P. B.; C., S. J.; Shelley, M. Y.; Klein, M. L. *Comp. Phys. Comm* **2002**, *147*, 1–6.
- [21] Landau, L. D.; Lifshitz, E. M. *Fluid Mechanics*; Pergamon Press, 1959.
- [22] Groot, R. D.; Rabone, K. L. *Biophys. J.* **2001**, *81*, 725–736.
- [23] Venturoli, M.; Smit, B. *Phys.Chem.Comm.* **1999**, *2*, art.no. 10.
- [24] Shillcock, J. C.; Lipowsky, R. *J. Chem. Phys.* **2002**, *117*, 5048–5061.
- [25] Kranenburg, M.; Venturoli, M.; Smit, B. *Phys. Rev. E* **2003**, *67*, art. no. 060901.
- [26] Kranenburg, M.; Venturoli, M.; Smit, B. *J. Phys. Chem. B* **2003**, *107*, 11491–11501.

- [27] Chen, C. M.; Lubensky, T. C.; Mackintosh, F. C. *Phys. Rev. E* **1995**, *51*, 504–513.
- [28] Lubensky, T. C.; MacKintosh, F. C. *Phys. Rev. Lett.* **1993**, *71*, 1565–1568.
- [29] Schwarz, U. S.; Gompper, G. *Phys. Rev. Lett.* **2000**, *85*, 1472–1475.
- [30] Marrink, S. J.; Tieleman, D. P. *J. Am. Chem. Soc.* **2001**, *123*, 12383–12391.
- [31] Hoogerbrugge, P. J.; Koelman, J. M. V. A. *Europhys. Lett.* **1992**, *19*, 155–160.
- [32] Frenkel, D.; Smit, B. *Understanding Molecular Simulations: from Algorithms to Applications*; Academic Press: San Diego, 2nd ed., 2002.
- [33] Scott, H. L. *Curr. Opin. Struct. Biol.* **2002**, *12*, 495–502.
- [34] Goetz, R.; Gompper, G.; Lipowsky, R. *Phys. Rev. Lett.* **1999**, *82*, 221–224.
- [35] Español, P.; Warren, P. *Europhys. Lett.* **1995**, *30*, 191–196.
- [36] Coveney, P. V.; Novik, K. E. *Phys. Rev. E* **1996**, *54*, 5134–4831.
- [37] Coveney, P. V.; Novik, K. E. *Phys. Rev. E* **1997**, *55*, 4831–4831.
- [38] Koelman, J. M. V. A.; Hoogerbrugge, P. J. *Europhys. Lett.* **1993**, *21*, 363.
- [39] Boek, E. S.; Coveney, P. V.; Lekkerkerker, H. N. W. *J. Phys. Condens. Matter* **1996**, *8*, 9509–9512.
- [40] Boek, E. S.; Coveney, P. V.; Lekkerkerker, H. N. W.; van Schoot, P. *Phys. Rev. E* **1997**, *55*, 3124–3133.
- [41] Groot, R. D.; Madden, T. J. *J. Phys. Chem.* **1998**, *108*, 8713–8724.
- [42] Warren, P. B. *Curr. Opinion Coll. Interface Sci.* **1998**, *3*, 620–624.
- [43] Wijmans, C. M.; Smit, B. *Macromolecules* **2002**, *35*, 7138–7148.
- [44] Zhang, K.; W., M. C. *Comput. Phys. Commun.* **2000**, *129*, 275–281.
- [45] van Vliet, R. E.; Hoefsloot, H. C.; Iedema, P. D. *Polymer* **2003**, *44*, 1757–1763.
- [46] Prinsen, P.; Warren, P. B.; J., M. M. A. *Phys. Rev. Lett.* **2002**, *89*, art. no. 148302.
- [47] Yamamoto, S.; Maruyama, Y.; Hyodo, S. *J. Chem. Phys.* **2002**, *116*, 5842–5849.
- [48] Ryjkina, E.; Kuhn, H.; Rehage, H.; Müller, F.; Peggau, J. *Angew. Chem. Int. Ed.* **2002**, *41*, 983–986.
- [49] Jury, S.; Bladon, P.; Cates, M.; Krishna, S.; Hagen, M.; Ruddock, N.; Warren, P. *Phys. chem. Chem. Phys.* **1999**, *1*, 2051–2056.
- [50] Groot, R. D. *Langmuir* **2000**, *16*, 7493–7502.
- [51] Kong, Y.; Manke, C. W.; Madden, W. G.; Schlijper, A. G. *J. Chem. Phys.* **1997**, *107*, 592–602.
- [52] Schlijper, A. G.; Manke, C. W.; Madden, W. G.; Kong, Y. *Int. J. of Mod. Phys. C* **1997**, *8*, 919–929.
- [53] Konstant, P. H.; Pearce, L. L.; Harvey, S. C. *Biophys. J.* **1994**, *67*, 713–719.
- [54] Spenley, N. A. *Europhys. Lett.* **2000**, *49*, 534–540.
- [55] Ayton, G.; Voth, G. A. *Biophys. J.* **2002**, *83*, 3357–3370.
- [56] Español, P. *SIMU, Challenges in Molecular Simulations* **2002**, *4*, 59–77.
- [57] Groot, R. D.; Warren, P. B. *J. Chem. Phys.* **1997**, *107*, 4423–4435.
- [58] Jähnig, F. *Biophys. J.* **1996**, *71*, 1348–1349.

- [59] Feller, S. E.; Pastor, R. W. *Biophys. J.* **1996**, *71*, 1350–1355.
- [60] Feller, S. E.; Pastor, R. W. *J. Chem. Phys.* **1999**, *111*, 1281–1287.
- [61] Chiu, S.-W.; Clark, M.; Subramaniam, S.; Scott, H. L.; Jakobsson, E. *Biophys. J.* **1995**, *69*, 1230–1245.
- [62] Zhang, R.; Sun, W.; Traistram-Nagle, S.; Headrick, R. L.; Suter, R. M.; Nagle, J. F. *Phys. Rev. Lett.* **1995**, *74*, 2832–2835.
- [63] Katsaras, J.; Gutberlet, T. *Lipid Bilayers. Structure and interactions*; Springer: Berlin, 2001.
- [64] Nagle, J. F.; Tristram-Nagle, S. *Curr. Opin. Struct. Biol* **2000**, *10*, 474–480.
- [65] Furuike, S.; Levadny, V. G.; Li, S. J.; Yamazaki, M. *Biophys. J.* **1999**, *77*, 2015–2023.
- [66] Simon, S. A.; McIntosh, T. J. *Biochim. Biophys. Acta* **1984**, *773*, 169–172.
- [67] Flyvbjerg, H.; Petersen, H. G. *J. Chem. Phys.* **1989**, *91*, 461–466.
- [68] Cevc, G.; Marsh, D. *Phospholipid bilayers: physical properties and models*; John Wiley and Sons: New York, 1987.
- [69] Petrache, H. I.; Dodd, S. W.; Brown, M. F. *Biophys. J.* **2000**, *79*, 3172–3192.
- [70] Sun, W.-J.; Tristram-Nagle, S.; Suter, R. M.; Nagle, J. F. *Biophys. J.* **1996**, *71*, 885–891.
- [71] Misquitta, Y.; Caffrey, M. *Biophys. J.* **2001**, *81*, 1047–1058.
- [72] Slater, J. L.; Huang, C. H. *Prog. Lipid. Res.* **1988**, *27*, 325–359.
- [73] Koynova, R.; Brankov, J.; Tenchov, B. *Eur. Biophys. J. Biophys. Lett.* **1997**, *25*, 261–274.
- [74] Takahashi, H.; Matsuo, A.; Hatta, I. *Phys. Chem. Chem. Phys.* **2002**, *4*, 2365–2370.
- [75] Iwanaga, T.; Suzuki, M.; Kunieda, H. *Langmuir* **1998**, *14*, 5775–5781.
- [76] Shelley, J. C.; Shelley, M. Y. *Curr. Opinion Coll. Interface Sci.* **2000**, *5*, 101–110.
- [77] Dlpoly 2.12. **2001**.
- [78] MacKerell, Jr., A. D.; Bashford, D.; Bellott, M.; Dunbrack, Jr., R. L.; Evanseck, J. D.; Field, M. J.; Fischer, S.; Gao, J.; Guo, H.; Ha, S.; Joseph-McCarthy, D.; Kuchnir, L.; Kuczera, K.; Lau, F. T. K.; Mattos, C.; Michnick, S.; Ngo, T.; Nguyen, D. T.; Prodhom, B.; Reiher, III, W. E.; Roux, B.; Schlenkrich, M.; Smith, J. C.; Stote, R.; Straub, J.; Watanabe, M.; Wiórkiewicz-Kuczera, J.; Yin, D.; Karplus, M. *J. Phys. Chem. B* **1998**, *102*, 3586–3616.
- [79] Jorgensen, W. L.; Chandrasekhar, J.; Madura, J. D.; Impey, R. W.; Klein, M. L. *J. Chem. Phys.* **1983**, *79*, 926–935.
- [80] Ryckaert, J. P.; Ciccotti, G.; Berendsen, H. J. C. *J. Comput. Phys.* **1977**, *23*, 327–341.
- [81] Essmann, U.; Perera, L.; Berkowitz, M. L.; Darden, T.; Lee, H.; Pedersen, L. G. *J. Chem. Phys.* **1995**, *103*, 8577–8593.
- [82] Hoover, W. G. *Phys. Rev. A* **1985**, *31*, 1695–1697.

- [83] Allen, M. P.; Tildesley, D. J. *Computer Simulation of Liquids*; Clarendon Press: Oxford, 1989.
- [84] Shinto, H.; Miyahara, M.; Higashitani, K. *Langmuir* **2000**, *16*, 3361–3371.
- [85] Armen, R. S.; Uitto, O. D.; Feller, S. E. *Biophys. J.* **1998**, *75*, 734–744.
- [86] Tschöpp, W.; Kremer, K.; Batoulis, J.; Bürger, T.; Hahn, O. *Acta Polymer.* **1998**, *49*, 61–74.
- [87] Tristram-Nagle, S.; Zhang, R.; Suter, R. M.; Worthington, C. R.; Sun, W. J.; Nagle, J. F. *Biophys. J.* **1993**, *64*, 1097–1109.
- [88] Tristram-Nagle, S.; Liu, Y.; Legleiter, J.; Nagle, J. F. *Biophys. J.* **2002**, *83*, 3324–3335.
- [89] Lewis, B. A.; Engelman, D. M. *J. Mol. Biol.* **1983**, *166*, 211–217.
- [90] Lis, L. J.; McAlister, M.; Fuller, N.; Rand, R. P.; Parsegian, V. A. *Biophys. J.* **1982**, *37*, 657–666.
- [91] Rand, R. P.; Parsegian, V. A. *Biochim. Biophys. Acta.* **1989**, *988*, 351–376.
- [92] Petrache, H. I.; Tristram-Nagle, S.; Nagle, J. F. *Chem. Phys. Lipids* **1998**, *95*, 83–94.
- [93] Nagle, J. F.; Wiener, M. C. *Biochim. Biophys. Acta* **1988**, *942*, 1–10.
- [94] Nagle, J. F.; Tristram-Nagle, S. *Biochim. Biophys. Acta* **2000**, *1496*, 159–195.
- [95] Jørgensen, K. *Biochim. Biophys. Acta* **1995**, *1240*, 111–114.
- [96] Heimburg, T. *Biophys. J.* **2000**, *78*, 1154–1165.
- [97] Tardieu, A.; Luzzatti, V.; Reman, F. C. *J. Mol. Biol.* **1973**, *75*, 711–733.
- [98] Woodward, J. T.; Zasadzinski, J. A. *Biophys. J.* **1997**, *72*, 964–976.
- [99] Sun, W.-J.; Tristram-Nagle, S.; Suter, R. M.; Nagle, J. F. *Proc. Natl. Acad. Sci. USA* **1996**, *93*, 7008–7012.
- [100] Sengupta, K.; Raghunathan, V. A.; Katsaras, J. *Phys. Rev. E* **1999**, *59*, 2455–2457.
- [101] Zasadzinski, J. A. N.; Schneir, J.; Gurley, J.; Elings, V.; Hansma, P. K. *Science* **1988**, *239*, 1013–1015.
- [102] Goldstein, R. E.; Leibler, S. *Phys. Rev. Lett.* **1988**, *61*, 2213–2216.
- [103] Doniach, S. *J. Chem. Phys.* **1979**, *70*, 4587–4596.
- [104] Carlson, J. M.; Sethna, J. P. *Phys. Rev. A* **1987**, *36*, 3359–3374.
- [105] Larsson, K. *Chem. Phys. Lipids* **1977**, *20*, 225–228.
- [106] Chen, C. M.; Mackintosh, F. C. *Phys. Rev. E* **1996**, *53*, 4933–4943.
- [107] Sengupta, K.; Raghunathan, V. A.; Hatwalne, Y. *Phys. Rev. Lett.* **2001**, *87*, art. no. 055705.
- [108] Cameron, D. G.; Casal, H. L.; Mantsch, H. H. *Biochemistry* **1980**, *19*, 3665–3672.
- [109] Marder, M. and Frisch, H. L.; Langer, J. S.; McConnell, H. M. *Proc. Natl. Acad. Sci. USA* **1984**, *81*, 6559–6561.
- [110] Rappolt, M.; Pabst, G.; Rapp, G.; Kriechbaum, M.; Amenitsch, H.; Krenn, C.; Bernstorff, S.; Laggner, P. *Eur. Biophys. J.* **2000**, *29*, 125–133.

- [111] Wittebort, R. J.; Schmidt, C. F.; Griffin, R. G. *Biochemistry* **1981**, *20*, 4223–4228.
- [112] Banerjee, S. *Physica A* **2002**, *308*, 89–100.
- [113] Falkovits, M. S.; Seul, M.; Frisch, H. L.; McConnell, H. M. *Proc. Natl. Acad. Sci. USA* **1982**, *79*, 3918–3921.
- [114] Nagle, J. E.; Petrache, H. I.; Gouliaev, N.; Tristram-Nagle, S.; Liu, Y.; Suter, R. M.; Gawrisch, K. *Phys. Rev. E* **1998**, *58*, 7769–7776.
- [115] Mason, P. C.; Nagle, J. E.; Epand, R. M.; Katsaras, J. *Phys. Rev. E* **2001**, *63*, art.no. 030902(R).
- [116] Fang, Y.; Yang, J. *J. Phys. Chem.* **1996**, *100*, 15614–15619.
- [117] Mason, P. C.; Gaulin, B. D.; Epand, R.; Wignall, G. D.; Lin, J. S. *Phys. Rev. E* **1999**, *59*, 3361–3367.
- [118] Takeda, T.; Ueno, S.; Kobayashi, H.; Komura, S.; Seto, H.; Toyoshima, Y. *Physica B* **1995**, *213&214*, 763–765.
- [119] Cunningham, B. A.; Brown, A.-D.; Wolfe, D. H.; Williams, W. P.; Brain, A. *Phys. Rev. E* **1998**, *58*, 3662–3672.
- [120] Tenchov, B.; Koynova, R.; Rapp, G. *Biophys. J.* **2001**, *80*, 1873–1890.
- [121] Pabst, G.; Katsaras, J.; Raghunathan, V. A.; Rappolt, M. *Langmuir* **2003**, *19*, 1716–1722.
- [122] Pabst, G.; Katsaras, J.; Raghunathan, V. A. *Phys. Rev. Lett.* **2002**, *12*, art. no. 128101.
- [123] Korreman, S.; Posselt, D. *Euro. Biophys. J.* **2001**, *30*, 121–128.
- [124] Korreman, S.; Posselt, D. *Euro. Phys. J. E* **2000**, *1*, 87–91.
- [125] Chen, F. Y.; Hung, W. C.; Huang, H. W. *Phys. Rev. Lett.* **1997**, *79*, 4026–4029.
- [126] Lemmich, J.; Mortensen, K.; Ipsen, J. H.; Honger, T.; Bauer, R.; Mouritsen, O. G. *Phys. Rev. E* **1996**, *53*, 5169–5180.
- [127] Misbah, C.; Duplat, J.; Houchmandzadeh, B. *Phys. Rev. Lett.* **1998**, *80*, 4598–4601.
- [128] Janiak, M. J.; Small, D. M.; Singer, M. A. *Biochemistry* **1976**, *15*, 4575–4580.
- [129] Luna, E. J.; McConnell, H. M. *Biochim. Biophys. Acta* **1977**, *466*, 381–392.
- [130] Heimburg, T. *Biochim. Biophys. Acta* **1998**, *1415*, 147–162.
- [131] Schneider, M. B.; Chan, W. K.; Webb, W. W. *Biophys. J.* **1983**, *43*, 157–165.
- [132] McIntosh, T. J.; McDaniel, R. V.; Simon, S. A. *Biochim. Biophys. Acta* **1983**, *731*, 109–114.
- [133] McIntosh, T. J.; Lin, H.; Li, S.; Huang, C.-H. *Biochim. Biophys. Acta* **2001**, *1510*, 219–230.
- [134] Adachi, T.; Takahashi, H.; Ohki, K.; Hatta, I. *Biophys. J.* **1995**, *68*, 1850–1855.
- [135] Hata, T.; Matsuki, H.; Kaneshina, S. *Biophys. Chem.* **2000**, *87*, 25–36.
- [136] Lewis, R. N. A. H.; Winter, I.; Kriechbaum, M.; Lohner, K.; McElhaney, R. N. *Biophys. J.* **2001**, *80*, 1329–1342.

- [137] Winter, I.; Pabst, G.; Rappolt, M.; Lohner, K. *Chem. Phys. Lipids* **2001**, *112*, 137–150.
- [138] Rowe, E. S. *Biochemistry* **1983**, *22*, 3299–3305.
- [139] Chiou, J.-S.; Krishna, P. R.; Kamaya, H.; Ueda, I. *Biochim. Biophys. Acta* **1992**, *1110*, 225–233.
- [140] Ohki, K.; Tamura, K.; Hatta, I. *Biochim. Biophys. Acta* **1990**, *1028*, 215–222.
- [141] Feller, S. E.; Brown, C. A.; Nizza, D. T.; Gawrisch, K. *biopj* **2002**, *82*, 1396–1404.
- [142] Rowe, E. S.; Campion, J. M. *Biophys. J.* **1994**, *67*, 1888–1895.
- [143] Nambi, P.; Rowe, E. S.; McIntosh, T. J. *Biochemistry* **1988**, *27*, 9175–9182.
- [144] Vierl, U.; Löbbecke, L.; Nagel, N.; Cevc, G. *Biophys. J.* **1994**, *67*, 1067–1079.
- [145] Löbbecke, L.; Cevc, G. *Biochim. Biophys. Acta* **1995**, *1237*, 59–69.
- [146] Veiro, J. A.; Nambi, P.; Herold, L. L.; Rowe, E. S. *Biochim. Biophys. Acta* **1987**, *900*, 230–238.
- [147] Nagel, N. E.; Cevc, G.; Kirchner, S. *Biochim. Biophys. Acta* **1992**, *1111*, 263–269.
- [148] Rosser, M. F. N.; Lu, H. M.; Dea, P. *Biophys. Chem.* **1999**, *81*, 33–44.
- [149] Tenchov, B. G.; Yao, H.; Hatta, I. *Biophys. J.* **1989**, *56*, 757–768.
- [150] Rowe, E. S. *Biochim. Biophys. Acta* **1985**, *813*, 321–330.
- [151] Mou, J.; Yang, J.; Huang, C.; Shao, Z. *Biochemistry* **1994**, *33*, 9981–9985.
- [152] Rowe, E. S.; Zhang, F.; Wu Leung, T.; Parr, J. S.; Guy, P. T. *Biochemistry* **37**, 1998, 2430–2440.
- [153] Connors, K. A. *Binding constants*; John Wiley and Sons: New York, 1987.
- [154] Simon, S. A.; Stone, W. L.; Busto-Latorre, P. *Biochim. Biophys. Acta* **1977**, *468*, 378–388.
- [155] Trandum, C.; Westh, P. *Prog. Anesth. Mech.* **2000**, page preprint.
- [156] Trandum, C.; Westh, P.; Jörgensen, K.; Mouritsen, O. G. *J. Phys. Chem. B* **1999**, *103*, 4751–4756.
- [157] Westh, P.; Trandum, C. *Biochim. Biophys. Acta* **1999**, *1421*, 261–272.
- [158] Westh, P.; Trandum, C.; Koga, Y. *Biophys. Chem.* **2001**, *89*, 53–63.
- [159] Zhang, F.; Rowe, E. S. *Biochemistry* **1992**, *31*, 2005–2011.
- [160] Pauling, L. *The nature of the chemical bond*; Cornell University Press: New York, 1960.
- [161] Adachi, T. *Chem. Phys. Lip.* **2000**, *107*, 93–97.
- [162] Rowe, E. S.; Cutrera, T. A. *Biochemistry* **1990**, *29*, 10398–10404.
- [163] Huang, C.; McIntosh, T. J. *Biophys. J.* **1997**, *72*, 2702–2709.
- [164] Risbo, J. adn Sperotto, M.; Mouritsen, O. G. *J. Phys. Chem.* **1995**, *103*, 3643–3656.
- [165] Jorgensen, K.; Sperotto, M.; Mouritsen, O. G.; Ipsen, J.; Zuckermann, M. *Biochim. Biophys. Acta* **1993**, *115*, 135–145.

Summary

Since lipids are an important component of biological membranes, knowledge of the behavior of these systems is relevant for our understanding of biological membranes. In addition, the ability of lipids to form various liquid crystalline and mesophases has implications for various processes in membrane biology such as membrane function or membrane protein crystallization.

Lipids can self-assemble in water to form bilayer structures, in which the hydrophilic part of the lipid is oriented towards the water phase (see figure 6.1). The formation of a specific phase is dependent on the molecular structure of the lipid, temperature and the environment, *i.e.* the addition of salts or small surfactants like alcohols and anesthetics to the system.

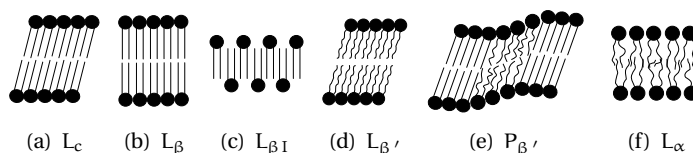


Figure 6.1: Schematical drawings of the various bilayer phases. The characteristics of these phases are explained in the text. The filled circles represent the hydrophilic head group of a phospholipid and the lines represent the hydrophobic tails.

The lowest temperature phase is the L_c phase, also called the subgel phase, which transforms to the gel phase or $L_{\beta'}$ phase upon heating. In both phases the hydrocarbon tails are tilted with respect to the bilayer normal, but in the L_c phase the tails are packed closer together than in the $L_{\beta'}$ phase. Increasing the temperature further leads to the formation of the rippled ($P_{\beta'}$) phase, in which the bilayer is not flat, but corrugated. Finally, the bilayer undergoes the transition to the liquid crystalline or fluid L_α phase. In this phase, the hydrocarbon chains become disordered and therefore the transition to the L_α phase is regarded as the melting of the bilayer. Dependent on the structure of the head group and the presence of small amphiphilic molecules, the low-temperature phases are the L_β phase or the interdigitated $L_{\beta I}$ phase, respectively. In the L_β phase the tails do not have a tilt with respect to the bilayer normal, and in the $L_{\beta I}$ phase, the terminal methyl groups of the lipid chains of two opposing layers do not face each other, but are located near the head group region of the opposing layer.

Despite recent developments of experimental techniques, many factors of the functions of membranes are still not well understood. Therefore, a better characterization of the (phase) behavior of lipid membranes is needed. This insight can be gained by performing computer simulations on model bilayers. Using state of the art molecular dynamics simulations, it is possible to obtain detailed structural informa-

tion of a single phase, but these are too time consuming to determine, for example, a complete phase diagram. An alternative approach is to use a mesoscopic model, in which general aspects of changes in the chemical structure and interactions between the lipids can be studied.

The aim of this thesis is twofold. The first question is how much detail should be added to a mesoscopic model of a lipid to reproduce the experimental observations. Once optimized, we can use the model to gain insight on the structure and phase behavior of a lipid bilayer.

In chapter 2, we describe the simulation techniques used in this thesis. We perform Dissipative Particle Dynamics (DPD) simulations on a tensionless bilayer. In a DPD simulation one uses a dissipative, a random force, and a conservative force between the particles. In analogy with previous simulations using the DPD technique, we use soft-repulsive interactions to mimic the coarse-grained interactions between the lipids and water molecules. In our model, we distinguish three types of particles to mimic the water and the head- and tail-atoms of a lipid. Lipids are constructed by connecting head and tail beads with springs. To ensure that our simulations are performed in a tensionless state we combine DPD with a Monte Carlo scheme, in which we can impose the surface tension.

In chapter 3 we study the phase behavior of the simplest mesoscopic model of a phospholipid, that consists of a hydrophilic head group and one hydrophobic tail. With the chosen set of parameters, we observe the formation of the liquid crystalline phase (L_α) and the interdigitated gel phase ($L_{\beta I}$). The $L_{\beta I}$ phase is known from bilayers consisting of double tail lipids, but in these bilayers this interdigitated phase has to be induced. For bilayers consisting of single-tail lipids only the non-interdigitated L_β and L_α phases are observed experimentally. We show that we can obtain all three phases in these bilayers by changing the interactions between the head groups of the lipid. This suggests that it might be possible to induce an $L_\beta \rightarrow L_{\beta I}$ transition by adding salts.

In chapter 4 we extended the mesoscopic lipid to a model comprising of a larger headgroup to which two hydrophobic tails are attached. We created two mesoscopic models of DMPC, which differ in their level of coarse graining. Using the results from MD simulations on a single lipid in water, an additional bond-bending potential between three subsequent beads was added, which is necessary to obtain the correct tail length dependence of the area per lipid. Using a model consisting of beads with a volume of 90 \AA^3 , we reproduce the experimental values of the area per lipid and the hydrophobic thickness at the reference temperature of $T^* = 1$. We also show that there is no linear relation between the repulsion parameter a_{ij} and the level of coarse

graining. The key factor in the formation of a lipid bilayer is the difference between the water-water and the water-hydrophobic tail repulsion parameters.

Once created the model, we investigate in chapter 5 the phase behavior of double tail lipids, as a function of temperature, headgroup interaction and tail length. At low values of the head-head repulsion parameter, the bilayer undergoes with increasing temperature the transitions $L_c \rightarrow L_\beta \rightarrow L_\alpha$, while for higher values of a_{hh} the transitions $L_c \rightarrow P_{\beta'} \rightarrow L_\alpha$ take place (see figure 6.1). Dependent on tail length, we find the $L_{\beta'}$ between the L_c and the $P_{\beta'}$ phase, of which the stability increases with increasing tail length. The rippled structure ($P_{\beta'}$) is only observed at high enough values of the head-head repulsion parameter in a narrow region around the line where we have approximately 50% L_c or $L_{\beta'}$ phase and 50% L_α phase. At this condition, the frustration between the surface area of the heads and the optimal lateral density of the tails, leads to the formation of a striped (rippled) phase. The anomalous swelling, observed at the $P_{\beta'} \rightarrow L_\alpha$, is caused by conformational changes of the lipid tails, but is not directly related to the rippled phase.

In chapter 6 we study the induced interdigitation of bilayers consisting of double-tail lipids. For mono-tail lipids interdigitation could be induced by changing only the head-head repulsion (chapter 3), but for double-tail lipids this is not sufficient. In these bilayers interdigitation is induced by adding an additional hydrophobic bead to the head group or by adding model alcohols to the bilayer. In case of the additional head bead, the headgroup becomes charged, which we mimic by increasing the head-head repulsion. The general cause of interdigitation is the increased area per headgroup, resulting in the formation of energetically unfavorable voids in the hydrophobic core of the bilayer. With the additional bead we find that an increased steric hindrance plays the crucial role in inducing interdigitation and that the charge facilitates the formation of this phase. In the case of adding alcohol, we reproduce the experimental observations, but at much lower concentrations at the interface than predicted experimentally. The $L_{\beta'} \rightarrow L_{\beta I}$ transition, via a coexistence region, depends both on the length of the alcohol, alcohol concentration and temperature.

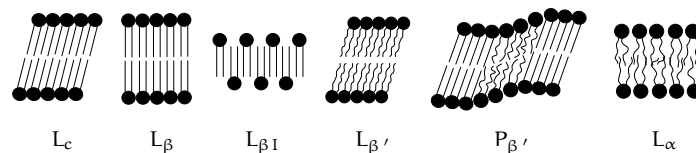
In this thesis we have shown that even with a coarse grained model some level of chemical detail can be implemented and the effect of molecular structure on the properties of model bilayers can be studied. This makes coarse grained models a powerful and flexible tool to study a large variety of systems.

Samenvatting

De cel is de belangrijkste eenheid in de biologie. Elk organisme bestaat uit cellen, die er over het algemeen hetzelfde uitzien en dezelfde grootte hebben. Toch kunnen cellen verschillende functies hebben, wat in sommige gevallen al door de naam duidelijk wordt: er zijn rode bloedcellen, witte bloedcellen, hersencellen, zenuwcellen, etcetera. Dat al deze cellen hun eigen functie kunnen uitoefenen, wordt mogelijk door het celmembraan. Het celmembraan is een "schil" die om de cel zit en deze afschermt van zijn omgeving. Hierdoor kan in de cel een eigen milieu ontstaan. De basis van een celmembraan is de lipide bilaag. In deze bilaag zitten eiwitten, die het transport verzorgen van stoffen door het membraan heen. Deze eiwitten zijn zeer specifiek: sommige stoffen worden wel doorgelaten en andere niet. Doordat het celmembraan van elk type cel een andere samenstelling heeft van lipiden en eiwitten, kan een cel zijn eigen specifieke functie uitoefenen.

Een lipide is een molecuul met een hydrofiële (waterminnende) kop en twee hydrofobe (waterafstotende) staarten. Doordat deze twee eigenschappen verenigd zijn in één molecuul, vormen lipiden in water een bilaag, waarbij de staarten elkaar opzoeken en de kopgroepen in het water steken. Er zijn meerdere lipiden: lipiden kunnen verschillen in de lengte van de staart en de samenstelling van de kopgroep.

De lipiden in een celmembraan hebben twee functies: ten eerste de afscherming van de cel van zijn omgeving en ten tweede hebben sommige lipiden interactie met de eiwitten, waardoor ze het functioneren van het eiwit beïnvloeden. De precieze structuur van de bilaag kan veel invloed hebben op het functioneren van het eiwit. Het is dus belangrijk om te weten hoe de structuur van de bilaag afhangt van de structuur van de lipiden zelf, van de temperatuur en van eventueel toegevoegde stoffen aan het systeem.



Figuur 1: De verschillende fases van een lipide bilaag op een rijtje. De kenmerken van deze fases worden in de tekst uitgelegd. Het zwarte bolletje stelt de hydrofiële kopgroep van een lipide voor en de lijnen de hydrofobe staarten. Naarmate de lijnen rechter zijn, zijn de staarten meer geordend.

De laatste jaren zijn er veel experimentele technieken ontwikkeld om de structuur van een lipide bilaag te onderzoeken. Ondanks deze ontwikkelingen blijven er toch nog veel onduidelijkheden bestaan over het gedrag en de structuur van bilagen.

Om deze onduidelijkheden weg te nemen, gebruiken wij computersimulaties. Een mogelijkheid om een bilaag te simuleren is om elk atoom van elk lipide in het model te stoppen. Het nadeel hiervan is dat het aantal atomen erg groot wordt, tot wel een miljoen. Het doorrekenen van zo'n model vraagt bijzonder veel rekentijd en daarom blijven deze berekeningen vaak beperkt tot een relatief klein systeem of een korte tijd. Om relevantere tijdschalen en grotere systemen te simuleren, maken we vaak gebruik van een simpeler model dat toch alle essentiële informatie bevat. In dit onderzoek gebruiken we hiervoor Dissipative Particle Dynamics (DPD), een methode waarin een groepje atomen wordt voorgesteld door een bolletje en waarin deze bolletjes onderling alleen afstotende krachten ondervinden. In het algemeen stelt een bolletje drie watermoleculen voor en bestaat een lipide uit een keten van hydrofiele en hydrofobe bolletjes. De interacties tussen de bolletjes worden zo gekozen dat de hydrofiele en hydrofobe deeltjes elkaar afstoten maar dat tussen deeltjes van eenzelfde type deze afstoting kleiner is. Tevens zorgen we er in onze simulaties voor dat er op het membraan geen spanning staat (een spanningsloos membraan is biologisch de meest relevante toestand), door DPD te combineren met een Monte Carlo schema. Deze combinatie maakt het mogelijk om overgangen van de ene structuur (fase) naar de andere waar te nemen.

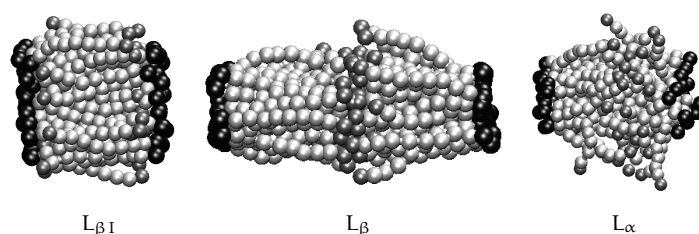
Het doel van dit proefschrift is tweeledig. De eerste vraag die ontstaat in de ontwikkeling van een model is hoeveel informatie een model moet bevatten om een "realistische" bilaag te simuleren. Als we dit eenmaal weten en het model geoptimaliseerd hebben, komen we bij de tweede vraag: kunnen we het model gebruiken om antwoord te geven op experimentele vragen over de structuur van bilagen?

In de hoofdstukken 3 en 4 wordt voornamelijk de eerste vraag bestudeerd: welke informatie is essentieel voor een model? Simpel gezegd komt het erop neer dat je met een heel eenvoudig model begint, dus alleen met de bolletjes die met de veertjes aan elkaar zijn gemaakt. Dan start je een simulatie, kijkt wat eruit komt en vergelijkt de resultaten met de experimenten. Komt dit overeen, dan is het mooi meegenomen, maar zo niet dan moet je wat meer details gaan toevoegen. De vragen die bij het ontwerpen van een model opkomen zijn:

- In hoeveel bolletjes moet je een lipide opdelen?
- Is een model met één staartje voldoende of moet je er twee hebben?
- Kan het model helemaal flexibel zijn of moeten we opleggen dat de hoek tussen bijvoorbeeld bolletje 6, 7 en 8 ongeveer 180° moet zijn?

In hoofdstuk 3 bestuderen we het meest simpele model voor een lipide, bestaand uit één hydrofiel bolletje in de kop en één hydrofobe staart, waarvan de lengte kan variëren. Met dit model kunnen we een bilaag simuleren die bij een hoge temperatuur de kenmerken heeft van een realistische bilaag (de vloeibare L_α fase, gekenmerkt door ongeordende staarten), maar bij lage temperaturen een andere fase geeft.

In een experimenteel systeem is bij lage temperatuur de bilaag in de gel fase, of $L_{\beta'}$ fase, waarin de twee lagen volledig gescheiden zijn, de staarten geordend zijn en een hoek hebben ten opzichte van de normaal van de bilaag (de staarten hebben een tilt). In onze simulaties vinden we dat er een andere fase ontstaat, waarin de staarten in elkaar grijpen en geen hoek meer vertonen. Deze fase staat in de literatuur wel bekend als de geïnterdigiteerde of $L_{\beta I}$ fase, maar wordt normaal niet spontaan gevormd (zie figuur 2). Nadere bestudering van de lipiden met een enkele staart laat zien dat het vormen van deze $L_{\beta I}$ fase afhangt van de interacties tussen de kopgroepen. Hoe meer de kopgroepen elkaar afstoten, des te eerder de $L_{\beta I}$ fase gevormd wordt. Als de kopgroepen elkaar minder afstoten, wordt de L_{β} fase gevormd, die overeenkomt met de $L_{\beta'}$ fase met dit verschil dat de staarten geen tilt hebben. Experimenteel komt het veranderen van de kopgroep repulsie overeen met het toevoegen van zout aan een systeem: door het toevoegen van een zout dat de kopgroepen van elkaar scheidt, kan de $L_{\beta I}$ fase geïnduceerd worden.

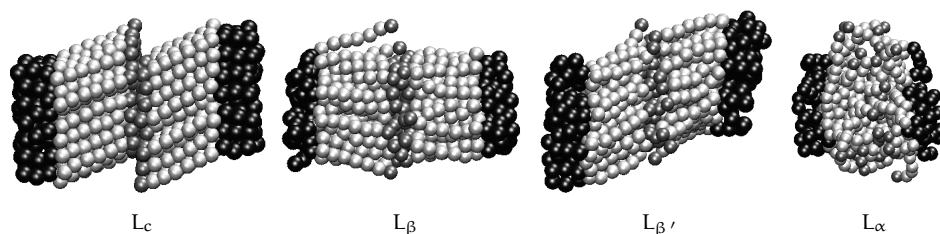


Figuur 2: Snapshots van simulaties aan een bilaag van een monotail lipide. Het model bestaat uit een hydrofiel bolletje (zwart) en een hydrofobe staart van negen bolletjes (grijs). De uiteinden van de staarten hebben een donkerder kleur grijs. Van links naar rechts: de geïnterdigiteerde fase $L_{\beta I}$, de niet-geïnterdigiteerde fase L_{β} en de vloeibare fase L_{α} .

In hoofdstuk 4 gaan we al uit van een model dat bestaat uit een kopgroep met meerdere hydrofiel bolletjes en twee hydrofobe staarten. Als uitgangspunt nemen we het fosfolipide DMPC en we vergelijken de resultaten van de simulaties met de experimentele resultaten, waarbij we het model en de repulsieparameters veranderen. Ook maken we het model wat stijver doordat we een hoek opleggen tussen drie opeenvolgende bolletjes. De waarden voor deze hoeken kunnen we verkrijgen door “realistische” simulaties aan een lipide uit te voeren. In het eerste model gaan we ervan uit dat een bolletje een watermolecuul voorstelt en hierdoor bestaat het lipide in totaal uit 38 bolletjes. Op dit model passen we twee parametersets toe, die met name verschillen in de waarde voor de water-staart interactie. Het blijkt dat we met beide sets de hoge temperatuurfase niet goed kunnen reproduceren, wat leidt tot de conclusie dat de vertaling van “één watermolecuul op een bolletje” te fijn is. In het tweede model gaan we ervan uit dat een bolletje drie watermoleculen voorstelt. Het lipide bestaat nu uit een kopgroep van drie hydrofiel bolletjes met daaraan vast

twee hydrofobe staarten, die ieder uit vijf bolletjes bestaan. Ook op dit model hebben we twee verschillende parametersets toegepast. Met dit model krijgen we voor beide parameter sets zowel de juiste hoge temperatuurfase als de lage temperatuurfase, waarbij ook de waarde voor de oppervlakte per lipide overeenkomt met de experimentele waarde.

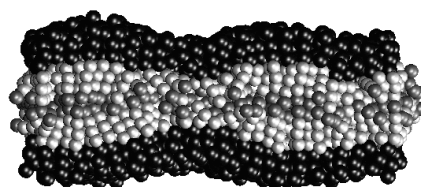
Nu we een goed model hebben, kunnen we het fasegedrag onderzoeken. In hoofdstuk 5 variëren we de temperatuur, de staartlengte en de interacties tussen de kopgroepen. Figuur 3 laat snapshots van simulaties aan een bilaag bij verschillende temperaturen zien. De hoge temperatuurfase is de L_α fase en bij de laagste temperaturen ontstaat de L_c fase, waarbij het verschil met de $L_{\beta'}$ fase is dat de staarten nog stijver zijn. De fases die hier tussenin zitten hangen af van de staartlengte en de interacties tussen de kopgroepen. Als de repulsie tussen de kopgroepen klein is (m.a.w. de kopgroepen zitten dicht op elkaar) dan zit tussen de L_c en de L_α fase de L_β fase, waarin de staarten wel geordend, maar niet getilt zijn. Bij hogere repulsie tussen de kopgroepen, vinden we verschillende fases, afhankelijk van de staartlengte. Bij korte staarten vinden we als we de temperatuur verhogen, de overgangen $L_c \rightarrow P_{\beta'} \rightarrow L_\alpha$, terwijl we bij langere staarten tussen de L_c en de $P_{\beta'}$ fase nog de $L_{\beta'}$ fase vinden. Deze fase is stabielere naarmate de lengte van de staarten toeneemt.



Figuur 3: Snapshots van simulaties aan een bilaag van een lipide met een dubbele staart. Het model bestaat uit een kopgroep met 3 hydrofiële bolletje (zwart) en twee hydrofobe staarten van ieder zeven bolletjes (grijs). De uiteinden van de staarten hebben een donkerder kleur grijs. Van links naar rechts: de subgel of L_c fase, de gel fase L_β , de gel fase $L_{\beta'}$, waarin de staarten een tilt hebben, en de vloeibare fase L_α

De $P_{\beta'}$ fase, die ook wel de “rippled fase” genoemd wordt, is de fase die tussen de geordende $L_{\beta'}$ of L_c fase en de ongeordende L_α fase inzit. Deze fase roept zowel bij experimentalisten als bij theoretici nogal wat vragen op. Het merkwaardige van de $P_{\beta'}$ fase is, dat de bilaag niet vlak is, zoals in de andere fases, maar een golf (een ripple) vertoont. In literatuur bestaan over het ontstaan van deze fase verschillende meningen. De ripple kan veroorzaakt worden door interacties tussen de bilagen, door coëxistentie tussen verschillende fases, door een variatie in tilt hoek van de staarten of door de ladingen van de kopgroepen. Ook blijkt dat de bilaag gaat opzwellen als de overgang naar de L_α fase plaatsvindt, maar het is niet zeker of dit

zwellgedrag samenhangt met de vorming van de rippled fase. Uit onze simulaties blijkt dat de voornaamste oorzaak van het ontstaan van de rippled fase de coëxistentie is tussen de L_c of $L_{\beta'}$ en we vinden de karakteristieke golfstructuur op de lijn waar we 50% van beide fases hebben (zie figuur 4). De structuur kan alleen ontstaan als de kopgroepen voldoende gehydrateerd zijn (m.a.w. omgeven zijn met water). Kennelijk is het energetisch gunstig om zoveel mogelijk kopgroepen te hydrateren en dit wordt alleen bereikt als het oppervlak van de bilaag zo groot mogelijk wordt. Omdat de temperatuur nog niet hoog genoeg is om de gehele bilaag te laten smelten naar de L_α fase, wordt deze oppervlaktevergroting bereikt door de bilaag te laten rippelen. Wanneer de kopgroepen elkaar meer aantrekken (de repulsie tussen de kopgroepen is klein), zullen de kopgroepen minder gehydrateerd zijn, en zal de rippled fase niet gevormd worden. Het zwellgedrag van de bilaag hangt niet samen met de vorming van de rippled fase, aangezien we het zwellen ook terugvinden als de rippled fase niet wordt gevormd. De oorzaak van het zwellen van de bilaag als de temperatuur omlaag wordt gebracht, is de ordening (het rechtekken) van de hydrofobe staarten, waardoor de bilaag aanzienlijk dikker wordt.



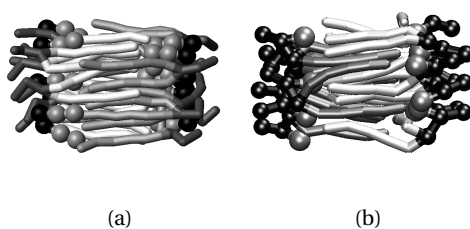
Figuur 4: De “rippled fase”: snapshot van een simulatie. De dikke en dunne gedeelten van de bilaag wisselen elkaar af. In het dikke gedeelten is de bilaag in de geordende L_c fase en in de dunne gedeelten in de vloeibare L_α fase.

In het laatste hoofdstuk grijpen we weer terug op de interdigitatie van een bilaag (de $L_{\beta I}$ fase), die we in hoofdstuk 3 spontaan vonden. In een bilaag van fosfolipiden is de lage temperatuurfase de L_c of de $L_{\beta'}$ fase, waarin de twee helften van de bilaag compleet gescheiden zijn. In de $L_{\beta I}$ fase grijpen de staarten van de twee helften compleet in elkaar, maar deze moet geïnduceerd worden door het veranderen van de structuur van het lipide of het toevoegen van een extra component aan het systeem. Bij de lipiden met een enkele staart hebben we de geïnterdigiteerde fase makkelijk kunnen induceren door de interacties tussen kopgroepen te veranderen. Bij het model met twee hydrofobe staarten is het aanpassen van de kopgroepinteracties niet voldoende. Twee experimentele methoden om interdigitatie te induceren zijn het toevoegen van een klein amfifiel molecuul, zoals een alcohol, aan het systeem of het veranderen van de kopgroep door er een extra hydrofobe groep aan te koppelen. In onze simulaties bestuderen we beide methodes en inderdaad vinden we bij lage temperatuur de geïnterdigiteerde fase (zie figuur 5). Het mechanisme is

in beide gevallen hetzelfde: de ruimte tussen de kopgroepen wordt vergroot doordat de extra groep of het alcohol precies op het grensvlak van de hydrofiele koppen en de hydrofobe staarten gaat zitten. Hierdoor wordt de afstand tussen de staarten ook groter, waardoor er “gaten” in de bilaag ontstaan. Deze gaten zijn energetisch ongunstig, en het systeem zoekt de oplossing in het in elkaar schuiven van de staarten. De uiteinden van de staarten komen niet in contact met het water, omdat de uiteinden worden afgeschermd door de extra hydrofobe groep in de kopgroep of door het hydrofobe staartje van het alcohol. Naarmate de staarten van het lipide langer worden, neemt de stabiliteit van de geïnterdigiteerde fase toe.

In het geval van het toevoegen van alcohol aan een bilaag, blijkt uit experimenten dat er een minimale concentratie nodig is om een volledig geïnterdigiteerde fase te krijgen en het algemene beeld is dat tegenover elke staart van het lipide een alcohol moet zitten. De simulaties laten zien dat dit niet het geval hoeft te zijn; er is inderdaad een minimum aantal alcoholmoleculen nodig om interdigitatie te induceren, maar dit aantal is lager dan het aantal staarten in de bilaag. Bij een lager aantal moleculen vindt er coëxistentie plaats tussen de geïnterdigiteerde fase en de niet-geïnterdigiteerde fase en bij nog lagere concentratie wordt de geïnterdigiteerde fase niet gevormd.

In het geval van het aankoppelen van een extra hydrofobe groep aan de hydrofiele kopgroep, treden er twee effecten op: de repulsie tussen de kopgroepen wordt groter, omdat er een lading gecreëerd wordt en er treedt sterische hindering op door de aanwezigheid van de hydrofobe groep zelf. In de literatuur wordt het ontstaan van de lading als de voornaamste reden aangeduid voor het vormen van de geïnterdigiteerde fase. De simulaties laten echter zien dat de extra groep de belangrijkste bijdrage heeft aan het ontstaan van de geïnterdigiteerde fase en dat de grotere kopgroeprepulsie de vorming vergemakkelijkt.



Figuur 5: Snapshots van de geïnterdigiteerde fase van een bilaag. (a) Interdigitatie door het toevoegen van alcohol en (b) interdigitatie door het aankoppelen van een extra hydrofobe groep aan de kopgroep van het lipide. In (a) zijn de lipiden met 'sticks' aangegeven en de alcoholmoleculen met bolletjes. In (b) wordt de extra groep weergegeven door een grotere bolletje.

Curriculum Vitae

- 31 juli 1976 geboren te Leiderdorp
- 1988-1994 VWO, Christelijk Lyceum Dr. W.A. Visser 't Hooft te Leiden
- 1994-1998 Hoger Laboratorium Onderwijs, Hogeschool Leiden
"The reactivity of *o*-hydroxybenzyl alcohol in solution at elevated temperatures"
- 1997-1999 Doctoraal Scheikunde, Universiteit Leiden
"The carbon-oxygen bond dissociation enthalpies in organic peroxy radicals"
- 1999-2003 Promotieonderzoek, Universiteit van Amsterdam
"Phase transitions of lipid bilayers: a mesoscopic approach"

Publications and presentations

Publications

- M. Kranenburg, M. Venturoli, and B. Smit, *J. Phys. Chem.*, **2003**, *107*, 11491-11501
“Phase behavior and induced interdigitation in bilayers studied with dissipative particle dynamics”
- M. Kranenburg and T.J.H. Vlugt <http://www.natuurkunde.nl/artikelen/>, **2003**
“Hoe werken anesthetica? Een numeriek model”
- L. Rekvig, M. Kranenburg, J. Vreede, B. Hafskjold, and B. Smit, *Langmuir*, **2003**, *19*, 8195-8205
“Investigating surfactant efficiency with Dissipative Particle Dynamics”
- L. Rekvig, M. Kranenburg, B. Hafskjold, and B. Smit, *Europhys. Lett.*, **2003**, *63*, 902-907
“Effect of surfactant structure on interfacial properties”
- M. Kranenburg, M. Venturoli, and B. Smit, *Phys. Rev. E*, **2003**, *67*, art.nr. 060901(R),
“Molecular simulations of mesoscopic bilayer phases”
- M. Kranenburg, M.V. Ciriano, A. Cherkasov, and P. Mulder, *J. Phys. Chem. A*, **2000**, *104*, 915-921
“The carbon-oxygen bond dissociation enthalpies in organic peroxy radicals”
- E. Dorrestijn, M. Kranenburg, D. Poinot, and P. Mulder, *Holzforschung*, **1999**, *53*, 111-116
“Lignin depolymerization in hydrogen donor solvents”
- E. Dorrestijn, M. Kranenburg, M.V. Ciriano, and P. Mulder, *J. Org. Chem.*, **1999**, *64*, 3012-3018
“The reactivity of *o*-hydroxybenzyl alcohol in solution at elevated temperatures”

Oral presentations

- M. Kranenburg and B. Smit, Summerschool “Coarse graining methods”, **2001**, Sjukulla, Finland
 - “On the mapping of a phospholipid on a coarse-grained model”
 - “DPD simulations of surfactants in an oil-water system”

Poster presentations

- M. Kranenburg, M. Venturoli, and B. Smit, SoftSimu 2002, **2002**, Helsinki, Finland
“Creating a DPD-model of a phospholipid bilayer”
- M. Kranenburg, M. Venturoli, and B. Smit, Physics meets biology, **2001**, Helsinki, Finland
“Creating a coarse-grained model of a phospholipid”
- M. Kranenburg, M. Venturoli, J.P. Nicolas, and B. Smit, Summerschool “Soft matter”, **2000**, Les Houches, France
“On the mapping of a phospholipid on a coarse-grained model”
- M. Kranenburg, M. Venturoli, and B. Smit, Biophysics Europe, **2000**, Munich, Germany
“Creating a coarse-grained model of a phospholipid”
- M. Kranenburg, M. Venturoli, J.P. Nicolas, and B. Smit, “Vloeistoffen en grensvlakken”, **2000**, Lunteren, The Netherlands
“On the mapping of a phospholipid on a coarse-grained model”

Dankwoord

En dan komen we nu bij het onderdeel dat iedereen toch waarschijnlijk als eerste leest: het dankwoord. Word ik nog genoemd, wie wordt er genoemd en wie wordt er vergeten? Ik ben er zeker van dat ik mensen vergeet. Zowel op de UvA als daarbuiten zijn er de laatste vier jaren velen geweest die mij op de één of andere wijze hebben bijgestaan. Toch wil ik een aantal mensen in het bijzonder bedanken.

Ten eerste natuurlijk mijn promotor Berend Smit. Hij heeft met mij hoge pieken en diepe dalen meegemaakt, maar Berend bleef altijd even enthousiast. Berend, bedankt voor de vele gesprekken, zowel wetenschappelijk als persoonlijk.

Op het wetenschappelijke vlak heb ik veel gehad aan de leden van mijn 'knutselclub'. Peter, Evert Jan, Christophe, Jocelyne, Live, Maddalena, Jean Pierre, Frank, René en Maarten, bedankt voor het meedenken tijdens deze uurtjes. Met 'mijn' studenten, Jocelyne, Daan, Lucas, Martijn en Martin, kwam ik eveneens tot leuke resultaten. Daarnaast wil ik Marijke en Stephen van de bieb bedanken. Elk artikel, uit welk vreemd boek dan ook, vond ik altijd keurig in mijn postvakje.

Ook mijn kamergenoten mogen niet ontbreken in dit dankwoord. De 'wisselende' bewoners: Live, Edith en Chris, maar zeker de vaste kern: David, Abdon en Merijn. We zijn serieus aan het werk geweest, maar ik heb met jullie ook erg veel lol gehad. De traditie van champagne met nootjes bij elk geaccepteerd artikel, de altijd aanwezige voorraad zoetheid en gewoon de sfeer onderling zorgden ervoor dat onze kamer iets unieks had. Ik zal B6.38 zeker gaan missen.

Uiteraard hebben alle collega's bijgedragen tot een leuke promotietijd, maar dat worden er teveel om op te noemen. 's Ochtends vroeg even koffie drinken bij Nicole met een vast cluppie, tussen de middag lunch met de lunsclub, ITS-radio: allemaal tekenen van een goede sfeer.

Natuurlijk bestaat er ook een wereld buiten die van de wetenschap, die niet minder belangrijk is. Allereerst wil ik Karin en Thijs noemen, die ik leerde kennen als collega, maar die in korte tijd goede vrienden zijn geworden. En naast mijn promotie vond ik de nodige afleiding in volleyballen en zingen. Lekker afreageren van een dag hard werken en even over iets anders praten dan over computersimulaties.

Nog een stapje verder op het persoonlijke vlak. Robert en Margriet, ik hoop dat ik nog lang een deel van het meubilair mag blijven. Marjolein en Renaldo, bedankt voor het urenlang spelletjes spelen en het voorzien van nuchtere opmerkingen. Pap en mam, voor jullie kan ik niets anders bedenken dan bedankt voor alles. Gooi: collega, vriend en nog zoveel meer. Thanks, Mik.